PFIZER
MEDICAL
RESEARCH
AWARD
since 2000

주관 : 대한민국의학한림원
at ona Academy of Med cine of Korea

후원 : Pfizer 한국화이자제약

대한민국의학한림원 제19회 화이자의학상

PFIZER
MEDICAL
RESEARCH
AWARD
since 2000

대한민국의학한림원
제19회 화이자의학상

시상식

2021. 11. 3(수) 18:00
서울대학교 의과대학 행정관 대강당(3층)

주관 : 대한민국의학한림원 National Academy of Medicine of Korea

후원 : Pfizer 한국화이자제약

PFIZER
MEDICAL
RESEARCH
AWARD
since 2000

대한민국의학한림원
제19회 화이자의학상

기초의학상

임상의학상

중개의학상

PFIZER
MEDICAL
RESEARCH
AWARD
since 2000

화이자의학상 제정 의의

대한민국의학한림원이 주관하고 한국화이자가 후원하는 '화이자의학상(Pfizer Medical Research Award)'은 한국 의학계의 비전을 제시하고, 의학 분야의 연구 경쟁력 제고에 기여하고 있는 국내 최고 권위의 순수 의학상입니다.

화이자의학상은 연구 개발을 통해 국내 의학계 발전을 도모하고 책임 있는 기업시민으로서 신뢰받는 동반자가 되겠다는 기업 사명 실현을 목적으로, 한국화이자제약 창립 30주년을 기념해 지난 1999년 제정되었습니다.

2009년부터는 한국 의학의 지속적인 진흥 창달과 선진화를 위해 의학, 치의학, 약학, 영양학, 간호학, 보건학 등 관련 전문 분야 최고의 석학들로 구성된 대한민국의학한림원이 주관과 심사를 맡으면서 상의 권위와 공정성이 한층 높아졌습니다.
화이자의학상은 기초의학, 임상의학, 중개의학의 3개 부문에서 당해 연도 기준 2년 이내에 발표된 개별 논문의 우수성, 창의성, 과학성, 공헌도, 그리고 우리나라 환자들이 해당 연구를 통해 받게 되는 실질적인 혜택 측면에서 가장 탁월한 논문을 선정해 각 3천 만원의 수상금을 부여하고 있습니다.

특히, 기초와 임상 부문 외에도 2016년부터 신설된 중개의학상 등 세 분야로 구분하여 시상을 진행해, 다양한 분야의 연구자들에게 균등한 수상기회를 부여한다는 측면에서 그 가치를 인정받고 있습니다. 또한, 객관적이고 공정한 심사기준에 따라 수상자를 선정함으로써 해를 거듭할수록 업계 내 가장 권위 있는 의학상으로 성장·발전해오고 있습니다.

식순안내

17:00 - 18:00	**RECEPTION**
18:00 - 18:30	**제 1 부**
개 회	사회자 : 대한민국의학한림원 학술위원 강훈철
국민의례	
주관기관대표 인사	대한민국의학한림원 원장 임태환
후원사대표 인사	한국화이자제약 대표이사 사장 오동욱
학술상 심사 보고	화이자의학상 심사위원장 이은직
수상자 발표	화이자의학상 운영위원장 유승흠
시 상	
축 사	대한의사협회 회장 이필수 / 대한의학회 회장 정지태 한국과학기술한림원 원장 한민구
18:30 - 19:10	**제 2 부**
수상자 강연	좌장 : 연세대학교 의과대학 학장 유대현
폐 회	
19:20 - 21:00	**제 3 부 (장소 이동 : 중식당 - 함춘원)**
디 너	

기초의학상 성학준 교수 (연세대학교 의과대학 의학공학교실)

수상논문
Development of a Shape-Memory Tube to Prevent Vascular Stenosis

임상의학상 박중원 교수 (국립암센터 간담도췌장암센터)

수상논문
Proton beam radiotherapy vs. radiofrequency ablation for recurrent hepatocellular carcinoma: A randomized phase III trial

중개의학상 최동호 교수 (한양대학교 의과대학 외과)

수상논문
Adenine base editing and prime editing of chemically derived hepatic progenitors rescue genetic liver disease

주관기관 대표 인사

대한민국의학한림원 원장
임태환

안녕하십니까. 대한민국의학한림원 원장 임태환입니다.
대한민국의학한림원이 주관하고 화이자제약이 후원하는 제19회 화이자의학상의 개최를 기쁘게 생각합니다. 바쁘신 가운데 시상식에 참석하여 자리를 빛내주신 내외 귀빈 여러분께 감사드리며, 무엇보다 오늘의 주인공인 영광의 수상자분들께 마음 깊은 축하의 말씀을 전합니다.

저희 대한민국의학한림원이 이 상을 주관하여 심사해 온 것이 13회째입니다. 올해는 코로나의 영향으로 시상식 현장에 최소한의 인원만을 모실 수 밖에 없었지만 온라인으로 생중계된다고 하니 오히려 더 많은 분들이 수상의 소식과 의미를 알 수 있지 않을까 싶습니다.

화이자의학상은 인류의 질병치료에 기여할 수 있는 연구 업적을 발굴하고 시상함으로써 의학자들의 연구 의욕을 고취하고 대한민국 의학 발전에 기여하기 위해 1999년에 제정되었습니다. 이제는 명실공히 우리나라 최고의 의학자에게 수여되는 상으로 자리매김하였으며, 의료 연구자에게 그 어떤 상보다 큰 영예가 되는 상이라고 할 수 있겠습니다. 이에 저희 의학한림원도 우리나라 보건의료분야 최고 권위의 법정 석학단체라는 자부심에 걸맞게 공정한 심사와 선정에 최선을 다했다는 말씀을 감히 드립니다.

이런 과정을 거쳐 올해 화이자의학상 수상자로 기초의학상에 연세대 의과대학 의학공학교실 성학준 교수님, 임상의학상에 국립암센터 간담도췌장암센터 박중원 교수님, 중개의학상에 한양대 의과대학 외과학교실 최동호 교수님이 선정되었습니다. 앞으로 더 큰 역할을 하시는데 오늘의 이 수상이 마중물이 되기를 바라며, 더욱더 연구에 정진하시어 앞으로도 우수한 연구 업적을 이루시고 우리나라 의학 발전과 더 나아가 인류의 건강증진에 더욱 힘써 주시기를 부탁드립니다.

그리고 이 자리를 빌려 화이자의학상을 후원하여주시는 한국화이자제약의 오동욱 사장님과 실무진께 진심으로 감사를 드리며, 수상자 선정을 위해 공정한 업적 평가 및 심사에 힘써 주신 대한민국의학한림원 학술상 심사위원회의 이은직 위원장님을 비롯한 위원 여러분과 운영위원회의 유승흠 위원장님을 비롯한 위원 여러분들의 노고에도 거듭 감사드립니다.

앞으로도 대한민국의학한림원은 지속적인 연구 업적 발굴을 통해 국내 의과학자들의 성과를 조명하고 한국 의학 발전에 더욱 기여할 수 있도록 노력하겠습니다. 여기 참석하신 많은 분들의 지속적인 관심과 격려를 부탁드리겠습니다.

후원사 대표 인사

한국화이자제약 대표이사 사장
오동욱

안녕하세요.
올해도 바쁘신 가운데 이번 제19회 화이자의학상 시상식에 참석해주신 분들과 멀리서나마 시청해주시는 내외빈 여러분께 깊이 감사드립니다.

화이자의학상은 한국 의학계의 비전을 제시하고 연구경쟁력을 높여 의학 발전에 기여하고자 제정된 순수 의학상으로 한국화이자제약 설립 30주년을 기념해 지난 1999년 처음 제정된 이래, 올해 19회를 맞이했으며 올해까지 총 46명의 수상자를 배출했습니다. 매년 화이자의학상을 통해 국내 의과학자들의 우수한 연구를 발굴하고 후원함으로써 대한민국 의학계 발전에 기여할 수 있다는 점에서 매우 영광스럽게 생각합니다.

특히 화이자의학상은 기초의학상, 중개의학상, 임상의학상의 수상 분야로 구분되어 국내 의학계 최고 권위의 순수 의학상으로서의 입지를 확고히하고 있습니다.

본 의학상이 지금에 이르기까지 주관과 심사를 맡아 큰 도움을 주신 대한민국의학한림원에 감사드립니다. 특히 대한민국 의학계의 비전을 제시하고 한국의학의 진흥과 선진화를 위해 애써주시는 대한민국의학한림원 임태환 회장님을 비롯하여 화이자의학상의 공정한 운영을 위해 노력해주신 유승흠 운영위원장님과 운영위원회, 엄정한 심사를 담당해주신 이은직 심사위원장님 외 심사위원회 여러분의 노고에도 감사를 드립니다.

아울러, 인류의 질병 치료에 기여할 수 있는 뛰어난 연구 업적을 통해 화이자의학상의 권위와 가치를 더욱 드높여주신 제19회 화이자의학상 기초의학상 수상자이신 연세대학교 의과대학 의학공학교실 성학준 교수님과 임상의학상 수상자이신 국립암센터 간담도췌장암센터 박중원 교수 님, 그리고 중개의학상 수상자이신 연세대학교 의과대학 소아과학교실 최동호 교수님께 진심으로 축하의 말씀 드립니다. 이번 수상을 계기로 앞으로도 늘 변함없는 열정으로 의학계의 발전과 질환 치료의 새로운 장을 열고, 대한민국을 넘어 전세계 인류의 건강 증진에 기여하실 수 있기를 기대합니다.

한국화이자는 앞으로도 의학계의 신뢰받는 파트너이자 제약업계를 선도하는 혁신적인 바이오제약 기업으로서 더욱 정진할 것을 약속드립니다. 앞으로도 환자들의 삶을 변화시키는 혁신을 추구하며 의약품에 대한 연구 개발과 공급을 통해 국민 건강 증진과 의약업계 발전에 기여하는 한편, 책임 있는 기업 시민으로서 다양한 사회공헌 활동을 통해 모두가 건강하게 나이 들며 행복한 삶을 누리는 데 기여하겠습니다.

잠잠해질줄 알았던 코로나 바이러스의 확산이 꾸준히 이어지면서 모두가 불확실성 속에서 많은 어려움을 겪고 있습니다. 최전선에서 고생해주신 의료진 분들의 노고가 대한 더욱 빛나는 한해였습니다. 다시 한번 의료계의 발전과 질환 치료를 위해 애써주시는 의료진 분들과 참석해주신 모든 분들께 감사드리며 여러분모두의 건강과 안녕을 기원합니다.

학술상 심사 보고

화이자의학상 심사위원장
이은직

제19회 화이자의학상 수상자 심사 및 선정은 대한민국의학한림원(이하 의학한림원)에서 주관하고 의학한림원 원장이 심사위원을 위촉하기로 한 운영 규정에 따라 심사위원 11인(심사위원장 포함)을 선정하였다. 심사위원회는 심사 결과를 운영위원회에 보고하고 운영위원회는 수상자를 추천하고, 의학한림원 이사회에서 최종 결정하였다.

1. 화이자의학상 모집 공고

제19회 화이자의학상 후보자 공모 접수는 2021년 7월 12일 공고하여 2021년 8월 15일까지 받았으며, 모집을 알리는 포스터를 제작하여 전국 의과대학, 종합병원, 연구소, 의료단체 및 학회 등에 발송하여 보다 많은 의학자들이 공모에 참여할 수 있도록 홍보하였다. 다양한 분야의 연구자들에게 균등하게 기회를 부여하기 위하여 기초의학, 임상의학, 중개의학 부문에 모집 마감일 전국 의과대학, 병원 및 연구소 등 12개 기관에서 26명의 의학자가 공모에 응하였다.

2. 논문심사

접수된 공모자 26명을 대상으로 다음과 같은 심사절차에 따라 심사를 진행하였다.

1차 심사위원회(2021년 8월 31일)에서 예년과 동일하게 신청 접수 마감일 현재 학술지에 게재된 논문을 대상으로 심사하기로 결정하고(In press Epub ahead of print는 제외), 금년도 4편이 응모된 기초 부문을 제외하고, 주 논문을 대상으로 심사위원들이 추천을 많이 받은 임상 5편, 중개 5편을 대상으로 임하여 2단계 서면 심사를 시행하였다. 2차 심사위원회(2021년 9월 07일)에는 2단계 온라인 심사에서 선정한 기초의학, 임상의학, 중개의학 각 부문별 3편을 대상으로 3단계 심사를 시행하였다.

1단계로 각 심사위원들이 대상자의 지원 분야 및 결격 사유를 포함, 주 논문 및 관련 논문의 평가결과와 대상자가 화이자의학상 수상자로서 충분한 연구 업적이 있는가를 취합하여 평가하고, 2단계로 각 위원별로 후보자 3명을 무순위로 추천하여 기초, 임상, 중개 각 부문 상위 3명을 선정했다. 마지막으로 3차 심사위원회(2021년 9월 14일)에서는 2단계 심사를 통해 선정된 각 후보별 주심제를 도입하여 주논문과 관련 논문의 수준을 비교 평가, 집중 토의를 거친 후 기초의학상 분야, 임상의학상 분야, 중개의학상 분야에서 각각 상위 2명을 순위별로 선정하여 운영위원회에 추천하였다.

3. 수상자 선정

심사위원회에서 기초의학상 부문, 임상의학상 부문, 중개의학상 부문 각각 2명을 선정하여 운영위원회에 보고하고, 2021년 9월 16일 운영위원회에서는 회의를 개최, 운영위원들의 투표로 기초의학상, 임상의학상, 중개의학상, 각 1명 총 3명을 수상 대상자로 선정하여 2021년 9월 27일 의학한림원 이사회에서 인준을 받아 최종 결정하였다.

축사

대한의사협회 회장
이필수

안녕하십니까. 대한의사협회 회장 이필수입니다.

대한민국 의학 최고의 석학단체인 대한민국의학한림원이 주관하고 글로벌 제약업계를 선도하는 한국화이자제약이 후원하는 제19회 화이자의학상 시상식 개최를 진심으로 축하합니다.

올해 수상의 영예를 안으시는 기초의학상 부문의 연세의대 의학공학교실 성학준 교수님, 임상의학상 부문의 국립암센터 간담도췌장암센터 박중원 교수님, 중개의학상 부분의 한양의대 외과 최동호 교수님께 존경과 축하의 박수를 보내드립니다.

아울러 뜻깊은 화이자의학상 시상식을 위하여 노고를 아끼지 않으신 대한민국의학한림원 임태환 원장님, 한국화이자제약 오동욱 대표이사 사장님을 비롯한 관계자 여러분, 그리고 바쁘신 일정에도 축하와 격려를 위해 참석해 주신 내빈 여러분께 감사드립니다.

지난 1999년에 제정된 화이자의학상은 기초의학과 임상의학, 그리고 중개의학 부문에서 각기 탁월한 성과를 일궈낸 의학자를 격려하기 위해 제정된 상으로, 우리나라 환자들에게 미치는 실질적인 혜택에 중점을 둔다는 점에서 가장 한국적인 의학상으로 그 가치를 인정받고 있습니다.

특히 대한민국의학한림원이 심사를 맡아 엄격하고 공정한 심사기준으로 수상자를 선정함으로써 해를 거듭할수록 가장 권위 있는 의학상으로 성장하고 있습니다.

이처럼 화이자의학상이 19회째를 맞이하기까지 훌륭한 의학자들을 적극적으로 발굴하고 격려해 온 대한민국의학한림원과 코로나19 백신 개발 및 공급 등 위기시국에 중요한 역할을 해온 한국화이자제약에 깊이 감사합니다.

오늘 영예의 수상자 분들께서는 어려운 환경 속에서도 탁월한 성취를 통해 질병으로 고통받는 국민들에게 희망을, 나아가 우리나라 의학이 세계적인 수준임을 보여주셨습니다.

수상하신 세 분이 앞으로 더 큰 연구업적을 남기고 더욱 더 세계적으로 명성을 떨칠 수 있도록 우리나라의 의료제도와 연구 환경 개선해 나가는데 저희 대한의사협회가 앞장서겠습니다.

아울러 앞으로도 코로나19와 같은 미지의 신종 감염병에 발빠르게 대처할 수 있도록 의학계와 제약계 간 유기적인 공조와 협업으로 역량을 키워 인류건강에 기여할 수 있길 바랍니다.

다시 한 번 화이자의학상 시상식 개최를 축하드리며, 수상하신 분들과 대한민국의학한림원, 그리고 한국화이자제약의 무궁한 발전과 참석해 주신 모든 분들의 건승을 기원합니다. 감사합니다.

축사

대한의학회 회장
정지태

대한민국 의학 관련 분야 최고 석학들로 구성되어, 한국 의학의 선진화에 앞장서 온 대한민국의학한림원이 주관하고 글로벌 제약업계를 선도하는 한국 화이자제약이 후원하는 국내 최고 권위있는 의학상인 제 19회 화이자 의학상을 수상하게 되신 기초의학상의 연세대학교 의과대학 의학공학교실 성학준 교수, 임상의학상의 국립암센터 간담도췌장암센터 박중원 교수, 중개의학상 부문의한양대학교 의과대학 외과학교실 최동호 교수 세 분께 대한민국 190개 중요한 의학 학술 단체를 대표하여 축하 인사 드립니다.

연세대학교 의과대학 의학공학교실 성학준 교수는 형상기억고분자(shape-memory polymer) 기반 기술을 활용한 이식관을 개발하여 인조 혈관을 삽입할 때 기존 혈관과 다른 직경으로 인해 발생하는 혈류장애 및 혈관 손상 등의 문제를 해결하여 기초의학상 수상자가 되었고, 국립암센터 간담도췌장암센터 박중원 교수는 양성자 치료의 안전성과 효능을 연구하여 이를 입증하는 논문을 작년 '저널 오브 헤파톨로지(Journal of Hepatology)'에 게재해 성과를 인정 받아 임상의학상에 선정되었으며,한양대학교 의과대학 외과학교실 최동호 교수는 정교한 유전자 교정 기술과 줄기세포 기술을 접목하여 유전성 간질환을 치료의 가능성을 제시하여 중개의학상 수장자로 선정되었습니다.

이는 수상자 개인의 영광 이기도 하지만, 소속한 기관의 영광 이기도 하고, 연구자 부모님과 가족의 자랑이기도 합니다. 특히 어려운 여건에서도 말없이 뒤에서 성원해 주신 배우자에게 특별히 감사를 드립니다. 이 세분의 연구 성과가 임상적으로 널리 적용되어 인류 건강 복지에 큰 기여를 하기를 바랍니다.

또한 이 연구자들의 특출 난 연구 결과를 발굴하여 시상하시는 대한민국의학한림원 임원과 관계자 여러분의 노고에 감사드리고, 꾸준히 후원해 주시는 한국화이자제약에도 심심한 감사 말씀 드립니다.

축사

한국과학기술한림원 원장
한민구

인류의 질병치료에 기여할 수 있는 연구 업적을 발굴하고 시상함으로써 의학자들의 연구 의욕을 고취하고 대한민국의 의학발전에 기여하고자 제정된 '화이자의학상'의 제19회 시상식을 축하드립니다.

대한민국의학한림원과 한국화이자제약이, '화이자의학상'을 통해 의약학 연구의 중요성을 인정하고 대한민국 의학 연구자들의 소중한 연구 결과를 발굴하고 포상을 해오신 높은 뜻에 과학기술인의 한 사람으로서 감사드립니다.

의학 연구의 중요성은 아무리 강조해도 지나치지 않습니다. 건강한 삶은 우리들의 가장 큰 소망입니다. 의학 연구는 인류 건강과 복지에 결정적인 영향력을 미침은 물론이고, 산업적으로도 국가 경제에 미치는 영향은 점점 확대되고 있습니다.

특히 전세계적으로 COVID-19 사태를 겪으면서 불과 2년도 안된 짧은 기간에 탁월한 효과를 갖는 백신이 개발되어 우리들 모두에게 큰 희망을 주고 있습니다. 우리나라는 세계적인 의학 수준을 자랑하고 있습니다만 연구개발면에서는 더 많은 투자가 필요합니다.

올해로 19회를 맞이하는 '화이자의학상'이 앞으로도 우리나라 의학 발전에 든든한 버팀목이 되어주시길 부탁드리고, 아울러 올해 수상의 영예를 안으신 기초의학 부문 성학준 교수님, 임상의학 부문 박종원 교수님, 중개의학 부문 최동호 교수님께 축하 인사를 전합니다. 이번 수상을 계기로 더욱더 연구에 정진하시기를 부탁드립니다.

오늘의 시상식 준비를 하여주신 임태환 대한민국의학한림원 회장님과 오동욱 한국화이자제약 대표이사님, 그리고 공정하고 엄정한 평가에 힘써주신 유승흠 운영위원장님과 이은직 심사위원장님을 비롯한 관계자분들의 노고에 감사드립니다.

화이자의학상이 우리 의학의 미래와 비전을 제시하여 보다 건강한 대한민국을 만들어주시길 기원합니다.

감사합니다.

화이자 의학상 운영위원회

위원장

유승흠 연세의대 명예교수

연세의대 졸업(1970)
예방의학

간사

이은직 연세의대 교수

연세의대 졸업(1984)
내과학

남궁성은 가톨릭의대 명예교수

가톨릭의대 졸업(1969)
산부인과학

박귀원 서울의대 명예교수

서울의대 졸업(1972)
외과학

박성수 한양의대 명예교수

한양의대 졸업(1974)
내과학

임태환 울산의대 명예교수

서울의대 졸업(1978)
영상의학

정남식 연세의대 명예교수

연세의대 졸업(1976)
내과학

정화순 이화의대 명예교수

이화의대 졸업(1974)
진단검사의학

최병인 서울의대 명예교수

서울의대 졸업(1974)
영상의학

< 가나다 순 >

PFIZER
MEDICAL
RESEARCH
AWARD
since 2000

대한민국의학한림원
제19회 화이자의학상

기초의학 부문

성학준 교수

연세대학교 의과대학 의학공학교실

대한민국의학한림원 제19회 화이자의학상

기초의학 부문 수상자

성학준 교수

연세대학교
의과대학
의학공학교실

학력

1993. 03 - 1999. 02	연세대학교 생화학과 (이학사)
1999. 03 - 2001. 02	연세대학교 의과대학 의학공학 교실 (공학석사)
2001. 03 - 2004. 02	죠지아 공대/에모리 의대 의공학과 (공학박사)

경력

2004. 05 - 2006. 05	죠지아 공대/에모리 의대 의공학과, 박사후 연구원
2006. 06 - 2009. 07	NJ 생체재료 센터, 팀장
2009. 08 - 2018. 08	반더빌트대학 공과대학-의공학과/의과대학-심장내과, 교수진
2016. 03 - 2018. 08	연세대학교 의과대학 의생명과학부, 특임교수
2018. 09 - 현재	연세대학교 의과대학 의학공학 교실, 교수
2021. 03 - 현재	연세대학교 의과대학 의학공학 교실, 주임교수

수상

2008.	미국 심장학회 과학자상
2009.	미국 보건 복지부 탐구개발 연구상
2011 .	미국 과학재단 올해의 과학자상
2014.	미국 과학재단 혁신 창업 대상상
2015.	미국 과학재단 혁신 기술 이전 대상상
2016 .	미국 과학재단 혁신 과학상
2019.	연세대 의대 우수 연구 업적 상
2021.	KCA 올해의 우수 전문인
2021.	국제 첨단소재 협회 (IAAM) 명예상

논문 요약 및 연구의 의의

의료 소재로 여겨왔던 형상기억 고분자 원천기술 개발을 통한 혈관 이식 및 결합 디바이스로의 응용 연구

본 연구에서는 형상의 회복이 가능한 새로운 소재인 형상기억고분자의 다세대 (multi-generation) 라이브러리를 구축하고, 혈관 이식 및 결합 부위에서 혈관 구조의 회복이 가능하며 혈류의 흐름을 안정화 시켜 혈관 협착 방지가 가능한 소구경 혈관 이식 및 결합 (문합) 적용 디바이스를 개발 하였음.

3mm 미만의 숙주 혈관에 문합기를 이식하여 성공한 첫 번째 연구 결과로써 소재적인 측면 뿐만 아니라 혈관 문합기 제품이 가진 오랜 문제를 해결할 수 있는 전례 없는 잠재력을 보여준 사례임. 이는 혈관 관련 연구 분야를 한 단계 더 나아갈 수 있는 기틀을 마련함과 동시에 다음과 같은 다양한 의료 분야의 발전에 기여할 수 있을 것으로 기대함. 1) 자동 문합 기능은 경험이 부족한 전공의사의 수술을 용이하게 해주고 봉합사나 기존의 문합기 (Ring-Pin) 사용해서 문합할 시 발생하는 단점들 (소요 시간 및 부작용 발생률)을 최소화할 수 있는 방안 제시됨. 2) Computational Fluid Dynamics를 이용해 여러 가지 혈관 그래프트의 이식에 따른 혈류의 변화 양상을 예측함으로써 restenosis등의 clinical adverse effect를 최소화하는데 활용됨. 3) 소재의 형상기억 능력과 3차원 프린팅 기술을 응용 (맞춤형 몰드 제작)으로 환자 맞춤형 의료기기 개발에 활용이 가능함. 4) 신장, 간장 이식 수술 시 혈관 부적합성을 극복하며, 문합의 편리함으로 혈관 부적합성이 없는 경우에도 범용 가능함. 5) 자유피판술 시 이전 치료로 인한 적합한 혈관의 부재 시 대안으로 사용 가능하며, 적합한 혈관이 있는 경우에도 문합의 효율을 증진 함.

형상기억고분자 산업은 연평균 성장률 25%에 이를 정도로 폭발적인 성장을 기록하고 있지만 현재 대한민국은 관련 특허 보유국 순위 권 밖일 정도로 경쟁력이 미비한 실정임. 본 연구를 통해 의료기기로의 적용 성이 높은 형상기억고분자 원천 소재를 개발함으로써 후속 연구의 파생이 가능하며, 이 분야의 의료 소재 국산화를 통해 국내 산업 발전 및 국가 경쟁력 강화에 파급 효과를 기대함.

수상 소감

코로나 시국에서 의미가 큰 상을 받게 되어 영광스럽습니다. 더욱 건강증진에 도움 이 될 수 연구를 열심히 하라는 의미로 새기고 정진하겠습니다. 시상의 주체측 과 심의과정에 수고해 주신모든 분들께 감사 드립니다. 함께한 모든 공동 연구자 및 저희 연구원 분들께도 이 기쁨을 함께 하고 공로를 돌리고 싶습니다.

다 학제간 융합 연구를 근본으로 하는 의공학자로서 의학상은 의미가 크게 다가 옵니다. 해외에서 오랜 기간을 일해 오다 귀국 후 연구에 대한 가치를 인정받은 듯하여 용기를 주는 상 이기도 합니다. 원천 의료소재에 대한 수입의존도가 절대적으로 높은 국내 현실을 볼 때 앞으로 국산화 가능한 소재로 성장 할 수 있다는 생각도 들게 되었습니다. 소년 시절 영화를 보고 만들고 싶었던 형상 기억 소재를 2008년경에 아이디어를 정립하고 지속적으로 라이브러리 형식으로 개발하여 현재 5세대에 걸치는 진보를 거듭하고 있습니다. 또한, 혈관 쪽 뿐만 아니라, 안과, 성형, 치과, 비혈관 내장 기관, 약물 전달 등으로 응용이 확장되는 발전을 거듭 하는 현재 연구 진보를 생각해 볼 때 앞으로의 성장에 큰 동기화가 되는 계기가 되었습니다. 열심히 하겠습니다.

마지막으로, 연구자로서 열심히 생활하고 활동할 수 있도록 버팀목이 된 가족 모두께 감사합니다.

Development of a Shape-Memory Tube to Prevent Vascular Stenosis

*Yong Cheol Shin, Jung Bok Lee, Dae-Hyun Kim, Taeyoung Kim, Grant Alexander, Young Min Shin, Ju Young Park, Sewoom Baek, Jeong-Kee Yoon, Yong Jae Lee, Gyeung Mi Seon, Mi Hee Lee, Mi-Lan Kang, Woo Soon Jang, Jong-Chul Park, Ho-Wook Jun, YongTae Kim, and Hak-Joon Sung**

Inserting a graft into vessels with different diameters frequently causes severe damage to the host vessels. Poor flow patency is an unresolved issue in grafts, particularly those with diameters less than 6 mm, because of vessel occlusion caused by disturbed blood flow following fast clotting. Herein, successful patency in the deployment of an ≈2 mm diameter graft into a porcine vessel is reported. A new library of property-tunable shape-memory polymers that prevent vessel damage by expanding the graft diameter circumferentially upon implantation is presented. The polymers undergo seven consecutive cycles of strain energy-preserved shape programming. Moreover, the new graft tube, which features a diffuser shape, minimizes disturbed flow formation and prevents thrombosis because its surface is coated with nitric-oxide-releasing peptides. Improved patency in a porcine vessel for 18 d is demonstrated while occlusive vascular remodeling occurs. These insights will help advance vascular graft design.

When the diameter of a host vessel reduces below 6 mm, the physical occlusion of grafts caused by thrombosis becomes unresolvable.[1] Moreover, grafting a construct frequently causes disturbed flow, which induces stenosis.[2] The diameter of conventional constructs cannot be customized to fit various vessel diameters, which results in vascular wall damage (Figure S1 and Video S1, Supporting Information). Vessel-damage-free deployment requires the shape recovery of a graft through circumferential tube expansion by ≈40%–50% to fit the host vessel after insertion (Videos S1–S3, Supporting Information). Hence, a new class of shape memory polymer (SMP) library was synthesized through ring opening polymerization[3] with ε-caprolactone (CL) and glycidyl methacrylate (GMA) monomers (**Figure 1**a; Figure S2, Supporting Information). Vessel property-matching optimization necessitated a combinatorial design strategy[4] to produce tunable SMP properties through a series of development steps (Figure 1b–g). First, the idea of decreasing the shape recovery temperature, which was represented by melting temperature (T_m), to the body temperature range was validated[5] by the differential scanning calorimetry (DSC) (Figure 1b). T_m decreased from the temperature of the base poly(ε-caprolactone) (PCL) to that of our SMPs because crosslinking reduced the crystallinity of PCL. This effect was more dominant compared to the increase in the tightness of the polymer chains owing to crosslinking, as illustrated previously.[5] T_m decreased further from the autocrosslinked state to the temperature of ultraviolet (UV)-crosslinked SMPs (i.e., before and after crosslinking, respectively) .

As further validation, when the amount of crosslinking points [poly(glycidyl methacrylate)% (PGMA%)][6] was increased from 4% to 8%, the corresponding T_m and crystallization temperature (T_c) values decreased in linear regression patterns (Figure 1c), which was matched by their enthalpy energies (H_m and H_c) (Figure 1d; Figure S3a, Supporting Information). The range of T_c was typically lower than T_m because polymer crystallization occurred at a temperature lower than T_m. However, an equal enthalpy energy was required to alter both the chain integration stages of our SMPs. In this manner, the SMP composition was determined to be 94%PCL-6%PGMA because it had a T_m of 35–40 °C, as planned (Figure 1e). Next, the polymer concentration was determined to be 100% as its stress was increased to ≈2 MPa when the strain was increased to 50% with the lowest viscosity and shear viscosity among the test concentrations (Figure 1f; Figure S4, Supporting Information). This matched with the behavior of native blood vessels.[7] The stress of the 200% concentration group increased to 4 MPa, which can damage a target vessel.[8] The 50% group was torn at ≈5% strain owing to the insufficient concentration-mediated loose integration of polymers. The crosslinking time was determined as 200 s because the ultimate tensile strain attained the maximum value (≈100%) at this point. However, it decreased considerably at 250 s because of the excessive heating by UV irradiation and the consequent recrystallization of the SMP through annealing (Figure 1g). The follow-up studies used 94%PCL-6%PGMA at 100% concentration after UV crosslinking for 200 s.

Dr. Y. C. Shin, Dr. J. B. Lee, Dr. D.-H. Kim, Dr. Y. M. Shin, S. Baek, Dr. J.-K. Yoon, Y. J. Lee, G. M. Seon, Dr. M. H. Lee, Dr. M.-L. Kang, Prof. J.-C. Park, Prof. H.-J. Sung
Department of Medical Engineering
Yonsei University College of Medicine
Seoul 03722, Republic of Korea
E-mail: hj72sung@yuhs.ac

T. Kim, Prof. Y. Kim
George W. Woodruff School of Mechanical Engineering
Wallace H. Coulter Department of Biomedical Engineering
Institute for Electronics and Nanotechnology
Parker H. Petit Institute for Bioengineering and Bioscience
Georgia Institute of Technology
Atlanta, GA 30332, USA

Dr. G. Alexander
Endomimetics LLC
Birmingham, AL 35203, USA

The ORCID identification number(s) for the author(s) of this article can be found under https://doi.org/10.1002/adma.201904476.

DOI: 10.1002/adma.201904476

J. Y. Park, Dr. W. S. Jang
Anas Meditech
Seoul 08504, Republic of Korea

Y. J. Lee
Department of Obstetrics and Gynecology
Yonsei University College of Medicine
Seoul 03722, Republic of Korea

G. M. Seon, Prof. J.-C. Park
Brain Korea 21 PLUS Project for Medical Science
Yonsei University College of Medicine
Seoul 03722, Republic of Korea

Dr. M.-L. Kang
TMD Lab.
Seoul 03722, Republic of Korea

Prof. H.-W. Jun
Department of Biomedical Engineering
University of Alabama at Birmingham
Birmingham, AL 35294, USA

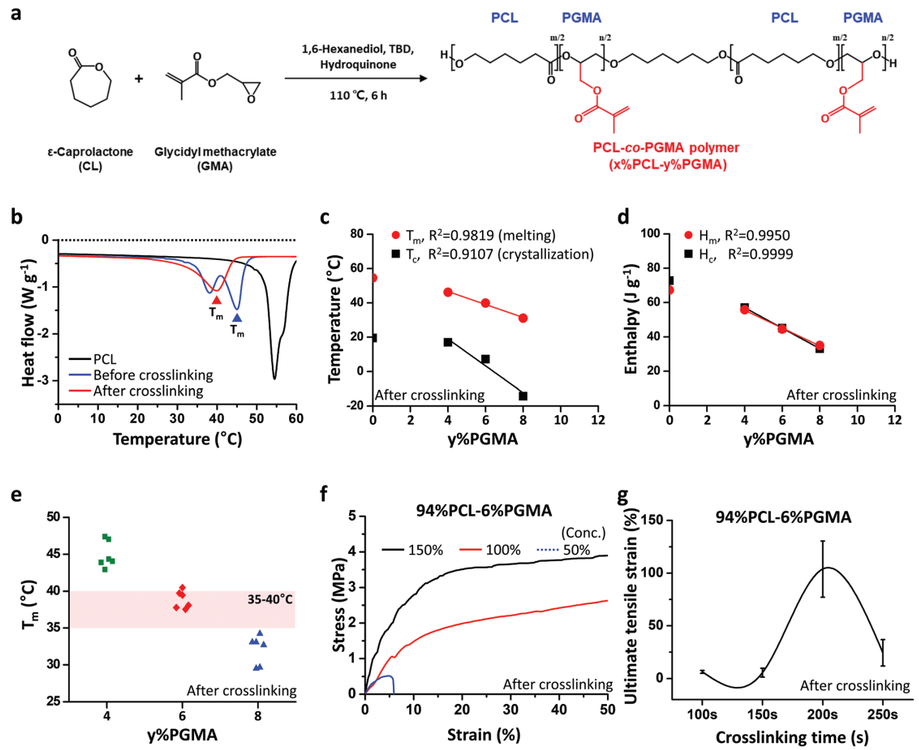

Figure 1. Synthesis and characterizations of x%PCL-y%PGMA copolymer library. a) Synthesis of x%PCL-y%PGMA copolymer (PCL-PGMA) is illustrated, in which ε-caprolactone (CL) and glycidyl methacrylate (GMA) monomers undergo ring opening polymerization. b,c) Differential scanning (DSC) characterization of PCL and PCL-PGMA copolymer before and after crosslinking b) with regression analysis of correlation between y% PGMA and post-crosslinking c). d) Melting enthalpy (H_m) and crystallization enthalpy (H_c). e) Determination of post-crosslinking y% PGMA as 6% because its T_m is close to the body temperature range. f) Determination of post-crosslinking 94%PCL-6%PGMA concentration as 100% (w/v) in the stress–strain curves (Crosslinking time: 200 s). g) Determination of 94%PCL-6%PGMA crosslinking time as 200 s because of the maximum ultimate tensile strain.

The new class of SMP library was successfully synthesized as the theoretical molar% values were close to the actual molar% values, with the expected number- and weight-average molecular weight (M_n and M_w) in a polydispersity index range of 1.3–1.6 before crosslinking (Table S1 – Top, Supporting Information). Then, the test SMPs were crosslinked at the determined conditions (polymer concentration: 100%; crosslinking time: 200 s) (Figure 1). As the amount of crosslinking points (PGMA%) increased from 4% to 8%, as evidenced by the decrease in water contact angles (Figure S3b, Supporting Information), the Young's modulus (E), and corresponding maximum stress (σ_{max}) decreased significantly. This is because the increased crosslinking degree reduced the polymer crystallinity and consequent stiffness (Table S1 – Middle, Supporting Information). In contrast, the maximum strain (ε_{max}) increased to the highest value (104% ± 26%) as the PGMA% increased from 4% to 6%. This result indicates that 6% crosslinking reduced the polymer crystallinity with insignificant influence on the crosslinking-mediated tightening of polymer chains. This is likely to have promoted polymer chain distensibility. However, as PGMA% increased further to 8%, crosslinking occurred even in the noncrystalline phase[9] with a more significant influence on the tightening of polymer chains, thereby decreasing the maximum strain of 8% PGMA to a level similar to that of 4% PGMA. These results further support the selection of 94%PCL-6%PGMA, because deployment into vessels requires sufficient strain to prevent the disruption of arterial pulsing motion with negligible degradation within 3 weeks of the critical remodeling period (Figure S5, Supporting Information).[10]

The thermal properties exhibited similar trends before and after the crosslinking of the test composition groups (Table S1 – Bottom, Supporting Information), indicating that autocrosslinking before UV exposure increased with PGMA%, similar to post-UV crosslinking. The increase in the crosslinking degree with PGMA% reduced the corresponding crystallinity (X_c). Hence, T_m, the melting enthalpy (ΔH_m), T_c, and the crystallization enthalpy (ΔH_c) decreased as PGMA% increased. This phenomenon supports the observations (Figure 1). There were marginal variations in the extent of decrease in each property. Overall, the glass transition temperature (T_g) values of the SMP library were higher than that of PCL (–60 °C) and increased marginally after crosslinking. This was most likely influenced by the variations in their M_w and GMA (side chain) availability, with consequent changes in the chain polarity of polymers compared to PCL.[11] Nonetheless, the negligible changes in the overall T_g values of the test SMPs indicate the preservation of PCL's thermal properties after PGMA polymerization and crosslinking.

The highly repeatable nature of shape programming and recovery for 94%PCL-6%PGMA was demonstrated by applying ≈40 kPa of tensile stress (i.e., ≈5% strain) in stress-controlled cyclic thermomechanical tensile tests (**Figure 2**). To preclude the possibility that a similar response is limited to low strain conditions, the strain was increased from 4% to 43%. The remarkable shape recovery of SMP was demonstrated in this case as well (Figure S6, Supporting Information). Although it is feasible theoretically for shape programming/recovery to be repeated until SMPs degrade,[12] it is realistically limited owing to the incremental energy dissipation during shape memory cycles. Hence, tremendous efforts have been applied to improve the efficiency of energy storage and thereby, the repeatability of shape memory cycles.[12,13] The robust maintenance of

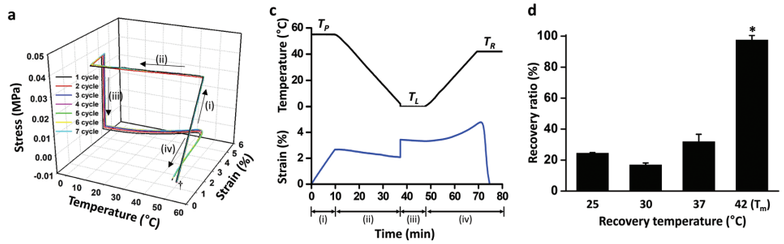

b

Cycles	1	2	3	4	5	6	7	Average
$R_f(N)$ (%‡)	94.55	95.03	95.15	95.84	95.19	95.26	95.35	**95.19 ± 0.36**
$R_r(N)$ (%)	97.53	99.65	100.5	99.95	96.36	96.03	91.39	**97.35 ± 2.94**
$R_r(1)$ (%)	97.53	97.27	97.87	97.82	94.28	98.23	89.78	**96.11 ± 2.86**

%‡=vs. original strain before subjecting to tensile stress

Figure 2. Shape memory properties of 94%PCL-6%PGMA after crosslinking. a) Stress-controlled thermomechanical cycling of 94%PCL-6%PGMA starting at 0% tensile strain and 55 °C (†), followed by seven consecutive cycles of i) deformation until a tensile stress of 39 kPa at 55 °C, ii) cooling down to 0 °C with set tensile stress, iii) decreasing tensile stress to 0 kPa, and iv) increasing temperature from 0 °C to 42 °C. b) Maintenance of shape recovery [$R_f(N)$] and shape fixity [$R_f(N)$] in the seven consecutive thermomechanical cycles. c) Time setting (x-axis) to control temperature and corresponding strain (y-axis) in the first thermomechanical cycle of 94%PCL-6%PGMA (T_P; programming temperature, T_L; cooling temperature, T_R; recovery temperature). d) Determination of 94%PCL-6%PGMA recovery temperature to 42 °C owing to the 100% recovery ratio. *$p < 0.05$.

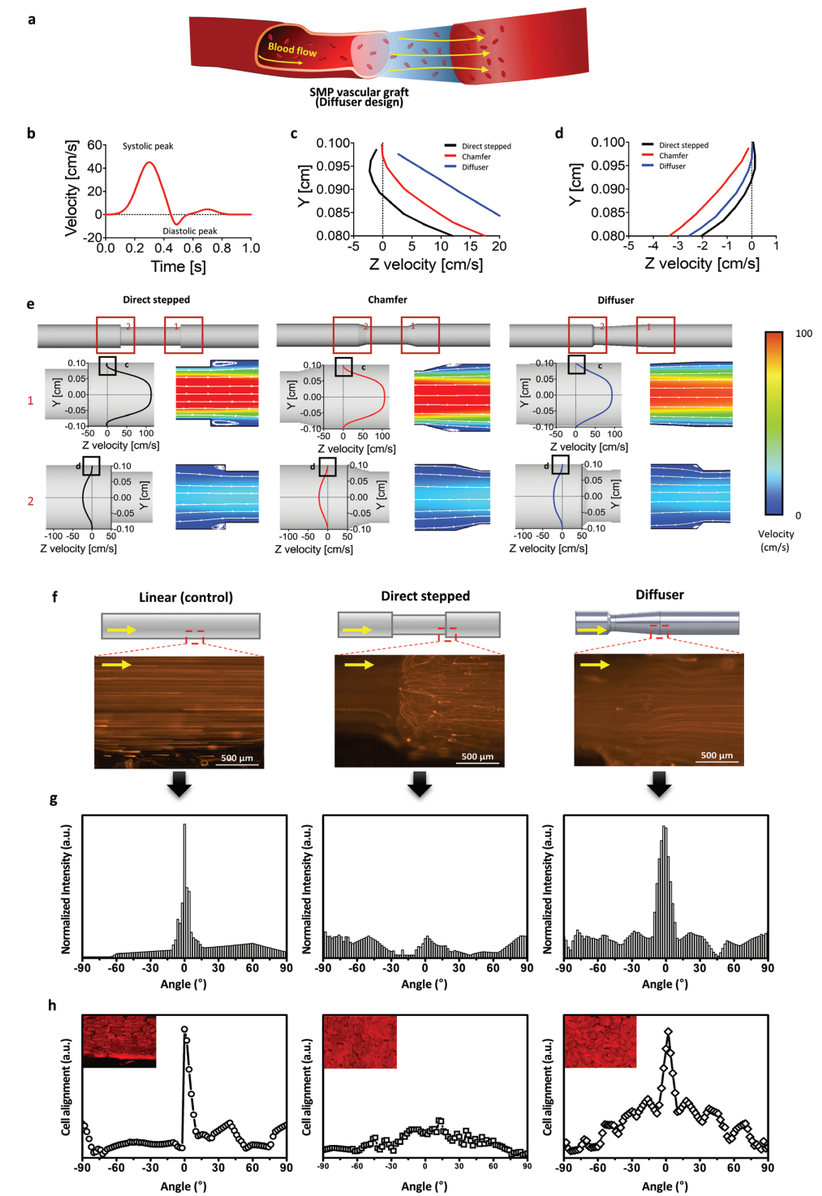

shape fixity (average R_f > 95%) and shape recovery (average R_r > 96%) during the seven consecutive thermomechanical cycles (Figure 2a,b; Figure S7, Supporting Information) represents a major breakthrough in SMP research. Six consecutive cycles without significant energy loss is the highest performance recorded till date, and even the material was a nonimplantable composite.[14] However, these results were obtained with ≈5% strain, while in the case shown in Figure S6 in the Supporting Information, the SMP sample was replaced with a new one when the strain level was increased. Therefore, the same SMP sample was used to verify that the robust shape recovery was maintained during the seven consecutive cycles under a higher strain range (14.6%–37.0%) (Figure S7, Supporting Information). The training effect implies that the initial shape recovery is different from the subsequent shape recovery, resulting in incremental R_f and R_r values from the lower values of the first cycle as the number of cycles increases, by training. This effect has been widely reported previously.[14,15] Although our first three cycles displayed an incremental pattern in the R_f and R_r values, which is likely to have been owing to the training, the robust high shape fixity and shape recovery [$R_f(1)$ = ≈95% and $R_r(1)$ > 98%] in the first cycle during the seven consecutive thermomechanical cycles (Figure 2a,b) indicates that pretraining is not necessary for our SMP. Moreover, circumventing pretraining reduces the residual stress and thereby aids in the preservation of strain energy for the subsequent cycles.[16]

The temperature-dependent changes in strain% enabled the programming of the shape memory function following a specific time frame (Figure 2c). In this manner, strain energy was stored as a form of heat in the temporary shape. At the cooling temperature (T_L), there was a 1% increase in strain% owing to the transition of the crosslinking bond status from flexible shrink to stiff freezing at 0 °C. This is similar the role of hydrogen bonding in frozen water.[17] Shape recovery started 20 min after heating to the recovery temperature (T_R) and ended within 10 min at T_R, as indicated by the decrease in strain% to zero. These procedures indicate that the shape programming of our SMPs is tightly controlled in a time-and-temperature-dependent manner. Shape recovery occurs rapidly and fully once the SMP graft is heated above the corresponding T_m. The temperature-dependent shape recovery efficiency of our SMPs was examined (Figure 2d). Shape recovery ratios were less than 30% when the temperature was below T_m but reached almost 100% at the corresponding T_m. This indicated the precision of recovery temperature setting, which minimizes unexpected SMP behavior while surgical grafting into vessels.

In our grafting strategy (**Figure 3**a), an SMP graft was inserted into amputated vessels with ≈40%–50% reduced diameter, followed by shape recovery to the host vessel diameter through rapid local heating. This minimized tissue damage during deployment. Three graft designs (i.e., direct stepped, chamfer, and diffuser) were examined to minimize disturbed flow formation (Figure 3b–h).[9] Computational fluid dynamics (CFD) modeling of the pulsatile flow in the coronary artery[18] was performed with the 1 Hz velocity profile of high systolic and low diastolic peaks (Figure 3b).[19] The analysis of the Z velocity at the systolic peak indicated that the direct stepped model clearly generated disturbed flow around the outlet position, with back flow at the step position (Figure 3c,e). In the chamfer model, the disturbed flow formation was attenuated to a certain degree. However, back flow stagnation persisted around the outlet vessel wall. In contrast, the diffuser model did not generate disturbed flow. A similar velocity analysis at the diastolic peak revealed clear formation of disturbed flow at the inlet vessel wall of the direct stepped model (Figure 3d), while this disturbed flow formation was not observed in the chamfer model. Interestingly, attenuated disturbed flow with stagnation appeared in the inlet vessel wall of the diffuser model. However, this flow pattern in the inlet vessel is absent in the coronary artery in vivo.[20] The aforementioned velocity and flow profiles are visualized with heatmap colors (Figure 3e; Video S4, Supporting Information). These results affirmed the selection of the diffuser model for minimizing the formation of disturbed flow while deploying the vascular graft.

To validate the CFD results, three types (linear, direct stepped, and diffuser) of microfluidic devices were fabricated through 3D printing,[21] followed by an analysis of the fluorescent particle flow[22] and endothelial cell (EC) alignment.[23] The fluorescent particle tracking of the flow profile verified the minimal formation of disturbed flow within the diffuser model (Figure 3; Video S5, Supporting Information). This result was supported by fast Fourier transform analysis;[24] the directions of particle movement and human umbilical vein endothelial cell (HUVEC) alignment were the most parallel with the flow direction (angle = 0°) in the diffuser model (Figure 3g,h). This validated the promising potential of the diffuser model for minimizing stenosis.[25]

Finally, the performance of the diffuser model was examined in a porcine model. The vascular compatible surface of a construct was coated with nitric oxide (NO)-releasing peptides to prevent thrombosis, as demonstrated in our previous studies (Figure S8, Supporting Information).[26] These constructs were sterilized safely (Figure S9, Supporting Information) and then grafted into both the cut ends (i.e., flow inlet and outlet points) of the femoral artery without vessel damage (Figure S10 and Video S1, Supporting Information). Doppler ultrasound imaging revealed a minimal flow patency in the direct stepped model. Meanwhile, the maximum flow patency was

Figure 3. Computer-modeling-based design of SMP vascular graft with experimental validation. a) Schematic illustration of SMP vascular graft with a diffuser design to minimize disturbed flow formation. b–d) Computational fluid dynamics (CFD) simulation of three designs (i.e., direct stepped, chamfer, and diffuser) of SMP vascular grafts. b) Pulsatile input flow: pulse from aorta is scaled down for blood flow in coronary artery. c) Comparison of velocity profile close to the vascular wall among the three graft designs at systolic and d) diastolic peaks. e) Comparison of velocity profile and contour among the three graft designs through CFD (systolic and diastolic peaks: red boxes 1 and 2, respectively). f) Linear design (control)-like minimization of disturbed flow formation in diffuser design was visualized in comparison with direct stepped design when the three designs were generated in polydimethylsiloxane (PDMS) bioreactors through the flow of red fluorescent microbeads (yellow arrow: flow direction), followed by g) quantitative profiling of deviation in the flow direction. h) Visualization of the consequent HUVEC alignment, followed by quantitative profiling of deviation in the cell alignment direction.

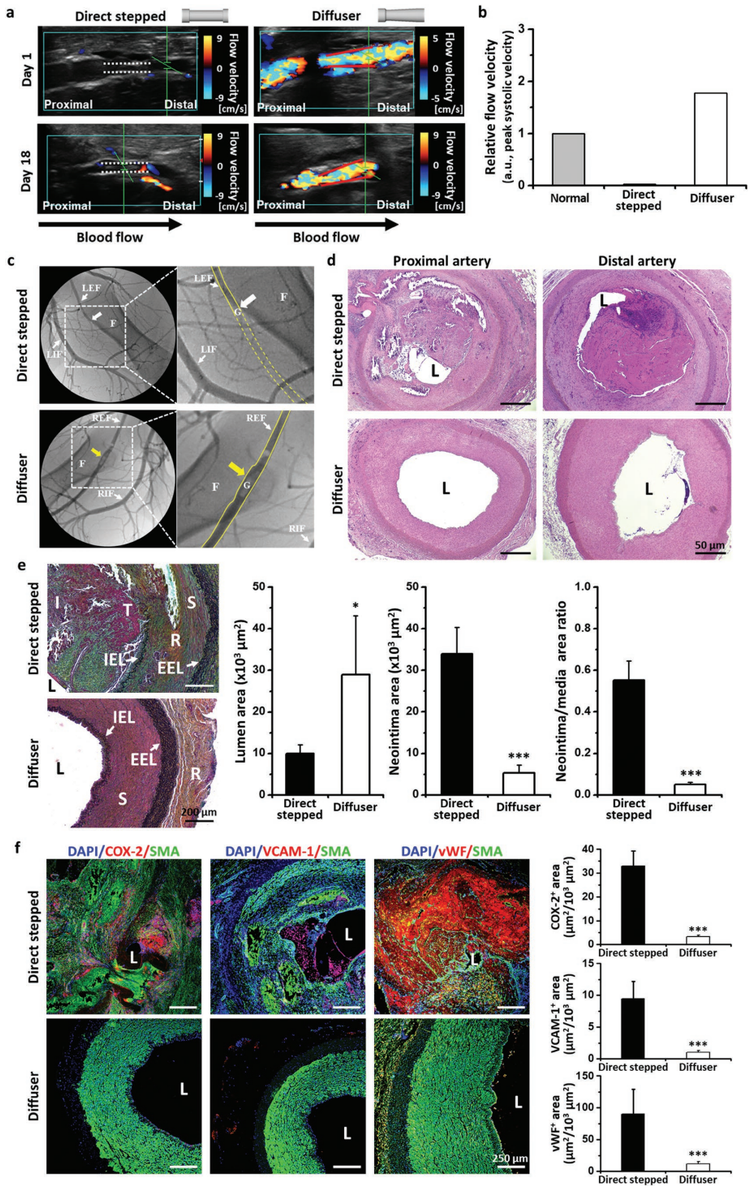

maintained in the diffuser model from day 1 to 18 after deployment (**Figure 4**a; Video S6, Supporting Information). This was supported by the higher flow velocity compared to those of the normal femoral artery and direct stepped model (Figure 4b). An angiography assessment affirmed these 18 d results by clearly visualizing normal-like pulsing blood flow in the diffuser graft. In contrast, there was almost no flow patency in the direct stepped group (Figure 4c; Figure S11 and Video S7, Supporting Information). This result was most likely a result of the occlusive formation of a stenotic lesion through a combination of thrombosis and inflammatory responses in the proximal (inlet) and distal (outlet) points of the host femoral artery (Figure 4d,e). These pathological responses were further evidenced in the direct stepped graft (in contrast to the normal-like histological features of the diffuser graft) by the marker expressions of inflammatory response [cyclooxygenase-2 (COX-2) and vascular cell adhesion protein-1 (VCAM-1)], EC thrombosis [von Willebrand factor (vWF)], and the location of smooth muscle cells [smooth muscle actin (SMA)] (Figure 4f).

Here, highly tunable SMP properties were generated by controlling the i) molar ratio during synthesis, ii) polymer concentration during construct casting, and iii) crosslinking time during graft fabrication. As a result, highly promising vascular grafting performance was demonstrated. This SMP underwent seven consecutive thermomechanical cycles with the shape fixity and recovery being maintained. It represents a breakthrough in the field of SMP research. The coating, design, and shape memory function of the present construct demonstrated significant potential for addressing long-standing vascular graft design issues. As another key benefit of the SMP property for vascular tube grafting, the inherited elastic nature of an SMP tube minimizes hindering cyclic contraction of arteries when inserted in vivo. Without this function, arterial contraction can be altered to result in pathological vascular remodeling, as generally observed in vein-to-artery grafting.

During the 18 d of the SMP construct having been grafted to a porcine femoral artery, the surface coating with the NO-releasing peptides prevented thrombosis with normal-like graft patency. More importantly, the computer-modeling-based diffuser design minimized the formation of disturbed flow. The SMP function enabled tissue-damage-free and operator-friendly grafting through shape programming.

An early SMP for biomaterial application, poly(ε-caprolactone)-dimethacrylate (PCL-DMA) was introduced in 2006–2007.[27] Although this SMP type provided a key foundation for significant progress during the past decade, the high shape transition temperature (T_s; ≈60 °C, which is beyond the point of protein denaturation) has been a significant obstacle to its application in the human body.[5,27] As a part of the accumulated efforts to reduce T_s to the body temperature through new polymer designs,[5,28] we have been developing a T_s-tunable SMP library through copolymerization of PCL and α-allyl carboxylate ε-caprolactone (ACPCL) since 2008. However, its long and laborious polymerization steps, the low yield (≈58%), and the number of repeatable shape memory cycles being limited to two have been significant challenges.[5] Since then, we have made significant progress in the development of the present class of SMP library by copolymerizing GMA into the backbone of PCL. This has resulted in i) a wide range of tuning T_s and material properties and ii) the robust preservation of strain energy during seven consecutive thermomechanical cycles.

To our knowledge, this is the first report on a successful vascular grafting into a host vessel of diameter smaller than 3 mm achieved through a combination of CFD modeling, microfluidic validation with human EC culture, and surface coating with NO-releasing peptides. It represents unprecedented potential to address the long-standing issues of present vascular graft products.

In the future, long-term and y-shape grafting performances will be investigated in the porcine model. The period in this study was limited to 18 d because the initial foundation of the essential stenotic events occurs within 3 weeks.[10] Thus, the prevention of these events indicates a promising long-term outcome. This study adds value to the present progress in the development of vascular constructs by demonstrating the successful performance of a small vascular graft with a diameter of ≈2 mm and thereby validating the urgent need to undertake clinical translation.

Supporting Information

Supporting Information is available from the Wiley Online Library or from the author.

Acknowledgements

Y.C.S. and J.B.L. contributed equally to this work. This study was financially supported by the National Research Foundation of Korea (NRF) (No. 2016M3A9E9941743).

Conflict of Interest

The authors declare no conflict of interest.

Figure 4. Porcine model of vascular patency after grafting SMP tube into femoral artery for 18 d. a) Doppler ultrasound imaging assessment of graft patency (white dashed line: direct stepped; red solid line: diffuser) with live monitoring of pulsation synchronization in the video (Supporting Information). b) Blood flow velocity inside SMP vascular grafts at day 18 after implantation with normalization based on the velocity inside the normal femoral artery without grafting. c) Angiography assessment of graft patency at day 18 after SMP tube grafting. The grafted femoral artery (left) is magnified (right), with the high and poor blood flow regions indicated by yellow solid and dashed lines, respectively, and the graft locations indicated by white (direct stepped) and yellow (diffuser) arrows (F-femur; G-graft location; LEF-left external femoral artery; LIF-left internal femoral artery; REF-right external femoral artery; RIF-right internal femoral artery). d,e) Cross-section of haematoxylin and eosin (H&E) d) and Movat staining images e) of harvested femoral arteries at day 18 after grafting of SMP test tubes, followed by quantitative analysis of patency structural factors (EEL-external elastic laminar; I-inflammation; T-thrombosis; IEL-internal elastic lamina; L-lumen; R-reticular fiber; S-smooth muscle). f) Immunostaining images and quantitative analysis of marker protein expression: inflammatory response [cyclooxygenase-2 (COX-2), vascular cell adhesion protein-1 (VCAM-1)], EC thrombosis [von Willebrand factor (vWF)], and smooth muscle cell [smooth muscle actin (SMA)]. *$p < 0.05$ and ***$p < 0.001$.

ADVANCED SCIENCE NEWS
www.advancedsciencenews.com
ADVANCED MATERIALS
www.advmat.de

Keywords

computational fluid dynamics, nitric oxide-releasing peptide, shape memory polymer, vascular graft, vascular remodeling

Received: July 12, 2019
Revised: August 9, 2019
Published online: August 27, 2019

[1] a) W. Wu, R. A. Allen, Y. Wang, *Nat. Med.* **2012**, *18*, 1148; b) K. Daenens, S. Schepers, I. Fourneau, S. Houthoofd, A. Nevelsteen, *J. Vasc. Surg.* **2009**, *49*, 1210.
[2] M. Gessaroli, C. Bombardi, M. Giunti, M. L. Bacci, *J. Vasc. Surg.* **2012**, *55*, 192.
[3] G. Becker, F. R. Wurm, *Chem. Soc. Rev.* **2018**, *47*, 7739.
[4] a) J. Kohn, *Nat. Mater.* **2004**, *3*, 745; b) Y. Yang, D. Bolikal, M. L. Becker, J. Kohn, D. N. Zeiger, C. G. Simon Jr., *Adv. Mater.* **2008**, *20*, 2037.
[5] T. C. Boire, M. K. Gupta, A. L. Zachman, S. H. Lee, D. A. Balikov, K. Kim, L. M. Bellan, H.-J. Sung, *Acta Biomater.* **2016**, *34*, 73.
[6] A. Lotierzo, B. W. Longbottom, W. H. Lee, S. A. F. Bon, *ACS Nano* **2019**, *13*, 399.
[7] S. Laurent, *Hypertension* **1995**, *26*, 355.
[8] F. Hansen, D. Bergqvist, P. Mangell, Å. Rydén, B. Sonesson, T. Länne, *Clin. Physiol.* **1993**, *13*, 631.
[9] H.-J. Sung, J. Su, J. D. Berglund, B. V. Russ, J. C. Meredith, Z. S. Galis, *Biomaterials* **2005**, *26*, 4557.
[10] a) R. M. Zwolak, M. C. Adams, A. W. Clowes, *J. Vasc. Surg.* **1987**, *5*, 126; b) M. Handa, W. Li, K. Morioka, A. Takamori, N. Yamada, A. Ihaya, *J. Vasc. Surg.* **2008**, *48*, 1566.
[11] M. Behl, M. Y. Razzaq, A. Lendlein, *Adv. Mater.* **2010**, *22*, 3388.
[12] A. Lendlein, O. E. C. Gould, *Nat. Rev. Mater.* **2019**, *4*, 116.
[13] a) Y. Zhang, Y. Li, W. Liu, *Adv. Funct. Mater.* **2015**, *25*, 471; b) J. Fan, G. Li, *Nat. Commun.* **2018**, *9*, 642.
[14] E. Wang, Y. Dong, M. D. Z. Islam, L. Yu, F. Liu, S. Chen, X. Qi, Y. Zhu, Y. Fu, Z. Xu, *Compos. Sci. Technol.* **2019**, *169*, 209.
[15] a) H. Tobushi, T. Hashimoto, N. Ito, S. Hayashi, E. Yamada, *J. Intell. Mater. Syst. Struct.* **1998**, *9*, 127; b) T. Ohki, Q.-Q. Ni, N. Ohsako, M. Iwamoto, *Composites, Part A* **2004**, *35*, 1065; c) Y. Dong, Q.-Q. Ni, Y. Fu, *Composites, Part A* **2015**, *72*, 1.
[16] J. Guo, Z. Wang, L. Tong, H. Lv, W. Liang, *Composites, Part A* **2015**, *76*, 162.
[17] S. Pothoczki, L. Pusztai, I. Bakó, *J. Phys. Chem. B* **2018**, *122*, 6790.
[18] a) R. Mazzitelli, F. Boyle, E. Murphy, A. Renzulli, G. Fragomeni, *Biocybern. Biomed. Eng.* **2016**, *36*, 327; b) A. Brandts, S. D. Roes, J. Doornbos, R. G. Weiss, A. De Roos, M. Stuber, J. J. M. Westenberg, *J. Magn. Reson. Imaging* **2010**, *31*, 1215.
[19] B. Kurşun, L. Uğur, G. Keskin, *Comput. Methods Programs Biomed.* **2018**, *158*, 31.
[20] K. Honda, Y. Okamura, Y. Nishimura, S. Uchita, M. Yuzaki, M. Kaneko, N. Yamamoto, T. Kubo, T. Akasaka, *J. Thorac. Cardiovasc. Surg.* **2015**, *149*, 1622.
[21] a) A. Enders, I. G. Siller, K. Urmann, M. R. Hoffmann, J. Bahnemann, *Small* **2019**, *15*, 1804326; b) F. Li, N. P. Macdonald, R. M. Guijt, M. C. Breadmore, *Anal. Chem.* **2019**, *91*, 1758.
[22] E. J. Carboni, B. H. Bognet, G. M. Bouchillon, A. L. Kadilak, L. M. Shor, M. D. Ward, A. W. K. Ma, *Biophys. J.* **2016**, *111*, 1487.
[23] A.-C. Vion, M. Kheloufi, A. Hammoutene, J. Poisson, J. Lasselin, C. Devue, I. Pic, N. Dupont, J. Busse, K. Stark, *Proc. Natl. Acad. Sci. USA* **2017**, *114*, E8675.
[24] V. Radotić, D. Braeken, D. Kovačić, *Eur. Biophys. J.* **2017**, *46*, 719.
[25] a) N. T. Jenkins, J. Padilla, L. J. Boyle, D. P. Credeur, M. H. Laughlin, P. J. Fadel, *Hypertension* **2013**, *61*, 615; b) L. Wang, J.-Y. Luo, B. Li, X. Y. Tian, L.-J. Chen, Y. Huang, J. Liu, D. Deng, C. W. Lau, S. Wan, *Nature* **2016**, *540*, 579.
[26] a) M. Kushwaha, J. M. Anderson, C. A. Bosworth, A. Andukuri, W. P. Minor, J. R. Lancaster Jr., P. G. Anderson, B. C. Brott, H.-W. Jun, *Biomaterials* **2010**, *31*, 1502; b) S.-J. Lee, Y.-D. Sohn, A. Andukuri, S. Kim, J. Byun, J. W. Han, I.-H. Park, H.-W. Jun, Y.-S. Yoon, *Circulation* **2017**, *136*, 1939; c) S. E. Paramonov, H.-W. Jun, J. D. Hartgerink, *J. Am. Chem. Soc.* **2006**, *128*, 7291.
[27] a) I. Bellin, S. Kelch, R. Langer, A. Lendlein, *Proc. Natl. Acad. Sci. USA* **2006**, *103*, 18043; b) I. Bellin, S. Kelch, A. Lendlein, *J. Mater. Chem.* **2007**, *17*, 2885.
[28] a) Y. Liu, Y. Li, G. Yang, X. Zheng, S. Zhou, *ACS Appl. Mater. Interfaces* **2015**, *7*, 4118; b) K. Hearon, M. A. Wierzbicki, L. D. Nash, T. L. Landsman, C. Laramy, A. T. Lonnecker, M. C. Gibbons, S. Ur, K. O. Cardinal, T. S. Wilson, *Adv. Healthcare Mater.* **2015**, *4*, 1386; c) B. Q. Y. Chan, Z. W. K. Low, S. J. W. Heng, S. Y. Chan, C. Owh, X. J. Loh, *ACS Appl. Mater. Interfaces* **2016**, *8*, 10070.

PFIZER
MEDICAL
RESEARCH
AWARD
since 2000

대한민국의학한림원
제19회 화이자의학상

임상의학 부문

박중원 교수

국립암센터 간담도췌장암센터

대한민국의학한림원 제19회 화이자의학상

임상의학 부문 수상자

박중원 교수

국립암센터
간담도
췌장암센터

학력

1977. 03 - 1984. 02	서울대학교 의과대학 (의학학사)
1990. 03 - 1992. 02	한양대학교 의과대학 (의학석사, 생리학)
1994. 03 - 1996. 02	서울대학교 의과대학 (의학박사, 내과학, 지도교수 김정룡)

경력

1985. 03 - 1989. 02	서울대학교병원 인턴 및 레지던트 (전공의 (내과))
1992. 05 - 1993. 02	서울대학교병원 내과학교실 (소화기내과 전임의)
1993. 03 - 2002. 02	중앙대학교 의과대학 내과학교실 (전임강사, 조교수, 부교수)
1997. 03 - 1999. 02	미국 Mayo Clinic 소화기병연구소 (전임연구원 (visiting scientist))
2002. 03 - 현재	국립암센터 (책임연구원, 최고연구원)
2002. 09 - 2011. 08	국립암센터 (간암센터장 및 연구소 과장, 부장)
2014. 03 - 현재	국립암센터 국제암대학원 (교수 (암관리학과))
2021. 05 - 현재	국립암센터 항암신약신치료개발사업단 (단장)
2017. 06 - 2018. 06	대한간암학회 (회장)
2016. 09 - 2020. 09	국제간암학회 (ILCA) (이사 (Governing Board))
2016. 07 - 현재	아태간암전문가학회 (APPLE) (학술위원장)
2021. 02 - 현재	대한민국의학한림원 (정회원)

수상

1995.	대한내과학회 최우수 학술상
1996.	아시아태평양 소화기학회 젊은 연구자상
1997.	대한소화기학회 최우수 논문상
2005.	대한간학회 최우수 논문상
2006.	대한간학회 간산학술상
2007.	국립암센터 연구상
2008.	대한간학회-GSK 학술상 수상
2008.	서울의대 함춘의학상 (연구업적부분)
2009.	국립암센터 연구상
2011.	암의날 보건복지부장관 표창
2014.	국립암센터 연구상
2015.	국립암센터 연구상
2016.	대한암학회 로슈 암학술상
2018.	국립암센터 연구상
2019.	대한간암학회 학술논문상
2020.	국립암센터 연구상
2020.	임상시험 국가유공자 보건복지부장관 표창

논문 요약 및 연구의 의의

간세포암종 (hepatocellular carcinoma, HCC) 중 3cm 이하 크기의 초기암은 완치를 위해서 우선적으로 절제술 치료 또는 고주파열치료(Radiofrequecy Ablation; RFA)이 권장된다. 고주파열치료는 간암을 고주파로 태워서 치료하는 국소치료법이다. 국립암센터에서 우리나라 최초로 시작한 양성자치료(Proton Beam Radiotherapy; PBT)는 전립선암, 안구암 등에서는 3상 대조군 연구를 통해 국제적으로 표준치료로 인정되어 사용되고 있으나, HCC의 경우 일본, 유럽, 미국 등을 포함하여 전세계적으로 HCC 환자들에게 적용되고 있었지만, 절제술이나 RFA와 같은 완치적 표준치료와 효과-부작용 등을 비교하는 무작위 대조군 3상 임상연구가 없어서 근거중심의학 기반의 표준치료로서 인정받지 못한 치료법이었다. 그러므로 3상 대조군 연구를 통해 HCC에서 양성자치료 효과를 입증할 필요가 있었다.

연구팀은 3cm 이하, 2개 이하로 재발된 HCC 환자 144명을 간기능등급과 병기에 따라 각각 양성자치료군 72명과 고주파열치료군 72명으로 무작위 배정했다. 배정 이후 배정된 치료가 기술적으로 불가능한 경우 상호교차 치료를 허용하였고 이에따라 실제 치료는 80명이 양성자치료를, 56명이 고주파열치료를 받았다.

그 결과, 2년 국소무진행생존율(local progression fress survival; LPFS)은 양성자치료군 94.8%, 고주파열치료군은 83.9%로 나타났다. 3년 및 4년 국소무진행생존율도 큰 차이가 없었다. 가장 흔한 부작용은 양성자치료군에서는 중증도 이하 방사선 폐렴(32.5%), 백혈구수감소(23.8%)가, 고주파열치료군에서는 알라닌아미노트랜스퍼라제 수치 증가(96.4%) 복통(30.4%)로서, 두 치료군 모두 심각한 부작용이나 사망 없이 안전한 치료임을 확인했다.

본 연구는 여러 가지 제한으로 인해 남들이 하지 못했던 전향적 대조군 3상 연구를 재발 환자 대상으로 비열등성 방법, 교차치료법 적용 등으로써 제한점을 극복한 연구로서 양성자치료가 재발 간세포암종을 완치시킬 수 있음을 최종적으로 입증하였다. 양성자치료는 기존 표준치료인 고주파열치료의 약점 (종양 위치에 따른 접근성, 주변 혈관 인접에 따른 효과 등)을 상호보완할 수 있는 새로운 치료법으로서 더욱 많은 간세포암종 환자들에게 도움을 줄 수 있을 것이다.

이 연구는 간분야의 최고 학술지인 Journal of Hepatology 3월호 '표지논문'으로 게재되었다.

수상 소감

언제나 그렇듯이 상을 받는다는 건 누구로부터 인정을 받았다는, 기분 좋고 뿌듯한 일입니다. 그 상이 화이자의학상과 같이 대한민국의학한림원이 대한민국 의학발전 및 인류건강복지에 기여한 의학자에게 수여하는 상일 때는 수상자가 받는 기쁨과 자부심은 너무나 큽니다. 본 상을 심사해 주신 여러 선생님들과 관계자분들께 깊은 감사를 드립니다.

오늘 이 상을 받을 수 있게 해준 임상연구에 저를 믿고 기꺼이 참여해주신 환자분들과 가족분들, 헌신적으로 연구를 수행해주신 공동연구자 김태현선생님, 고영환선생님 외 여러 선생님들, 연구간호사들과, 또한 너무나 까다로운 통계분석을 도와주신 박보람선생님께 다시금 감사드립니다.

제게 간장학 연구의 실체적 방향과 목적을 가르쳐 주신, 이제는 고인이 되신 은사 김정룡교수님께 감사드립니다. 임상연구 의사는 어떠한 경우에라도 환자의 안전과 이익을 환자편에서 생각하고 연구를 수행해야 함을 깨닫게 해준 많은 연구참여 환자분들께 깊이 감사드립니다.

1965년 광화문 수송초등학교 1학년 첫 짝으로 만나서 지금까지 56년동안 제 곁을 지켜준 아내 나혜경과 진료와 연구를 한답시고 모자라게 군 아버지를 이해하려 노력해준 두 아들, 상우, 상연에게 고마움을 전합니다.

감사합니다.

Research Article
Hepatic and Biliary Cancer

JOURNAL
OF HEPATOLOGY

Proton beam radiotherapy *vs.* radiofrequency ablation for recurrent hepatocellular carcinoma: A randomized phase III trial

Tae Hyun Kim[1,2,†], Young Hwan Koh[1,3,†], Bo Hyun Kim[1], Min Ju Kim[3], Ju Hee Lee[1,3], Boram Park[4], Joong-Won Park[1,*]

[1]Center for Liver and Pancreatobiliary Cancer, National Cancer Center, Goyang, Republic of Korea; [2]Center for Proton Therapy, National Cancer Center, Goyang, Republic of Korea; [3]Department of Radiology, National Cancer Center, Goyang, Republic of Korea; [4]Biostatistics Collaboration Team, Research Core Center, National Cancer Center, Goyang, Republic of Korea

Background & Aims: Proton beam radiotherapy (PBT) has recently been applied to treat hepatocellular carcinoma (HCC); however, there is no randomized controlled trial-based evidence on its safety and efficacy. We compared the outcomes of PBT and radiofrequency ablation (RFA) in patients with recurrent/residual HCC (rHCC) in a phase III non-inferiority trial.

Methods: Patients with rHCC (size <3 cm, number ≤2) were randomly assigned to receive PBT or RFA according to Child-Pugh score and tumor stage. After randomization, if the assigned treatment was technically infeasible, crossover was allowed. The primary endpoint was 2-year local progression-free survival (LPFS), with a non-inferiority margin of 15% in the per-protocol (PP) population; a complementary analysis was performed in the intention-to-treat (ITT) population (NCT01963429).

Results: The ITT population comprised 144 patients receiving either PBT (n = 72) or RFA (n = 72). Six patients switched from the PBT arm to the RFA arm and 19 patients switched from the RFA arm to the PBT arm. In the PP population, the 2-year LPFS rate with PBT (n = 80) *vs.* RFA (n = 56) was 94.8% *vs.* 83.9%, a difference of 10.9 percentage points (90% CI 1.8–20.0; p <0.001); in the ITT population, the 2-year LPFS rate with PBT *vs.* RFA was 92.8% *vs.* 83.2%, a difference of 9.6 percentage points (90% CI 0.7–18.4; p <0.001), meeting the criteria for non-inferiority. The 3- and 4-year LPFS rates for PBT were also non-inferior to those for RFA. The most common adverse events were radiation pneumonitis (32.5%) and decreased leukocyte counts (23.8%) for PBT and increased alanine aminotransferase levels (96.4%) and abdominal pain (30.4%) for RFA. No Grade 4 adverse events or mortality were noted.

Conclusions: PBT showed LPFS values that were non-inferior to those for RFA; in addition, PBT was tolerable and safe.

Clinical trial number: #NCT01963429 (ClinicalTrials.gov).

Lay summary: Radiofrequency ablation is the standard of care for patients with small hepatocellular carcinoma in whom surgery is not feasible. This study is the first phase III randomized controlled trial to evaluate the clinical outcomes of proton beam radiotherapy *vs.* radiofrequency ablation in patients with recurrent small HCC. Our findings show that this new technique is not inferior and can be applied safely in patients with small recurrent hepatocellular carcinoma.

Keywords: Hepatocellular carcinoma; Radiofrequency ablation: proton beam therapy; local progression-free survival; Randomised controlled trial.
Received 21 April 2020; received in revised form 23 September 2020; accepted 23 September 2020; available online 5 October 2020

* Corresponding author. Address: Center for Liver and Pancreatobiliary Cancer, Research Institute and Hospital, National Cancer Center, 323 Ilsan-ro, Ilsandong-gu, Goyang-si, Gyeonggi-do, 10408, South Korea. Tel.: +82-31-920-1605; fax: +82-31-920-0149.
E-mail address: jwpark@ncc.re.kr (J.-W. Park).
† T.H.K. and Y.H. K. contributed equally to this study.

https://doi.org/10.1016/j.jhep.2020.09.026

Introduction

Primary liver cancer, including hepatocellular carcinoma (HCC), is the fifth most commonly observed cancer worldwide. HCC-related prognoses remain poor owing to the presence of underlying chronic liver disease, late diagnosis, and frequent recurrence or progression after treatment.[1,2] The initial treatment modality for HCC is generally based on tumor stage, underlying liver function, and performance.[3–5] Surgical resection is considered the best treatment for HCC, but for small HCC cases, in which resection is not feasible, radiofrequency ablation (RFA) is recommended; RFA is also the primary recommendation for tumors smaller than 2 cm.[3,4] The recurrence rate of HCC after resection or RFA is significant. In the case of local recurrence, despite the lack of sufficient evidence, the treatment method is generally selected according to the first-line treatment principle.[3,4]

Proton beam radiotherapy (PBT) is a type of radiation therapy that has been proven to be effective as a primary treatment for ocular tumor and prostatic cancer.[6,7] PBT has recently been applied to HCC treatment, and its safety and local control effects have been reported in various studies.[8–10] A previous phase II study in HCC patients demonstrated the safety and promising outcomes associated with PBT.[8,10–12] However, as there is no strong randomized controlled trial (RCT)-based evidence on PBT, it is not generally recommended for HCC treatment. Therefore, we conducted an RCT to evaluate and compare the local efficacy and clinical outcomes of PBT and RFA in patients with recurrent or residual HCC (rHCC).

Patients and methods

Study population

This phase III investigator-initiated, randomized, single-center, open-label clinical trial was performed at the National Cancer Center (NCC), Goyang, Republic of Korea. The eligibility criteria

for this study were as follows: HCC diagnosis was confirmed either histologically or clinically according to the Korean Liver Cancer Study Group and NCC Korea guidelines[13,14]; presence of recurrent or residual HCC lesions without vascular invasion after other treatment; the largest diameter and number of target lesion(s) were <3 cm and ≤2, respectively; no history of prior radiotherapy to targeted lesion(s); no evidence of extrahepatic metastasis; Child-Pugh score ≤7 without uncontrolled ascites; Eastern Cooperative Oncology Group performance status ≤2; age ≥18 years; adequate bone marrow (white blood cell count ≥2,000/μl, platelet count ≥50,000/μl, and hemoglobin level ≥7.5 g/dl) and liver function (total bilirubin level ≤3.0 mg/dl, and aspartate aminotransferase and alanine aminotransferase level <5.0× the upper limit of normal). All patients were unresectable or unwilling to undergo resection. All patients provided written informed consent before enrollment (supplementary information; study protocol). This study was approved by the NCC institutional review board and complied with the Declaration of Helsinki and Good Clinical Practice guideline.

Study design and treatment

Eligible patients were randomly assigned (1:1) to the PBT arm or RFA arm with stratification according to the Child-Pugh classification (A *vs.* B7) and tumor stage (American Joint Committee on Cancer [AJCC] 7th edition stage I–II *vs.* III). After randomization to each treatment arm, if the assigned method was not technically feasible, the patients were allowed to be treated with the other method. Patients and all investigators were unmasked to the treatment assignment (supplementary information; study protocol).

RFA was performed percutaneously using a monopolar water-cooling electrode system (Covidien-Medtronic, Minneapolis, MN, USA; and STARmed, Goyang, Korea) under ultrasound or CT guidance. The number of electrodes for single or multiple electrodes and overlapping RFA procedures were determined by the tumor size. RFA was performed under local anesthesia with intravenous analgesia or monitored anesthesia care. During RFA procedures, the output power was initially set at 50W and gradually increased from 90W to 200W, where it was maintained until the impedance reached a maximum value. Cold saline was infused into the electrode lumen using the pump to keep the tip temperature below 20°C. RFA procedures were continued until the entire tumor and border area sizes greater than 5 mm were included in the detected target lesion(s) on ultrasound or CT. Immediately after RFA, contrast-enhanced dynamic liver CT was conducted, and the results were carefully reviewed by the radiologist for the assessment of the technical success and procedure-related complications. If the level of ablation was considered insufficient, additional RFA was repeated during the same hospital stay.

PBT was performed using 230 MeV passively scattered proton beams (Proteus 235; Ion Beam Applications, S.A., Louvain-la-Neuve, Belgium). A contrast-enhanced four-dimensional CT scan was obtained in each patient. The internal target volume (ITV) was calculated as the sum of the gross tumor volumes in each CT image during the gated (exhalation) phases (30% of the total respiratory cycle). The planning target volumes (PTVs) were defined as the ITVs plus 5–7 mm margins in all directions. The prescribed dose to the PTV was 66 Gray equivalent (GyE) in 10 fractions, 5 fractions per week.[15,16] All patients was asked to fast for at least 4 hours before PBT at each treatment, and radiation was delivered under gated phases with a respiratory-gated technique.

Planned clinical, laboratory, and tumor assessment via contrast-enhanced multiphasic CT or MRI was performed within 2 weeks before each treatment, at the first month after the completion of RFA or PBT, every 3 months for the following 2 years, and every 6 months thereafter. Clinical and laboratory tests were performed before discharge after RFA treatment and during PBT treatment every week.

Outcomes and assessments

The primary endpoint was 2-year local progression-free survival (LPFS), defined as the time from the commencement date of each intervention to the date of local progression, and it was censored at the date of the last follow-up when the patients had no evidence of local progression. The secondary endpoints were progression-free survival (PFS), defined as time from the commencement date of each treatment to the date of local, intrahepatic or distant progression or death from any cause; overall survival (OS), defined as time from the commencement date of each treatment to date of death from any cause; and safety, defined as the presentation of adverse events (AEs) related to the treatments that were assessed according to the Common Terminology Criteria for Adverse Events version 3.0. Tumor assessment including size and response, and the evaluation of disease progression were conducted by 2 radiologists (Y-HK and JHL), and reviewed by an independent radiologist (MJK) according to RECIST version 1.1.[17]

Local progression was defined as the presence of regrowth or new tumor growth within 1 cm from the margin of the ablative zone in RFA or 1 cm from the margin of the PTV in PBT, respectively. Intrahepatic progression was defined as the regrowth of a previously treated non-target tumor or new tumor growth within the liver, except for local progression.

Statistical analysis

Efficacy was assessed in all the randomized patients (intention-to-treat [ITT] population) and patients treated per the protocol (per-protocol [PP] population), and safety was assessed in the PP population. Since this RCT had a non-inferiority crossover design, the analysis of the PP population was given priority, and the ITT analysis was performed complementarily.[18] Previous studies reported 2-year LPFS rates of 62.5–96.8% for RFA[19–25] and 54.6–96.0% for PBT[8,10–12,15] in treatment-naïve or rHCC (Tables S1 and S2). Because there was no LPFS data for RFA *vs.* placebo, this study was designed with reference to a previous RCT of RFA *vs.* percutaneous ethanol injection (PEI) in patients with HCCs <3 cm[23]; the difference of 2-year LRFS rate between RFA *vs.* PEI was 20%. We assumed that PBT could be more effective than PEI; the non-inferiority margin was calculated as 15%. A total of 144 patients (72 patients per arm) were required for the achievement of a power of 80%, a type I error level of 5%, and a follow-up loss rate of 5%. The primary endpoint, 2-year LPFS, was tested for non-inferiority with a margin of 15% – preferentially in the PP population and complementarily in ITT population – and its critical value was evaluated using the Com-Nougue approach[26] calculating the Z-statistic with standard error estimated by Greenwood's formula.

Differences in the incidence of AEs between the arms were evaluated using the χ^2 test and Fisher's exact test. Survival outcomes and hazard ratios (HRs) were estimated using the Kaplan-Meier method and a Cox proportional hazard model, respectively. A p value <0.05 was considered statistically significant, and all statistical tests were performed using SAS software (version 9.4; SAS Institute Inc., Cary, NC, USA) and R software (version 3.6.2; R Project for Statistical Computing).

Table 1. Patients' characteristics between the proton beam radiotherapy and radiofrequency ablation arms.

	Intention-to-treat population			Per-protocol population		
Characteristics	**PBT (n = 72)**	**RFA (n = 72)**	***p* value**	**PBT (n = 80)**	**RFA (n = 56)**	***p* value**
Sex						
Male	61 (84.7)	59 (81.9)	0.655*	69 (86.3)	45 (80.4)	0.358*
Female	11 (15.3)	13 (18.1)		11 (13.8)	11 (19.6)	
Age, years						
Median (range)	60 (46-78)	61.5 (40-82)	0.351‡	61 (40-82)	61 (44-77)	0.974‡
<60	33 (45.8)	28 (38.9)	0.399*	34 (42.5)	23 (41.1)	0.868*
≥60	39 (54.2)	44 (61.1)		46 (57.5)	33 (58.9)	
ECOG PS						
0	65 (90.3)	67 (93.1)	0.547*	73 (91.3)	51 (91.1)	1.000†
1	7 (9.7)	5 (6.9)		7 (8.8)	5 (8.9)	
Etiology						
HBV	61 (84.7)	60 (83.3)	0.820*	67 (83.8)	47 (83.9)	0.978
Others	11 (15.3)	12 (16.7)		13 (16.3)	9 (16.1)	
Child-Pugh classification						
A	70 (97.2)	70 (97.2)	1.000†	77 (96.3)	55 (98.2)	0.643†
B7	2 (2.8)	2 (2.8)		3 (3.8)	1 (1.8)	
AFP, ng/ml#	4.9 (0.7-411.8)	5.1 (1.4-963.6)	0.984‡	5.1 (0.7-411.8)	5.1 (1.5-963.6)	0.804‡
<10	49 (68.1)	49 (68.1)	1.000*	57 (71.3)	36 (64.3)	0.390*
≥10	23 (31.9)	23 (31.9)		23 (28.8)	20 (35.7)	
Tumor size, cm#	1.2 (1.0-2.5)	1.2 (1.0-2.9)	0.439‡	1.2 (1.0-2.9)	1.2 (1.0-2.2)	0.956‡
<2	63 (88.7)	65 (90.3)	0.763*	68 (86.1)	52 (92.9)	0.217*
≥2	8 (11.3)	7 (9.7)		11 (13.9)	4 (7.1)	
No. of treated lesion(s)						
1	67 (93.1)	66 (91.7)	0.754*	75 (93.8)	54 (96.4)	0.700†
2	5 (6.9)	6 (8.3)		5 (6.3)	2 (3.6)	
AJCC stage						
I	20 (27.8)	20 (27.8)	1.000†	21 (26.3)	18 (32.1)	0.476†
II	50 (69.4)	50 (69.4)		58 (72.5)	36 (64.3)	
III	2 (2.8)	2 (2.8)		1 (1.3)	2 (3.6)	
mUICC stage						
I	15 (20.8)	16 (22.2)	0.693†	16 (20.0)	14 (25.0)	0.868†
II	24 (33.3)	30 (41.7)		30 (37.5)	21 (37.5)	
III	32 (44.4)	25 (34.7)		33 (41.3)	20 (35.7)	
IVA	1 (1.4)	1 (1.4)		1 (1.3)	1 (1.8)	
BCLC stage						
0	4 (5.6)	5 (6.9)	0.908†	5 (6.3)	4 (7.1)	0.988†
A	39 (54.2)	38 (52.8)		43 (53.8)	31 (55.4)	
B	24 (33.3)	26 (36.1)		28 (35.0)	18 (32.1)	
C	5 (6.9)	3 (4.2)		4 (5.0)	3 (5.4)	
Diagnosis						
Pathologic	22 (30.6)	28 (38.9)	0.294*	23 (28.8)	22 (39.3)	0.199*
Imaging-based	50 (69.4)	44 (61.1)		57 (71.3)	34 (60.7)	
Pre-Tx to target site(s)						
No	41 (56.9)	33 (45.8)	0.182*	42 (52.5)	30 (53.6)	0.902*
Yes	31 (43.1)	39 (54.2)		38 (47.5)	26 (46.4)	
TACE	29 (40.3)	35 (48.6)		37 (46.3)	21 (37.5)	
RFA	1 (1.4)	3 (4.2)		0 (0.0)	4 (7.1)	
TACE + RFA	1 (1.4)	1 (1.4)		1 (1.3)	1 (1.8)	
Pre-Tx to non-target site(s)						
No	3 (4.2)	4 (5.6)	1.000†	4 (5.0)	3 (5.4)	1.000†
Yes	69 (95.8)	68 (94.4)		76 (95.0)	53 (94.6)	

AFP, α-fetoprotein; AJCC stage, American Joint Committee on Cancer stage; BCLC stage, Barcelona Clinic Liver Cancer stage; ECOG PS, Eastern Cooperative Oncology Group performance status; mUICC stage, modified International Union Against Cancer stage; PBT, proton beam radiotherapy; RFA, radiofrequency ablation; TACE, transarterial chemoembolization; Tx, treatment.
#Continuous variables presented as median (range).
*Pearson's Chi-square test.
†Fisher's exact test.
‡Wilcoxon rank-sum test.

Results

Patients

Of the 154 patients assessed for eligibility between December 2013 and December 2017, 144 were randomly assigned to the PBT arm (n = 72) and RFA arm (n = 72), and they comprised the ITT population (Fig. 1). The last patient completed the trial on

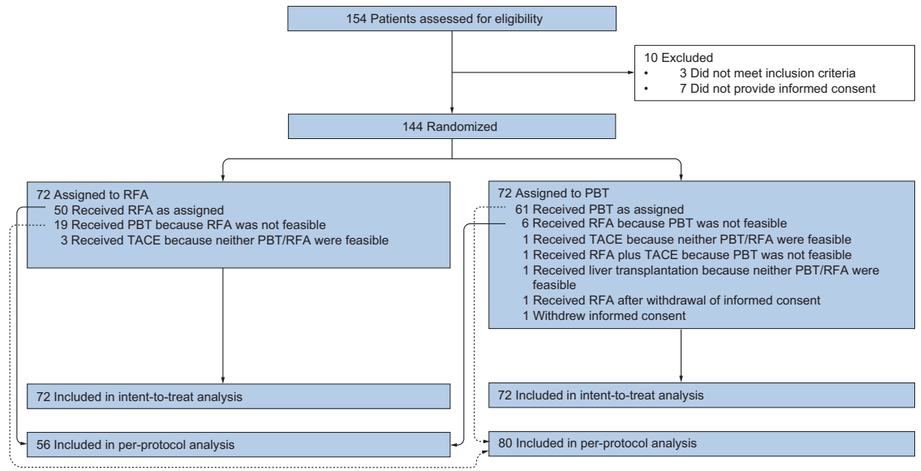

Fig. 1. CONSORT diagram. PBT, proton beam radiotherapy; RFA, radiofrequency ablation; TACE, transarterial chemoembolization.

January 2020. In the PBT arm, due to the proximity of the gastrointestinal organ to the targeted tumor(s) (n = 9) or withdrawal of informed consent (n = 2), finally 6 (8.3%) patients crossed over to the RFA arm and 5 patients received another treatment. In the RFA arm, due to the presence of a non-echogenic tumor, inadequate electrode path or the proximity of major vessels and bile ducts to the targeted tumor(s) (n = 22), 19 (26.4%) patients crossed over to the PBT arm and 3 received another treatment (Fig. 1). Thus, the PP population comprised 80 patients in the PBT arm and 56 patients in the RFA arm. The rate of crossover to the other arm due to technical infeasibility was significantly higher in the RFA arm (26.4%) than the PBT arm (8.3%) (p = 0.004). The median follow-up duration was 51.6 months (90% CI 45.6–59.5) (IQR 39.3–67.8) in the PBT arm and 50.7 months (90% CI 45.8–57.7) (IQR 41.4–67.4) in the RFA arm. Between both arms, the baseline characteristics of the ITT population were well-balanced (Tables 1 and S3).

Outcomes

In the PP population, for all patients (n = 136), the 2-year LPFS rate associated with PBT *vs.* RFA was 94.8% *vs.* 83.9% (difference of 10.9%; 90% CI 1.8–20.0), and for all target lesions (n = 143), the corresponding values were 95.1% *vs.* 84.4%, respectively. In the ITT population, for all patients, the 2-year LPFS rate associated with PBT *vs.* RFA was 92.8% *vs.* 83.2% (difference of 9.6%; 90% CI 0.7–18.4), and for all target lesions, the corresponding values were 93.3% *vs.* 83.2%, respectively; both analyses met the criteria for non-inferiority (Table 2, Fig. 2). The HRs of LPFS between the PBT and RFA arms for all target lesions and all patients were not significantly different (p >0.05 each) (Fig. 3A–D). The lower boundary of the CI of the differences (PBT minus RFA) in the 2-year LPFS did not include the non-inferiority margin of −15% (Fig. 2); thus, the non-inferiority of PBT in terms of LPFS was declared. In addition, in the PP population, for all patients, the 3- and 4-year LPFS rates were 88.3% (79.9–93.3%) and 85.8% (76.3–91.7%) in the PBT arm and 77.6% (66.4–85.5%) and 77.6% (66.4–85.5%) in the RFA arm, respectively, and the differences in the 3- and 4-year LPFS rates between the 2 arms were 10.7% (−0.8 to 22.1%) and 8.2% (−3.9 to 21.2%), respectively (Table 2, Fig. 2). The median PFS values in the PBT arm were 13.4 months (90% CI 10.32–16.76) and 13.4 months (90% CI 7.69–16.76), and those in the RFA arm were 13.6 months (90% CI 9.03–21.72) and 13.7 months (90% CI 9.86–18.89) in the PP and ITT populations, respectively. In the PP and ITT populations, the 2-year PFS rates were 28.7% and 31.9% in the PBT arm, and 37.5% and 31.9% in the RFA arm, respectively (Table 2); the HRs of the 2-year PFS rate between the PBT and RFA arms were not different (HR 1.10; 95% CI 0.76–1.59; HR 0.99; 95% CI 0.70–1.33, respectively) (Fig. 3E–F). The 3- and 4-year PFS rates were 20.9% and 15.6% in the PBT arm, and 23.1% and 13.8% in RFA arm, respectively, in the PP population (Table 2).

The median OS value was not reached in both arms and both populations. In the PP and ITT populations, the 2-year OS rates were 88.8% and 91.7% in the PBT arm, and 92.9% and 90.3% in the RFA arm, respectively (Table 2); the HRs of the OS rate between the PBT and RFA arms were not different (HR 1.19; 95% CI 0.62–2.27; HR 1.07; 95% CI 0.58–1.98, respectively) (Fig. 3G–H). The 3- and 4-year OS rates were 79.0% and 74.0%, respectively, in the PBT arm and 87.2% and 78.0%, respectively, in the RFA arm in the PP population (Table 2).

In the PP population, the best tumor responses in the PBT arm and RFA arm for all target lesions (n = 155) were complete response (CR) in 71 patients (83.5%) and 56 patients (96.6%); partial response in 6 patients (7.1%) and 1 patient (1.7%); stable disease in 8 patients (9.4%) and 1 patient (1.7%); and progressive disease in no patient, respectively (p = 0.063) (Fig. S1). Median

Table 2. Local progression-free survival, progression-free survival and overall survival in the proton beam radiotherapy and radiofrequency ablation arms in the per-protocol and intention-to-treat populations.

	N	PBT	RFA	Hazard ratio	p value*
Per-protocol population					
LPFS (for all target lesions), % (90% CI)	143				
2 year		95.1 (89.1–97.8)	84.4 (74.6–90.7)	0.51 (0.26–1.03)	0.114
3 year		88.9 (80.9–93.7)	78.3 (67.3–86.0)		
4 year		86.5 (77.4–92.1)	78.3 (67.3–86.0)		
LPFS (for all patients), % (90% CI)	136				
2 year		94.8 (88.5–97.7)	83.9 (73.8–90.4)	0.52 (0.26–1.05)	0.123
3 year		88.3 (79.9–93.3)	77.6 (66.4–85.5)		
4 year		85.8 (76.3–91.7)	77.6 (66.4–85.5)		
PFS (for all patients), % (95% CI)	136				
2 year		28.7 (19.3–38.9)	37.5 (25.0–49.9)	1.10 (0.76–1.59)	0.623
3 year		20.9 (12.7–30.5)	23.1 (13.1–34.8)		
4 year		15.6 (8.3–25.0)	13.8 (6.0–24.9)		
OS (for all patients), % (95% CI)	136				
2 year		88.8 (79.5–94.0)	92.9 (82.1–97.3)	1.19 (0.62–2.27)	0.600
3 year		79.0 (67.9–86.6)	87.2 (74.9–93.7)		
4 year		74.0 (62.1–82.7)	78.0 (63.6–87.3)		
Intention-to-treat population					
LPFS (for all target lesions), % (90% CI)	155				
2 year		93.3 (86.5–96.7)	83.2 (74.7–89.0)	0.68 (0.37–1.26)	0.306
3 year		86.8 (78.2–92.2)	78.4 (69.1–85.2)		
4 year		84.3 (74.7–90.5)	78.4 (69.1–85.2)		
LPFS (for all patients),% (90% CI)	144				
2 year		92.8 (85.6–96.5)	83.2 (74.4–89.2)	0.73 (0.39–1.38)	0.419
3 year		85.8 (76.5–91.6)	78.3 (68.6–85.3)		
4 year		83.0 (72.6–89.7)	78.3 (68.6–85.3)		
PFS (for all patients), % (95% CI)	144				
2 year		31.9 (21.6–42.8)	31.9 (21.6–42.8)	0.99 (0.70–1.41)	0.958
3 year		26.3 (16.8–36.8)	17.9 (10.1–27.6)		
4 year		18.7 (10.2–29.1)	12.6 (5.9–21.8)		
OS (for all patients), % (95% CI)	144				
2 year		91.7 (82.4–96.2)	90.3 (80.7–95.2)	1.07 (0.58–1.98)	0.821
3 year		80.8 (69.2–88.4)	86.0 (69.2–88.4)		
4 year		75.4 (62.8–84.2)	77.0 (64.5–85.6)		

LPFS, local progression-free survival; OS, overall survival; PBT, proton beam radiotherapy; PFS, progression-free survival; RFA, radiofrequency ablation.
*Cox proportional hazards model.

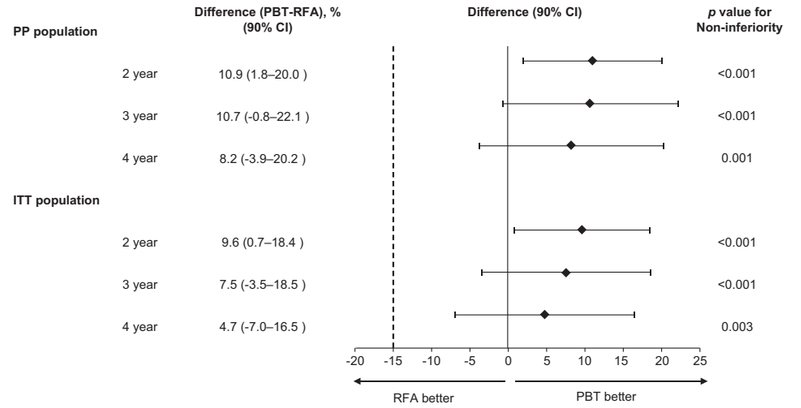

Fig. 2. Forest plots of local progression-free survival in all patients. p value was calculated for the hypothesis of non-inferiority with a non-inferiority margin of −15.0%. A 1-sided p value <0.05 was considered statistically significant (Cox-proportional hazard model). ITT, intention-to-treat; PBT, proton beam radiotherapy; PP, per-protocol; RFA, radiofrequency ablation.

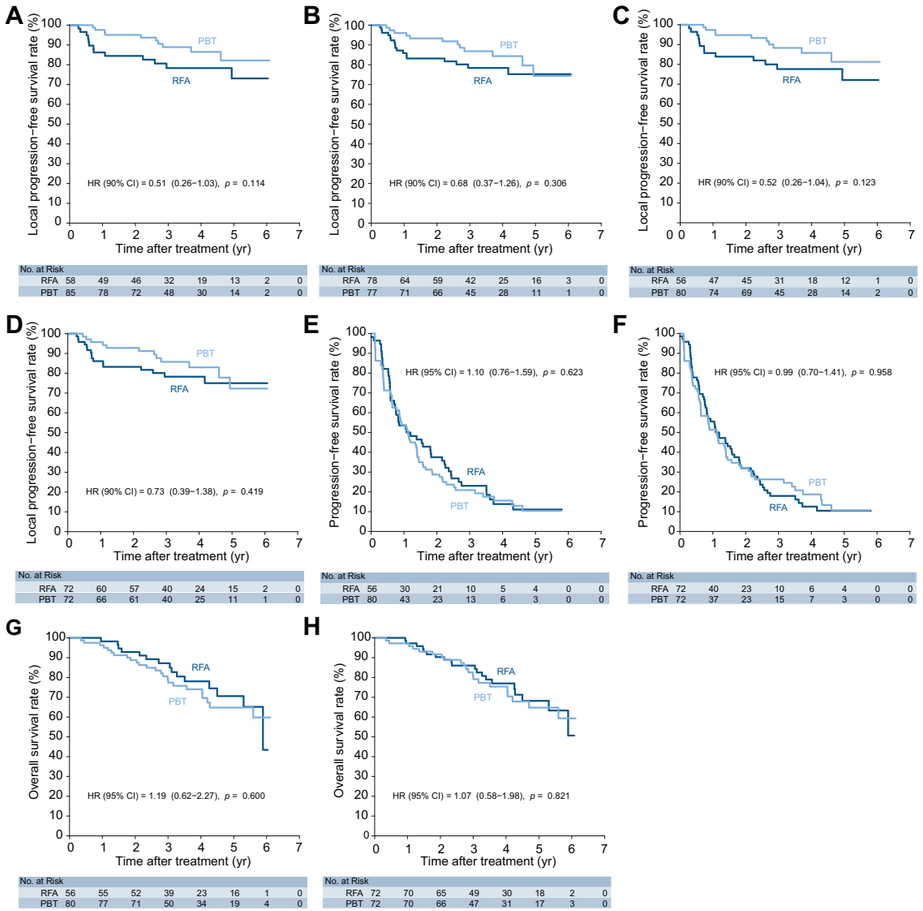

Fig. 3. Survival curves in the PP population and ITT population. (A) LPFS curves for all target lesions in the PP population. (B) LPFS curves in the ITT population. (C) LPFS curves for all patients in the PP population. (D) LPFS curves for all patients in the ITT population. (E) PFS curves in the PP population. (F) PFS curves in the ITT population. (G) OS curves in the PP population. (H) OS curves in the ITT population. Kaplan-Meier method and a Cox proportional hazard model was used. HR, hazard ratio; ITT, intention-to-treat; LPFS, local progression-free survival; OS, overall survival; PFS, progression-free survival; PBT, proton beam radiotherapy; PP, per-protocol; RFA, radiofrequency ablation.

time to the best tumor response was 4.4 months (range 1–13) in the PBT arm and 1 month (range 0.8–1.2) in the RFA arm (p <0.001). In the PP population, of the 80 patients in the PBT group, 65 (81.3%) had disease progression and 24 (30%) died from disease progression (n = 21), an unknown cause (n = 1), chronic renal failure (n = 1), and pneumonia (n = 1) unrelated to the treatment. Cumulative local, intrahepatic and extrahepatic progression were observed in 10 (12.5%), 65 (81.3%), and 10 patients (12.5%), respectively (Fig. S2). Of the 56 patients in the RFA group, 42 (82.1%) had disease progression and 15 (26.8%) died from disease progression unrelated to the treatment. Cumulative local, intrahepatic and extrahepatic progression occurred in 13 (23.2%), 41 (73.2%), and 11 patients (19.6%), respectively (Fig. S2). After disease progression development, subsequent treatment

Table 3. Adverse events after proton beam radiotherapy and radiofrequency ablation.

	PBT (n = 80), n (%)				RFA (n = 56), n (%)				
CTCAE grade	Grade 1	Grade 2	Grade 3	Grade 4	Grade 1	Grade 2	Grade 3	Grade 4	*p* value
WBC increase	0 (0.0)	0 (0.0)	0 (0.0)	0 (0.0)	1 (1.8)	0 (0.0)	0 (0.0)	0 (0.0)	0.412†
WBC decrease	18 (22.5)	1 (1.3)	0 (0.0)	0 (0.0)	9 (16.1)	0 (0.0)	0 (0.0)	0 (0.0)	0.569†
PLT decrease	15 (18.8)	0 (0.0)	0 (0.0)	0 (0.0)	16 (28.6)	0 (0.0)	0 (0.0)	0 (0.0)	0.179*
ALT/AST increase	10 (12.5)	3 (3.8)	0 (0.0)	0 (0.0)	14 (25.0)	32 (57.1)	8 (14.3)	0 (0.0)	<0.001†
Albumin decrease	5 (6.3)	0 (0.0)	0 (0.0)	0 (0.0)	3 (5.4)	0 (0.0)	0 (0.0)	0 (0.0)	1.000†
Bilirubin increase	8 (10.0)	0 (0.0)	0 (0.0)	0 (0.0)	8 (14.3)	0 (0.0)	0 (0.0)	0 (0.0)	0.445*
Fever	0 (0.0)	0 (0.0)	0 (0.0)	0 (0.0)	5 (8.9)	1 (1.8)	0 (0.0)	0 (0.0)	0.004†
Pain	0 (0.0)	1 (1.3)	0 (0.0)	0 (0.0)	10 (17.9)	7 (12.5)	0 (0.0)	0 (0.0)	<0.001†
Nausea	0 (0.0)	1 (1.3)	0 (0.0)	0 (0.0)	5 (8.9)	1 (1.8)	0 (0.0)	0 (0.0)	0.011†
Bleeding	0 (0.0)	0 (0.0)	0 (0.0)	0 (0.0)	0 (0.0)	0 (0.0)	1 (1.8)	0 (0.0)	0.412†
Dermatitis	14 (17.5)	0 (0.0)	0 (0.0)	0 (0.0)	0 (0.0)	0 (0.0)	0 (0.0)	0 (0.0)	0.001*
Radiation pneumonitis	26 (32.5)	0 (0.0)	0 (0.0)	0 (0.0)	0 (0.0)	0 (0.0)	0 (0.0)	0 (0.0)	<0.001*
Ascites	0 (0.0)	0 (0.0)	0 (0.0)	0 (0.0)	0 (0.0)	0 (0.0)	0 (0.0)	0 (0.0)	-
Upper gastrointestinal ulcer	0 (0.0)	0 (0.0)	0 (0.0)	0 (0.0)	0 (0.0)	0 (0.0)	0 (0.0)	0 (0.0)	-
No. of patients with ≥ Grade 3 AEs	0 (0.0)				9 (16.1)				<0.001†
Change of Child-Pugh score	−1	0	+1	+2	−1	0	+1	+2	0.049†
	2 (2.5)	72 (90.0)	6 (7.5)	0 (0)	0 (0)	45 (80.4)	11 (19.6)	0 (0)	

AE, adverse event; ALT, alanine aminotransferase; AST, aspartate aminotransferase; PBT, proton beam radiotherapy; PLT, platelet; RFA, radiofrequency ablation; WBC, white blood cell.
*Chi-square test.
†Fisher's exact test.

was performed; there was no significant difference between the PBT and RFA arms (p >0.05) (Table S4).

Safety

In the PP population, the incidence rates of leukopenia, thrombocytopenia, hyperbilirubinemia and hypoalbuminemia were similar in both arms (p >0.05 each) (Table 3). The incidences of elevated alanine aminotransferase levels were higher in the RFA arm than the PBT arm (grade 1, 25% *vs.* 12.5%; grade 2, 57.1% *vs.* 3.8%; and grade 3, 14.3% *vs.* 0%; p <0.001), and those of increased Child-Pugh score were higher in the RFA arm than the PBT arm (1-point decrease, 0% *vs.* 2.5%; no change, 80.4% *vs.* 90%; 1-point increase, 19.6% *vs.* 7.5%; p = 0.049). The incidence of dermatitis and radiation pneumonitis were higher in the PBT group than the RFA group (grade 1, 17.5% *vs.* 0%, p <0.001; and grade 1, 32.5% *vs.* 0%, p <0.001, respectively). The incidence of radiation pneumonitis is relatively high, but all were asymptomatic, radiographic changes (grade 1). Although grade 3 AEs occurred more frequently in the RFA group than the PBT group (16.1% *vs.* 0%, p <0.001), these toxicities were transient and all patients recovered. The RFA arm showed no major biliary and pulmonary AEs, except for 1 (1.8%) patient who had bleeding in the inferior phrenic artery after RFA that was controlled by embolization. The median length of hospital stay in the RFA arm was 3.1 days (range 2–8), and the median out-patient clinic duration in the PBT arm was 12.7 days (p <0.001). In both arms, treatment-related late hepatic failure and death without evidence of disease progression and/or subsequent treatment were not observed.

Discussion

This study demonstrated that PBT yielded LPFS values that were comparable to those obtained on RFA in patients with rHCC. Although the rate of crossover to other treatments after randomization was relatively high in both arms, PBT showed consistently non-inferior values, in terms of LPFS, to RFA in both the ITT and PP analyses. Despite crossover, patient characteristics between both arms in ITT and PP population were not significantly different (Table 1). In confirmatory trials with a superiority design, the ITT set is usually used in the primary analysis. However, in non-inferiority, crossover clinical trials, such as the present one, the analysis of the PP population was given priority and ITT analysis was performed complementarily.[18] Until the planning of this study, we lacked sufficient evidence for the application of PBT as a first-line treatment, so we performed this RCT with PBT as a second-line treatment in patients with rHCC. Because a non-inferiority trial is a research method that is selected when the treatment to be studied is considered to be equivalent and to be complementary to the standard treatment (for cases of technical infeasibility). We assumed that PBT had an equivalent effect on local control and could be applied as complementary to RFA treatment. Thus, we selected a non-inferiority crossover trial for this study. Additionally, selecting patients eligible for both therapies could have excluded the majority of real-world patients who may benefit from either treatment; this study compared the outcomes of PBT *vs.* RFA for tumors with the same tumor conditions.

RFA is frequently not feasible for HCC lesion(s) due to their invisibility under ultrasound guidance and limited accessibility of the tumor location.[27] In the present study, RFA was not feasible in 30.6% (22 of 72) of the patients in the RFA arm. Of these patients, PBT was feasible in 86.4% (19 of 22) of the patients and not feasible in 13.6% (3 of 22) patients due to proximity to the gastrointestinal organs (Fig. 1). In the PBT arm, PBT was not feasible in 15.3% (11 of 72) of the patients due to the technical infeasibility of PBT (12.5% [9/72]) and withdrawal of informed consent (2.7% [2/72]). Of the patients showing infeasibility to PBT, RFA was feasible in 66.7% (6 of 9) of the patients and infeasible in 33.3% (3 of 9). The rate of crossover to the other treatment due to technical infeasibility was significantly higher in RFA than PBT (19/72 [26.4%] *vs.* 6/72 [8.3%], p <0.05); owing to the single-institution nature of this study and the fact that RFA was conducted by an expert with more than 10 years of experience, PBT showed better feasibility than RFA. RFA is generally

limited by echogenicity, sub-phrenic location and proximity of vascular and biliary structures and PBT can be limited by the proximity of tumor(s) to radiosensitive gastrointestinal structures. Conversely, RFA is relatively not limited by proximity to gastrointestinal structures and PBT is relatively not limited by echogenicity, sub-phrenic location, and proximity of vascular and biliary structures. These findings suggested that RFA and PBT could be used in a complementary approach by cross-covering the technical infeasibility of each arm. However, 3 patients from each arm received another treatment because neither PBT nor RFA were feasible after randomization (Fig. 1); this is a limitation of study design.

RFA, as a first-line treatment for small HCC, has shown excellent outcomes, with 2- or 3-year LPFS rates of 70.2–96.8%.[20,22–25,28–29] As a second-line treatment for rHCC, it has shown a 2-year LPFS rate of 62.5–68.5%.[21,31] Although this study enrolled rHCC patients and 46.4% (26 of 56) of the patients in the RFA arm had a history of other local treatments for target lesions (Table 1), RFA showed comparable outcomes with 2- and 3-year LPFS rates of 83.9% and 77.6%, respectively, similar to previous reports.[20,21,25,31] Other studies with PBT showed outcomes with 2- or 3-year LPFS rates of 71.4–96% in patients with HCC.[8–10,12,15] In this study, 47.5% (38 of 80) of the patients in the PBT arm had a history of prior local treatment for target lesions, and despite the inclusion of a broader PTV than that used in other studies, PBT showed comparable outcomes, with 2- and 3-year LPFS rates of 94.8% and 88.3%, respectively, similar to previous reports.

On comparing the LPFS, PFS, and OS values, we observed different patterns in the PP and ITT populations (Fig. 2). Although there was no statistical difference (Table 1), the subtle discrepancies in the patients' characteristics between the 2 populations may contribute to these outcome differences; after crossover, the proportion of patients with tumor sizes > 2 cm decreased (PBT 13.9% *vs.* RFA 7.1%) and that of patients with AJCC stage I disease increased (PBT 26.3% *vs.* RFA 32.1%) in the RFA arm (Table 1). These results are considered to be limitations associated with the crossover trial design. However, PBT and RFA yielded OS rates that were similar to those observed for RFA in randomized trials comparing the efficacy of RFA and surgical resection in early HCC.[32–35] Although the non-inferiority of PBT compared to RFA was not shown in terms of the 2-year PFS as well as 3- and 4-year OS in the PP analysis (Fig. 2), the HRs in the PFS and OS between RFA and PBT were consistently not significant in both the ITT and PP analyses (p >0.05 each) (Fig. 3E–H). In the best tumor response evaluation, there was a lag in local control with PBT, unlike RFA, so the median time to the best tumor response was 4.4 months (range 1–13). The CR of the PBT arm was only 83.5%, because the criterion was RECIST. If it were based on modified RECIST, it would be possible to obtain a higher CR rate (Fig. S1).

This study has several limitations. First, the primary outcome measure was 2-year LPFS, rather than PFS or OS. As frequent intrahepatic recurrence is a biological characteristic of HCC, which results in subsequent treatments that may affect survival outcomes,[36] the most important goal of locoregional therapy such as RFA and PBT is local control, including LPFS. Considering the presence of a moderate correlation between PFS or time to progression and OS in advanced HCC,[37] LPFS was used as the primary outcome measure in this RCT. Second, this study had a single-center design and predominantly included patients with chronic hepatitis B; in order for our results to be generalizable, further studies must be conducted across other institutions including patients with various etiologies. Only a percutaneous RFA with ultrasound or CT guidance (the most popular method in real-world practice) was performed in this study. However, laparoscopic RFA and/or multi-bipolar RFA with real-time ultrasound/CT or ultrasound/MRI fusion image navigation can improve the feasibility and outcomes of RFA.[38–40] During study design, due to a lack of LPFS data on RFA *vs.* placebo, we assumed a non-inferiority margin of 15% based on the RCT data of RFA *vs.* PEI.[23] This margin seems to be relatively wide, but the lower boundary of CI of actual differences (PBT minus RFA) of 2-, 3-, and 4-year LPFS in the PP population was within - 5%. Lastly, PBT entails high costs and exclusive equipment, so our results cannot be applied to all patients with HCC.

In conclusion, this prospective randomized study demonstrated that PBT is associated with LPFS rates that are comparable to those observed for RFA in patients with rHCC with ≤2 tumor(s) of <3 cm. PBT was also tolerable and safe, consistent with the known profile. The associated good feasibility and comparable clinical outcomes suggest that PBT may be a promising treatment option for small HCC.

Abbreviations

AE, adverse events; AJCC, American Joint Committee on Cancer; CR, complete response; HCC, hepatocellular carcinoma; HR, hazard ratio; ITT, intention-to-treat; ITV, internal target volume; LPFS, local progression-free survival; NCC, National Cancer Center; OS, overall survival; PEI, percutaneous ethanol injection; PBT, proton beam radiotherapy; PFS, progression-free survival; PP, per-protocol; PTV, planning target volumes; RCT, randomized controlled trial; RFA, radiofrequency ablation; rHCC, recurrent/residual HCC.

Financial support

This study was supported by the National Cancer Center Grant, Korea (NCC 1810271, 1810031 and 1710030). The funding source had no role in the study design, data curation, or the analysis and interpretation of data.

Conflict of interest

J-WP has served in a consulting or advisory role for Roche, Genetech, BMS, Bayer, Eisai, Ipsen, AstraZeneca; received honoraria from Bayer, Eisai; and participated in research sponsored by Ono-BMS, AstraZeneca, Blueprint, Roche, Eisai, Exelicis, Kowa, Merk. BHK has participated in research sponsored by Ono-BMS and received honoraria from Abbvie. The other authors declare that they have no conflict of interest related to this manuscript.

Please refer to the accompanying ICMJE disclosure forms for further details.

Authors' contributions

Conception and study design: J-WP, THK, YHK; Funding acquisition: J-WP; Supervision: J-WP; Investigation and data curation: J-WP, THK, YHK, BHK, JHL, and MJK, Data analysis and interpretation: BP, THK, JWP, YHK, BHK; Writing – original draft: THK; Writing-review and editing: J-WP, THK, YHK, BHK, JHL, MJK, and BP. All authors reviewed and approved the final draft.

Data availability statement

Informed consent was not obtained from patients to share raw information in a public repository.

Acknowledgments

Byung-Ho Nam, Ph.D., President, HERINGS, Korea, assisted with the study design, sample size calculation and analysis plan. Ju Hee Lee's current affiliation is the Department of Radiology, Asan Medical Center, Korea, and Min Ju Kim's current affiliation is the Department of Radiology, Ehwa's Women's University Hospital, Korea. We are grateful to all APROH trial patients, their family and collaborators of APROH trials.

Supplementary data

Supplementary data to this article can be found online at https://doi.org/10.1016/j.jhep.2020.09.026.

References

[1] Akinyemiju T, Abera S, Ahmed M, Alam N, Alemayohu MA, Allen C, et al., Global Burden of Disease Liver Cancer Collaboration. The burden of primary liver cancer and underlying etiologies from 1990 to 2015 at the global, regional, and national level: results from the Global Burden of Disease study 2015. JAMA Oncol 2017;3:1683–1691.
[2] Park JW, Chen M, Colombo M, Roberts LR, Schwartz M, Chen PJ, et al. Global patterns of hepatocellular carcinoma management from diagnosis to death: the BRIDGE Study. Liver Int 2015;35:2155–2166.
[3] European Association for the Study of the Liver. EASL clinical practice guidelines: management of hepatocellular carcinoma. J Hepatol 2018;69:182–236.
[4] Korean Liver Cancer Association, National Cancer Center. 2018 Korean Liver Cancer Association-National Cancer Center Korea practice guidelines for the management of hepatocellular carcinoma. Gut and liver 2019;13:227–299.
[5] Marrero JA, Kulik LM, Sirlin CB, Zhu AX, Finn RS, Abecassis MM, et al. Diagnosis, staging, and management of hepatocellular carcinoma: 2018 practice guidance by the American Association for the Study of Liver Diseases. Hepatology 2018;68:723–750.
[6] Levin WP, Kooy H, Loeffler JS, DeLaney TF. Proton beam therapy. Br J Cancer 2005;93:849–854.
[7] Zietman AL, Bae K, Slater JD, Shipley WU, Efstathiou JA, Coen JJ, et al. Randomized trial comparing conventional-dose with high-dose conformal radiation therapy in early-stage adenocarcinoma of the prostate: long-term results from proton radiation oncology group/american college of radiology 95-09. J Clin Oncol 2010;28:1106–1111.
[8] Bush DA, Kayali Z, Grove R, Slater JD. The safety and efficacy of high-dose proton beam radiotherapy for hepatocellular carcinoma: a phase 2 prospective trial. Cancer 2011;117:3053–3059.
[9] Kim TH, Park JW, Kim YJ, Kim BH, Woo SM, Moon SH, et al. Phase I dose-escalation study of proton beam therapy for inoperable hepatocellular carcinoma. Cancer Res Teat 2015;47:34–45.
[10] Hong TS, Wo JY, Yeap BY, Ben-Josef E, McDonnell EI, Blaszkowsky LS, et al. Multi-institutional phase II study of high-dose hypofractionated proton beam therapy in patients with Localized, unresectable hepatocellular carcinoma and intrahepatic cholangiocarcinoma. J Clin Oncol 2016;34:460–468.
[11] Kim TH, Park JW, Kim BH, Oh ES, Youn SH, Moon SH, et al. Phase II study of hypofractionated proton beam therapy for hepatocellular carcinoma. Front Oncol 2020;10:542.
[12] Kawashima M, Furuse J, Nishio T, Konishi M, Ishii H, Kinoshita T, et al. Phase II study of radiotherapy employing proton beam for hepatocellular carcinoma. J Clin Oncol 2005;23:1839–1846.
[13] Korean Liver Cancer Study Group, National Cancer Center. Practice guidelines for management of hepatocellular carcinoma 2009. Korean J Hepatol 2009;15:391–423.
[14] Korean Liver Cancer Study Group, National Cancer Center. 2014 KLCSG-NCC Korea practice guideline for the management of hepatocellular carcinoma. Gut Liver 2015;9:267–317.
[15] Fukumitsu N, Sugahara S, Nakayama H, Fukuda K, Mizumoto M, Abei M, et al. A prospective study of hypofractionated proton beam therapy for patients with hepatocellular carcinoma. Int J Radiat Oncol Biol Phys 2009;74:831–836.
[16] Mizumoto M, Okumura T, Hashimoto T, Fukuda K, Oshiro Y, Fukumitsu N, et al. Proton beam therapy for hepatocellular carcinoma: a comparison of three treatment protocols. Int J Radiat Oncol Biol Phys 2011;81:1039–1045.
[17] Eisenhauer EA, Therasse P, Bogaerts J, Schwartz LH, Sargent D, Ford R, et al. New response evaluation criteria in solid tumours: revised RECIST guideline (version 1.1). Eur J Cancer 2009;45:228–247.
[18] Parpia S, Julian JA, Thabane L, Gu C, Whelan TJ, Levine MN. Treatment crossovers in time-to-event non-inferiority randomised trials of radiotherapy in patients with breast cancer. BMJ Open 2014;4:e006531.
[19] Choi D, Lim HK, Rhim H, Kim YS, Yoo BC, Paik SW, et al. Percutaneous radiofrequency ablation for recurrent hepatocellular carcinoma after hepatectomy: long-term results and prognostic factors. Ann Surg Oncol 2007;14:2319–2329.
[20] Kim YS, Lim HK, Rhim H, Lee MW, Choi D, Lee WJ, et al. Ten-year outcomes of percutaneous radiofrequency ablation as first-line therapy of early hepatocellular carcinoma: analysis of prognostic factors. J Hepatol 2013;58:89–97.
[21] Koh YH, Choi JI, Kim HB, Kim MJ. Computed tomographic-guided radiofrequency ablation of recurrent or residual hepatocellular carcinomas around retained iodized oil after transarterial chemoembolization. Korean J Radiol 2013;14:733–742.
[22] Lencioni RA, Allgaier HP, Cioni D, Olschewski M, Deibert P, Crocetti L, et al. Small hepatocellular carcinoma in cirrhosis: randomized comparison of radio-frequency thermal ablation versus percutaneous ethanol injection. Radiology 2003;228:235–240.
[23] Lin SM, Lin CJ, Lin CC, Hsu CW, Chen YC. Randomised controlled trial comparing percutaneous radiofrequency thermal ablation, percutaneous ethanol injection, and percutaneous acetic acid injection to treat hepatocellular carcinoma of 3 cm or less. Gut 2005;54:1151–1156.
[24] Nakazawa T, Kokubu S, Shibuya A, Ono K, Watanabe M, Hidaka H, et al. Radiofrequency ablation of hepatocellular carcinoma: correlation between local tumor progression after ablation and ablative margin. AJR Am J Roentgenol 2007;188:480–488.
[25] Shiina S, Tateishi R, Arano T, Uchino K, Enooku K, Nakagawa H, et al. Radiofrequency ablation for hepatocellular carcinoma: 10-year outcome and prognostic factors. Am J Gastroenterol 2012;107:569–577. quiz 578.
[26] Com-Nougue C, Rodary C, Patte C. How to establish equivalence when data are censored: a randomized trial of treatments for B non-Hodgkin lymphoma. Stat Med 1993;12:1353–1364.
[27] Rhim H, Lee MH, Kim YS, Choi D, Lee WJ, Lim HK. Planning sonography to assess the feasibility of percutaneous radiofrequency ablation of hepatocellular carcinomas. AJR Am J Roentgenol 2008;190:1324–1330.
[28] Kono M, Inoue T, Kudo M, Chishina H, Arizumi T, Takita M, et al. Radiofrequency ablation for hepatocellular carcinoma measuring 2 cm or smaller: results and risk factors for local recurrence. Dig Dis 2014;32:670–677.
[29] Lee LH, Hwang JI, Cheng YC, Wu CY, Lee SW, Yang SS, et al. Comparable outcomes of ultrasound versus computed tomography in the guidance of radiofrequency ablation for hepatocellular carcinoma. PLoS one 2017;12:e0169655.
[30] Lee DH, Lee JM, Lee JY, Kim SH, Han JK, Choi BI. Radiofrequency ablation for intrahepatic recurrent hepatocellular carcinoma: long-term results and prognostic factors in 168 patients with cirrhosis. Cardiovasc Intervent Radiol 2014;37:705–715.
[31] Kim N, Kim HJ, Won JY, Kim DY, Han KH, Jung I, et al. Retrospective analysis of stereotactic body radiation therapy efficacy over radiofrequency ablation for hepatocellular carcinoma. Radiother Oncol 2019;131:81–87.
[32] Feng K, Yan J, Li X, Xia F, Ma K, Wang S, et al. A randomized controlled trial of radiofrequency ablation and surgical resection in the treatment of small hepatocellular carcinoma. J Hepatol 2012;57:794–802.
[33] Chen MS, Li JQ, Zheng Y, Guo RP, Liang HH, Zhang YQ, et al. A prospective randomized trial comparing percutaneous local ablative therapy and partial hepatectomy for small hepatocellular carcinoma. Ann Surg 2006;243:321–328.
[34] Xia Y, Li J, Liu G, Wang K, Qian G, Lu Z, et al. Long-term effects of repeat hepatectomy *vs.* percutaneous radiofrequency ablation among patients with recurrent hepatocellular carcinoma: a randomized clinical trial. JAMA Oncol 2020;6(2):255–263.
[35] Huang J, Yan L, Cheng Z, Wu H, Du L, Wang J, et al. A randomized trial comparing radiofrequency ablation and surgical resection for HCC conforming to the Milan criteria. Ann Surg 2010;252:903–912.

[36] Moon H, Choi JE, Lee IJ, Kim TH, Kim SH, Ko YH, et al. All-treatment array of hepatocellular carcinoma from initial diagnosis to death: observation of cumulative treatments. J Cancer Res Clin Oncol 2017;143:2327–2339.
[37] Llovet JM, Montal R, Villanueva A. Randomized trials and endpoints in advanced HCC: role of PFS as a surrogate of survival. J Hepatol 2019;70:1262–1277.
[38] Seror O, N'Kontchou G, Nault JC, Rabahi Y, Nahon P, Ganne-Carrie N, et al. Hepatocellular carcinoma within Milan criteria: no-touch multibipolar radiofrequency ablation for treatment-long-term results. Radiology 2016;180(2):611–621.
[39] Ahn SJ, Lee JM, Lee DH, Lee SM, Yoon JH, Kim YJ, et al. Real-time US-CT/MR fusion imaging for percutaneous radiofrequency ablation of hepatocellular carcinoma. J Hepatol 2017;66(2):347–354.
[40] Song KD, Lee MW, Rhin H, Kang TW, Cha DI, Sinn DH, et al. Percutaneous US/MRI fusion-guided radiofrequency ablation for recurrent subcentimeter hepatocellular carcinoma: technical feasibility and therapeutic outcomes. Radiology 2018;288(3):878–886.

PFIZER
MEDICAL
RESEARCH
AWARD
since 2000

대한민국의학한림원
제19회 화이자의학상

중개의학 부문

최동호 교수

한양대학교 의과대학 외과

대한민국의학한림원 제19회 화이자의학상

중개의학 부문 수상자

최동호 교수

한양대학교
의과대학 외과

학력

1987. 02 - 1993. 02 한양대학교 의과대학 (의학학사)
1994. 08 - 1996. 08 한양대학교 의과대학 (의학석사)
1998. 03 - 2003. 08 한양대학교 의과대학 (의학박사)

경력

2001. - 2002. 국립보건원 객원연구원
2003. – 2012. 순천향대학교병원 조교수, 부교수
2013.09 – 현재 한양대학교 의과대학 교수
2019.07 – 현재 한양대학교 병원 연구부원장
2019.11 – 현재 한양대학교 병원 의학연구원장

수상

2004. 학술상 (한국간담췌외과학회)
2006. 우수논문상 (순천향대학교 의과대학 교수협의회)
2006. 종근당학술상 (대한이식학회)
2009. 락천의학 학술상 (순천향대학교)
2010. 학술발표상 (한국간담췌외과학회)
2010. 우수 총회구연 (대한간학회)
2010. 학술발표상 (한국간담췌외과학회)
2015. 자유연제 최우수상 (대한이식학회 추계학술대회)
2015. Best Paper Award (한국간담췌외과학회)

수상

2016. 제3회 한양 미래 R&D 공모전 우수상 (한양대학교 산학협력단)
2016. 제4회 한양 미래 R&D 공모전 우수상 (한양대학교 산학협력단)
2017. 제6회 한양 미래 R&D 공모전 우수상 (한양대학교 산학협력단)
2020. 제10회 에쓰-오일 우수학위논문상 (에쓰-오일 과학문화재단)
2021. 2021년 HYU 학술상

논문 요약 및 연구의 의의

유전성 난치질환은 효율적인 치료방법이 없어 치명적이거나, 만성화되어 평생 치료가 필요한 경우가 많습니다. 현재 약물을 이용한 치료방법들은 대부분 근본적인 해결보다는 질환의 진행을 늦추거나, 현 상태를 유지시키는 등의 보존적인 치료에 국한되고 있습니다. 유전성 난치질환의 근본적인 해결을 위해 유전자가위를 이용한 유전자치료 등이 크게 각광받고 있는데, 현재까지 대부분의 유전자치료는 유전자가위를 생체 내 (in vivo)에 직접 주입하는 방법을 사용하고 있습니다. 하지만 유전자가위를 생체 내로 전달할 때 효율적인 전달을 위하여, 바이러스 등을 전달체로 사용하기 때문에 바이러스에 관련된 위험성 및 유전자가위 과발현에 의한 표적 이탈 효과 (off-target effect) 등이 문제점으로 지적되고 있습니다.

본 연구진은 '저분자 화합물 유래 간 전구/줄기세포 제작 연구'를 발표한 바 있습니다 (Kim et al. Journal of Hepatology). 이번 연구에는 한양대학교 배상수 교수 연구팀과 함께 저분자 화합물을 통해 유전성 난치질환 모델 마우스 유래 간 전구/줄기세포를 제작하고, 차세대 유전자교정 기술인 염기교정 (base editing)과 프라임교정 (prime editing)을 통해 돌연변이 유전자를 교정한 후, 다시 생체 내로 이식하여 질병을 치료하는 전략 (ex vivo gene therapy)을 이용하여 한번의 치료만으로도 유전성 난치질환인 티로신혈증 (Hereditary tyrosinemia type I) 동물 모델에서 생존율이 크게 개선되는 등 유전성 간 난치질환에 대한 근본적인 치료방법을 제시한 것이 중요한 성과라고 하겠습니다.

이번 연구결과를 바탕으로 앞으로 유전성 난치질환 환자의 세포를 추출하여, 체외에서 염기교정 및 프라임교정 기술을 이용하여 교정한 후 다시 환자에게 이식하여 난치성 질환을 치료하는 유전자 세포치료제로서 유용하게 사용될 수 있을 것으로 기대합니다. 또한 off-target effect와 교정 효율 (editing efficiency) 등을 체외에서 확인 및 선별하여 환자에게 이식할 수 있기 때문에 기존 생체 내 직접 주입 유전자치료 (in vivo gene therapy)의 문제점을 크게 해결할 수 있을 것이라고 생각됩니다

마지막으로 이번연구가 본 연구진이 연구하고 있는 재생의학 (Regenerative medicine)을 기반으로 한 줄기세포, 유전자치료, 인공장기 관련된 연구의 중요한 융합연구의 성과라로 생각합니다

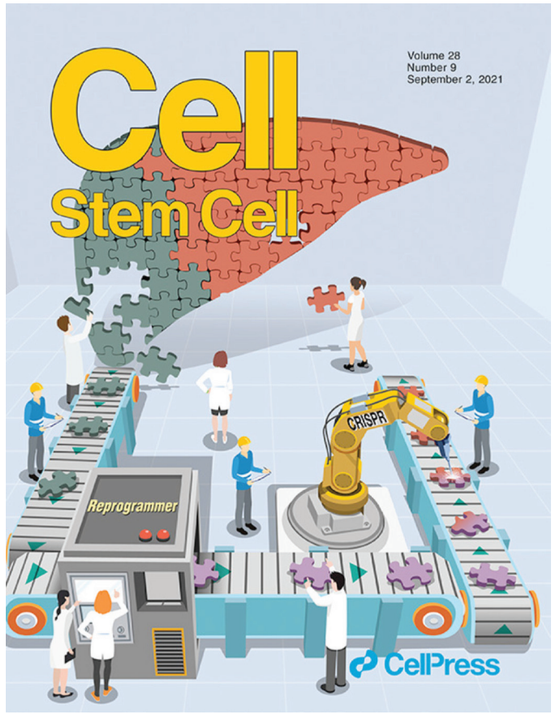

그림 1. 유전질환으로 손상된 간세포를 저분자 화합물을 이용하여 리프로그래밍하여 간줄기세포로 만들고 유전자 가위를 이용하여 손상된 유전자를 교정하여 건강한 간세포를 생체 외에서 만들고 그 간세포를 다시 이식하여 유전성 간질환을 치료하는 모식도
(표지논문 Cell Stem Cells Sep 2021)

수상 소감

권위있는 화이자 의학상을 수상하게 되어 개인적으로 큰 영광입니다. 심사해주시고 선정과정에 관여해 주신 관계자 여러분께 감사드립니다. 우선 저와 함께 같이 연구하여 온 학생과 연구원들에게 감사드리며, 저만 이와 같은 영광을 누리게 되어 죄송스러운 마음입니다. 특히 독일에 포탁으로 가 있는 김요한 박사, 불철주야 저와 같이 오직 연구만을 생각하고 있는 정재민 교수, 그리고 공동연구자로서 너무나 훌륭한 업적으로 저와 협업하는 배상수교수에게 감사드립니다. 그리고 정신없이 살고 있는 가장을 잘 이해해주는 제 아내 (이숙진) 그리고 두 딸(최민경, 최수경)에게도 미안하고 고마운 마음을 전합니다.

외과의사로서 그것도 간이식을 하고 간담췌외과를 하는 저에게 연구를 한다는 것이 쉽지는 않은 일이었습니다. 하지만 처음 의과대학에 오면서 생각한 마음들 그리고 의사가 되면서 다짐 했던 것들 을 초심으로 유지하면서 외과의사와 간담췌외과의사가 되면서 자연스럽게 저에게 남겨진 숙제들을 풀기위해서 앞으로도 묵묵히 연구를 진행해 나가겠습니다.

남은 저의 연구인생 동안 더욱 열심히 연구하여 간질환으로 고통받는 환자들에게 희망을 줄 수 있는 외과의사가 되기 위해서 노력하겠습니다. 비록 제가 한 연구가 미흡하여 당장 성과를 내지는 못하겠지만 이 연구가 도화선이 되어서 제 후배나 제자들이 꼭 치료법을 완성해 나가리라 믿습니다.

다시 한번 영광스러운 상을 제정하고 수상해주신 오동욱 대표님과 화이자관계자 및 임태환 의학한림원장 및 심사위원교수님들께도 감사드립니다

Short Article

Cell Stem Cell

Adenine base editing and prime editing of chemically derived hepatic progenitors rescue genetic liver disease

Graphical abstract

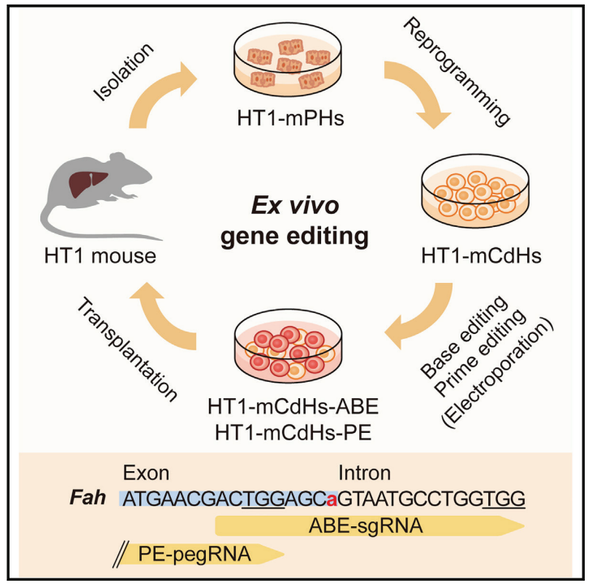

Highlights

- Chemically derived hepatic progenitors (CdHs) were derived from an HT1 mouse model
- Mutant HT1-CdHs can be successfully corrected using base editors and prime editors
- Corrected HT1-CdHs show no significant off-target editing
- Edited HT1-CdHs repopulate the liver and promote survival

Authors

Yohan Kim, Sung-Ah Hong, Jihyeon Yu, ..., Jaemin Jeong, Sangsu Bae, Dongho Choi

Correspondence

jmj1103@gmail.com (J.J.), sangsubae@hanyang.ac.kr (S.B.), crane87@hanyang.ac.kr (D.C.)

In brief

Kim et al. demonstrate an *ex vivo* therapeutic editing strategy for hereditary tyrosinemia type 1 (HT1) treatment using chemically derived hepatic progenitors (CdHs). CdHs generated from HT1 mice are genetically corrected by adenine base editors or prime editors. Corrected CdHs can repopulate the HT1 mice liver with a Fah-positive population.

Kim et al., 2021, Cell Stem Cell *28*, 1–11
September 2, 2021
https://doi.org/10.1016/j.stem.2021.04.010

Please cite this article in press as: Kim et al., Adenine base editing and prime editing of chemically derived hepatic progenitors rescue genetic liver disease, Cell Stem Cell (2021), https://doi.org/10.1016/j.stem.2021.04.010

Cell Stem Cell

CellPress

Short Article

Adenine base editing and prime editing of chemically derived hepatic progenitors rescue genetic liver disease

Yohan Kim,[1,2,9] Sung-Ah Hong,[3,9] Jihyeon Yu,[3,8,9] Jeongyun Eom,[4] Kiseok Jang,[4] Sangtae Yoon,[1,2] Da Hee Hong,[1,2] Daekwan Seo,[5] Seu-Na Lee,[6] Jae-Sung Woo,[6] Jaemin Jeong,[1,2,*] Sangsu Bae,[3,10,*] and Dongho Choi[1,2,7,*]

[1]Department of Surgery, Hanyang University College of Medicine, Seoul 04763, Republic of Korea
[2]HY Indang Center of Regenerative Medicine and Stem Cell Research, Hanyang University, Seoul 04763, Republic of Korea
[3]Department of Chemistry and Research Institute for Convergence of Basic Sciences, Hanyang University, Seoul 04763, Republic of Korea
[4]Department of Pathology, Hanyang University College of Medicine, Seoul 04763, Republic of Korea
[5]Psomagen, Inc., 1330 Piccard Drive, Suite 103, Rockville, MD 20850, USA
[6]Department of Life Sciences, Korea University, Seoul 02841, Republic of Korea
[7]Department of HY-KIST Bio-convergence, Hanyang University, Seoul 04763, Republic of Korea
[8]Present address: Division of Life Science, Korea Polar Research Institute, Incheon 21990, Republic of Korea
[9]These authors contributed equally
[10]Lead contact
*Correspondence: jmj1103@gmail.com (J.J.), sangsubae@hanyang.ac.kr (S.B.), crane87@hanyang.ac.kr (D.C.)
https://doi.org/10.1016/j.stem.2021.04.010

SUMMARY

DNA base editors and prime editing technology enable therapeutic *in situ* correction of disease-causing alleles. These techniques could have broad applications for *ex vivo* editing of cells prior to transplantation in a range of diseases, but it is critical that the target population is efficiently modified and engrafts into the host. Chemically derived hepatic progenitors (CdHs) are a multipotent population capable of robust engraftment and hepatocyte differentiation. Here we reprogrammed hepatocytes from a mouse model of hereditary tyrosinemia type 1 (HT1) into expandable CdHs and successfully corrected the disease-causing mutation using both adenine base editors (ABEs) and prime editors (PEs). ABE- and PE-corrected CdHs repopulated the liver with fumarylacetoacetate hydrolase-positive cells and dramatically increased survival of mutant HT1 mice. These results demonstrate the feasibility of precise gene editing in transplantable cell populations for potential treatment of genetic liver disease.

INTRODUCTION

Hereditary tyrosinemia type 1 (HT1), an autosomal recessive disorder caused by a deficiency in fumarylacetoacetase (FAH), results in liver failure due to the accumulation of toxic metabolites from the tyrosine metabolic pathway and can lead to hepatocellular carcinoma (HCC) (Chinsky et al., 2017; Nobili et al., 2010). Although 2-[2-nitro-4-trifluoromethylbenzoyl]-1,3-cyclohexanedione (NTBC) is used therapeutically, it does not treat the fundamental HT1 deficiency. Moreover, some patients lack NTBC sensitivity, and a risk for HCC remains during therapy (van Ginkel et al., 2019). Previously, several groups tried gene therapy approaches involving virus-mediated delivery of full-length *Fah* complementary DNA (cDNA) into the liver in HT1 ($Fah^{-/-}$) model mice (Grompe et al., 1998; Overturf et al., 1997). However, these strategies have potential limitations: the exogenous gene, unaffected by the native chromatin structure of the endogenous locus, will be constitutively expressed, at levels that differ from that of the endogenous gene, and there is a possibility of insertional mutagenesis as a result of viral vector integration into the host genome.

In a different strategy, CRISPR-mediated therapeutic editing approaches have been applied to alter a second gene in the disease pathway, thereby lessening the effects of the *Fah* mutation. Pankowicz et al. (2016) showed that in HT1 model mice, Cas9 nuclease-mediated disruption of the hydroxyphenylpyruvate dioxygenase (*Hpd*) gene, which has a role in the second step of tyrosine catabolism, alleviated the disease symptoms such that the mice exhibited a benign HT3 phenotype. Using a similar strategy, Rossidis et al. (2018) used a cytosine base editor, instead of Cas9, to disrupt the *Hpd* gene by inducing a premature termination codon in the middle of the gene. Both experiments involved the direct delivery of CRISPR-associated tools via lentivirus or adeno-associated virus (AAV); that is, they represent *in vivo* gene editing strategies. Thus, their clinical application would involve potential challenges such as safety issues associated with viral delivery and the possibility of insertional mutagenesis caused by integration of the viral vectors. Recently, Song et al. (2020) demonstrated successful base conversion of the *Fah* gene mutation via hydrodynamic tail vein injection of adenine base editors (ABEs), which mediate A-to-G conversion, with a non-viral delivery system. However, although the *in vivo*

Please cite this article in press as: Kim et al., Adenine base editing and prime editing of chemically derived hepatic progenitors rescue genetic liver disease, Cell Stem Cell (2021), https://doi.org/10.1016/j.stem.2021.04.010

Cell Stem Cell

CellPress

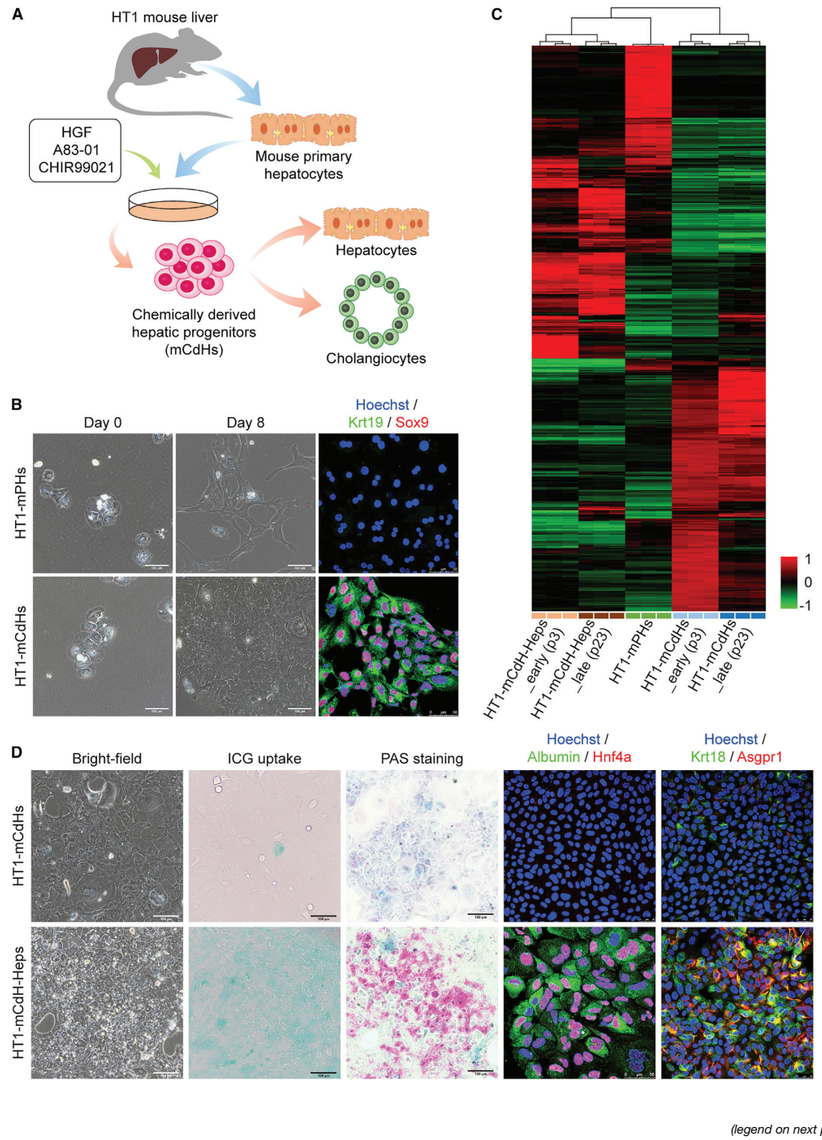

(legend on next page)

Please cite this article in press as: Kim et al., Adenine base editing and prime editing of chemically derived hepatic progenitors rescue genetic liver disease, Cell Stem Cell (2021), https://doi.org/10.1016/j.stem.2021.04.010

editing strategy is advantageous, it is difficult to control the transfection dosage of CRISPR-associated tools and to select corrected cells by excluding cells containing undesired mutations or CRISPR-mediated off-target effects, which may be a potential limitation to clinical applications.

Alternatively, *ex vivo* gene editing strategies can bypass the potential drawbacks of *in vivo* strategies; the concentration of CRISPR-associated tools can be easily tuned, and gene-corrected cells and cells validated to be free of off-target effects can be selected to increase efficiency and safety, respectively. Furthermore, recipients would not be exposed to CRISPR effectors, which may circumvent pre-existing immunological responses in humans (Crudele and Chamberlain, 2018). To date, a few studies have explored *ex vivo* gene editing strategies for applications in HT1 model mice and porcine, but most trials used primary hepatocytes (PHs) as the source cell for gene correction and transplantation (Hickey et al., 2016; VanLith et al., 2018). Because PHs cannot proliferate and maintain their function in an *in vitro* environment, after transplantation the corrected cells became engrafted with low efficiency and caused short-term gene rescue effects. In addition, lentiviral vectors or AAVs were used for CRISPR delivery because of the low transfection efficiency in PHs, raising the possibility of virus-associated safety issues. Instead of PHs, differentiable cells such as embryonic stem cells (ESCs) (Basma et al., 2009; Rambhatla et al., 2003), induced pluripotent stem cells (Chen et al., 2012; Sullivan et al., 2010), mesenchymal stem cells (Banas et al., 2007; Lee et al., 2004), and direct converted cells (Huang et al., 2014; Sekiya and Suzuki, 2011) can alternatively be used as sources of cells for transplantation. However, those cells are associated with potential challenges for clinical applications, such as low differentiation efficiency, incomplete function of differentiated cells compared with primary cells (Song et al., 2009; Wu and Tao, 2012), immune rejection (Rong et al., 2014), risk for tumorigenesis (Lee et al., 2013; Miura et al., 2009), use of viral vectors (Huang et al., 2014; Yu et al., 2007), and ethical issues in the case of ESCs (Zacharias et al., 2011).

As an alternative, we and another group recently developed chemically derived hepatic progenitors (CdHs) from primary human (Kim et al., 2019b) or mouse (Katsuda et al., 2017) hepatocytes. CdHs have the capacity for rapid proliferation after reprogramming, can be stably cultured over ten passages, exhibit adequate differentiation into hepatocytes and biliary epithelial cells, and can repopulate the liver in model disease mice after transplantation. Here, we generated mouse CdHs (mCdHs) from HT1 mouse hepatocytes by the addition of relevant chemical compounds and used the cells for *ex vivo* gene editing therapy. We corrected the *Fah* gene mutation using ABEs or prime editors (PEs) (Anzalone et al., 2019), which were transfected into the cells through electroporation, a non-viral method. In particular, PEs are capable of inducing all types of substitutions (i.e., transversion and transition mutations) as well as insertion and deletion (indel) mutations, which cannot be achieved by conventional base editors. The corrected mCdHs were transplanted into the liver of HT1 model mice, and the transplanted mice survived even after NTBC withdrawal, indicating that our *ex vivo* gene editing strategy could be a suitable and reliable tool for clinical applications in hereditary liver diseases.

RESULTS

Generation and characterization of CdHs from HT1 mice (HT1-mCdHs)

To generate mCdHs from HT1 model mice, we examined whether the previous protocol used for human hepatocyte reprogramming could also be applied to PHs from mice (HT1-mPHs). To this end, we treated the HT1-mPHs with one growth factor and two chemical compounds (referred to as HAC), namely, hepatocyte growth factor (HGF), A83-01 (TGF-β inhibitor), and CHIR99021 (GSK-3 inhibitor) (Figure 1A). Interestingly, we found that HAC-treated HT1-mPHs exhibited a small epithelial cell morphology 3 days after treatment and that the cell populations expanded to cover the dishes after 8 days (Figure 1B). We confirmed that those proliferating cells expressed hepatic stem- or progenitor-specific markers, including Krt19, Sox9, and Afp (Figures 1B, S1A, and S1B); thus, we defined the cells as CdHs from HT1 mice (HT1-mCdHs).

We further investigated the characteristics of HT1-mCdHs using RNA sequencing (RNA-seq). Hierarchical clustering analysis of gene expression data revealed that transcriptome-wide gene expression patterns of HT1-mCdHs were substantially different from those of HT1-mPHs, especially the expression of cell cycle-related genes, which was highly elevated in HT1-mCdHs (Figures S1C and S1D). Gene set enrichment analysis (GSEA) also indicated a clear enrichment of gene sets associated with the cell cycle and stem cells in HT1-mCdHs (Figure S1E). On the other hand, the HT1-mCdHs showed no significant differences in gene expression levels or proliferation capacity compared with CdHs from a wild-type C57BL/6N mouse (WT-mCdHs) (Figures S1A and S1F). In addition, the HT1-mCdHs were passaged stably 23 times, through which transcriptome-wide gene expression levels were maintained, indicating that these cells function as a stable cell line that could produce gene-corrected clones (Figures 1C and S1G). We further compared the HT1-mCdHs with chemically induced liver progenitors (CLiPs), which were previously constructed by another group (Katsuda et al., 2017). We found that both CLiPs and CdHs were stably converted into hepatic progenitors by day 7, and the expression levels of progenitor marker genes were comparable (Figures S1H and S1I).

Figure 1. Generation and characterization of HT1-mCdHs

(A) Schematic diagram of the reprogramming method used to generate chemically derived hepatic progenitors from the HT1 mouse.

(B) Freshly isolated HT1 mouse primary hepatocytes (PHs) were cultured in reprogramming medium for 8 days in the absence or presence of HAC. Immunofluorescence staining of hepatic progenitor markers Krt19 (green) and Sox9 (red) is shown. Nuclei were counterstained with Hoechst 33342. Scale bars, 100 and 50 μm.

(C) Hierarchical cluster analysis of 2,999 differentially expressed gene profiles (≥2-fold changes and $p < 0.05$) in early (passage 3 [p3]) and late (p23) stage HT1-mCdH and HT1-mCdH-Hep cultures, as well as HT1-mPH cultures (n = 3). Red and green represent higher and lower gene expression levels, respectively.

(D) Characteristics of HT1-mCdHs after culture under hepatic differentiation conditions, when they exhibit a mature hepatocyte phenotype. Bright-field, ICG uptake, PAS staining, and immunofluorescence staining for mature hepatocyte-specific markers are shown. Nuclei were counterstained with Hoechst 33342. Scale bars, 100 and 50 μm.

Please cite this article in press as: Kim et al., Adenine base editing and prime editing of chemically derived hepatic progenitors rescue genetic liver disease, Cell Stem Cell (2021), https://doi.org/10.1016/j.stem.2021.04.010

CellPress
Cell Stem Cell
Short Article

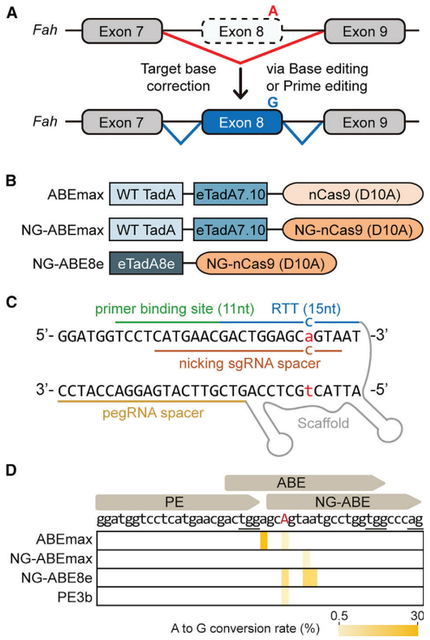

Figure 2. Gene editing in HT1-mCdHs with various ABE and PE systems

(A) Schematic of the gene editing procedure used to correct the pathogenic mutation in HT1-mCdHs.

(B) Schematic diagrams of ABEmax-, NG-ABEmax-, and NG-ABE8e-encoding plasmid constructs.

(C) Design of pegRNA1 and nicking sgRNA1b, which were used for A-to-G conversion of the pathogenic mutation (shown in red) in the *Fah* gene in this study.

(D) Heatmap visualizing A-to-G conversion rates analyzed by high-throughput sequencing. Brown arrows indicate the target sites, and PAM sequences are underlined.

Bipotent differentiation capacity of HT1-mCdHs

Hepatic progenitor cells have the capacity to differentiate into both mature hepatic cells and cholangiocytes. To examine the differentiation capacities of HT1-mCdHs, we first cultured them under hepatic differentiation conditions. We found that the hepatocyte-like cells differentiated from HT1-mCdHs (HT1-mCdH-Heps) had acquired both a mature hepatocyte morphology and mature hepatic characteristics, as shown by analysis of indocyanine green (ICG) uptake and periodic acid-Schiff (PAS) staining (Figure 1D). Immunofluorescence staining showed that mature hepatocyte-specific markers, including albumin (ALB), Hnf4a, Krt18, and Asgpr1, were expressed after hepatic differentiation (Figure 1D), indicating that the mCdHs can re-differentiate into mature hepatocytes under the proper conditions. These characteristics were confirmed using quantitative real-time PCR (see Mendeley Dataset 1A at Mendeley Data: https://doi.org/10.17632/rf6wscfvhw.1). RNA-seq data showed that global gene expression patterns in HT1-mCdHs were largely altered after differentiation (HT1-mCdH-Heps) (Figure 1C), and GSEA and Blue-Pink O' Gram confirmed that HT1-mCdH-Heps showed a strong induction of liver- and hepatocyte-specific gene expression, in contrast to HT1-mCdHs, consistent with a less differentiated phenotype in this cell type (Mendeley Datasets 1B and 1C). In addition, the altered patterns in HT1-mCdH-Heps exhibited a close relationship to that of HT1-mPHs (Figure 1C), supporting the hepatocyte differentiation ability of HT1-mCdHs. We observed that even in passage 23 (p23), HT1-mCdHs could differentiate into mature hepatocytes; we also confirmed that the global gene expression patterns of HT1-mCdH-Heps in p23 were substantially similar to that of HT1-mCdH-Heps in passage 3 (p3). We further conducted another experiment, involving three-dimensional culture methods, in which we induced HT1-mCdHs to differentiate into cholangiocytes. The resulting differentiated cells (HT1-mCdH-Chols) formed characteristic tubular-like structures (Mendeley Dataset 1D) and expressed higher levels of the cholangiocytic-specific markers *Krt19*, *Cftr*, *Ae2*, and *Aqpr1* than did HT1-mCdHs (Mendeley Dataset 1E). Taken together, these results show that we successfully established HT1-mCdHs that have a bipotent capacity to differentiate into both hepatocytes and cholangiocytes.

Adenine base editing and prime editing for correcting a *Fah* mutation in HT1-mCdHs

We next sought to establish a precise gene correction strategy for the HT1-mCdHs. The HT1 model mouse has a G > A point mutation at the 3′ end of *Fah* exon 8 that causes exon 8 skipping during the splicing process, resulting in production of non-functional Fah enzyme (Figure 2A). As a means of correcting the pathogenic mutation in HT1-mCdHs, we tested both ABEs (Figure 2B) and PEs (Figure 2C). We first designed a single-guide RNA (sgRNA) for use with a previously developed version of ABE, ABEmax, which recognizes an NGG protospacer adjacent motif (PAM) (Koblan et al., 2018). In this approach, the point mutation was positioned near but not in the editing window (fourth to seventh). We transfected the ABEmax-encoding plasmid together with the sgRNA-encoding plasmid into the HT1-mCdHs via electroporation; 3 days later, base editing outcomes in bulk cell populations were assessed using high-throughput sequencing. The results showed that the adenosine at the position at which the change was desired (A9) underwent base conversion with an average efficiency of 2.4%, whereas a bystander A (A6) was more efficiently converted, with an average efficiency of 29.3% (Figures 2B, 2D, S2A, and S2B), which is an expected result because ABEmax more readily edits the sixth versus the ninth position. With the aim of reducing the frequency of this bystander base conversion, we tested a version of ABEmax that recognizes an NG PAM (NG-ABEmax) (Jeong et al., 2019; Nishimasu et al.,

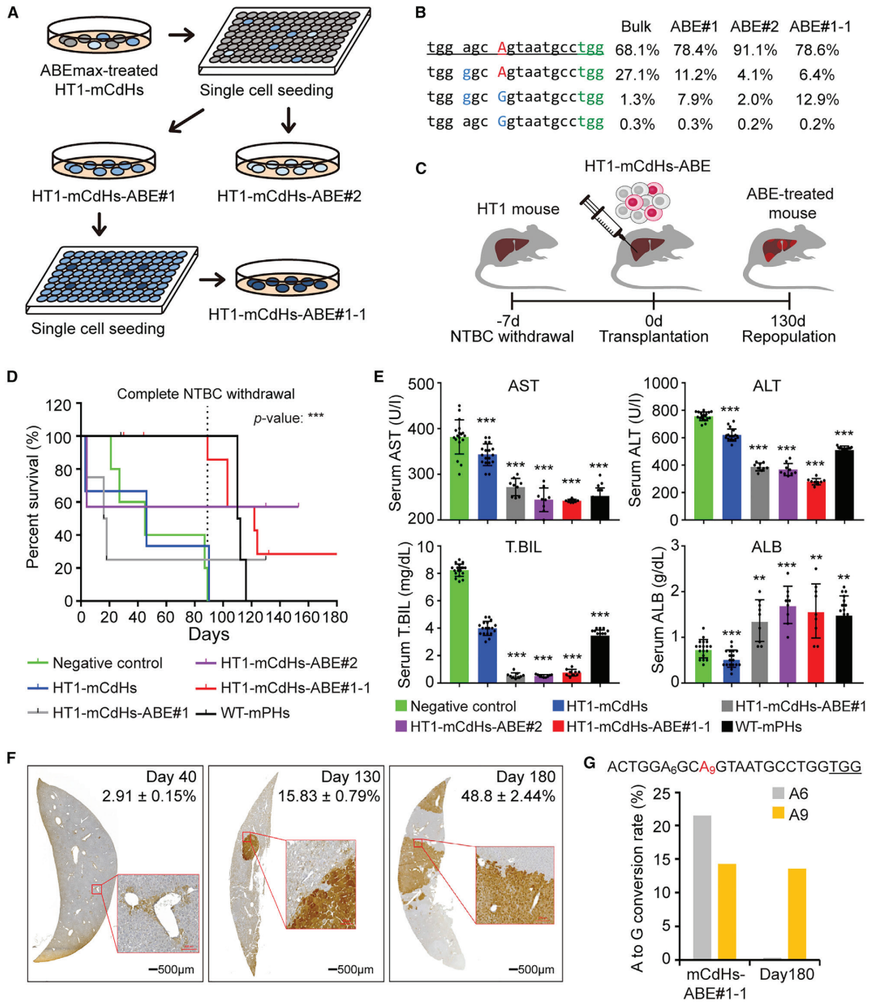

Figure 3. Therapeutic effects of HT1-mCdHs-ABE lines in HT1 model mice

(A) Isolation of clonal cell lines containing the corrected *Fah* gene. ABE-treated HT1-mCdHs were seeded into a 96-well plate (one cell per well), and two cell lines were selected (HT1-mCdHs-ABE#1 and -ABE#2). HT1-mCdHs-ABE#1 cells were again seeded into a 96-well plate, to obtain HT1-mCdHs-ABE#1-1. The base editing efficiency in each cell line was determined using high-throughput sequencing.

(B) Sequences at the target site and the proportion of each sequence in a HT1-mCdHs-ABE bulk population and in HT1-mCdHs-ABE#1, HT1-mCdHs-ABE#2, and HT1-mCdHs-ABE#1-1 lines assessed using high-throughput sequencing. The wild-type (WT) sequence is underlined, the pathogenic mutation is shown in red, the edited sequences in blue, and the PAM sequence in green.

(legend continued on next page)

Please cite this article in press as: Kim et al., Adenine base editing and prime editing of chemically derived hepatic progenitors rescue genetic liver disease, Cell Stem Cell (2021), https://doi.org/10.1016/j.stem.2021.04.010

CellPress

Cell Stem Cell
Short Article

2018) but found that the desired adenosine (now A3) was rarely converted (0.2%) (Figures 2B, 2D, S2A, and S2B). To increase the editing efficiency, we then adopted a recently developed ABE variant (ABE8e), which has faster deamination kinetics; we used a version of ABE8e that recognizes an NG PAM (NG-ABE8e) (Richter et al., 2020). When the HT1-mCdHs were treated with NG-ABE8e, the conversion rates of the adenosine at the desired position (A3) were substantially improved, to an average of 9.2%, and bystander As (A6 and A7) in intron sites were also converted at high rates (12.4% and 11% on average) (Figures 2B, 2D, S2A, and S2B).

Finally, we tested PEs to see if we could achieve highly precise base conversion without any bystander effects. A third prime editing system (PE3 or PE3b) requires a prime editing guide RNA (pegRNA) together with an additional nicking sgRNA. The pegRNA consists of guide RNA spacer sequences as well as a reverse transcription template (RTT) and a primer binding site (Figure 2C). To optimize PE3 editing activity, we designed two different PE targets and tested various pegRNAs, which contained a 15 nt RTT combined with primer binding sites of different lengths ranging from 9 to 15 nt (Figures S2C–S2F). Additionally, we designed two nicking sgRNAs for each pegRNA so that we could use both PE3 and PE3b. Ultimately, we selected pegRNA1 with 11 nt length of prime binding site and nicking sgRNA1b, which together resulted in the highest editing rate (average 2.3%) without any bystander effects (Figures 2D and S2F). Taken together, our results show that we have established various ABE- and PE-based mutation correction strategies in HT1-mCdHs.

Isolation of corrected HT1-mCdHs-ABE lines and examination of ABE-mediated genome-wide off-target effects

For further experiments, we first used ABEmax-treated HT1-mCdHs. To isolate clonal cell lines that contain the corrected *Fah* gene, we diluted the bulk population of ABE-treated cells and determined whether the corrected sequence was present in each resulting clonal cell line using high-throughput sequencing (Table S1). Among the *Fah* corrected clonal cell lines, we selected two lines showing high editing efficiencies, named HT1-mCdHs-ABE#1 and HT1-mCdHs-ABE#2 (Figure 3A). Notably, each cell line was associated with at least four different sequence patterns at the site of interest (Figure 3B). To exclude the possibility that these lines were not clonal, we diluted the HT1-mCdHs-ABE#1 cell population again to isolate single cells and determined the presence of the corrected sequence in each clonal cell line using high-throughput sequencing (Table S1). We consistently observed that all resulting clones had at least four different sequence patterns, suggesting that the HT1-mCdHs might be polyploid, similar to PHs. Previous studies revealed the polyploidy feature of hepatocytes in adult mammals and reported that about 90% of the entire hepatic cell population in rodents was polyploid (Duncan et al., 2010; Wilkinson et al., 2019). We confirmed the polyploid nature of the HT1-mCdHs using flow cytometry analysis (see Mendeley Dataset 2A at Mendeley Data: https://doi.org/10.17632/zxxb72tkxk.1). When we isolated diploid (2c) HT1-mCdHs and cultivated them for 14 days, we found that their ploidy distribution shifted to tetraploid (4c) or octaploid (8c), as seen in the original population (Mendeley Dataset 2B).

From the second set of clones, we selected the cell line (named HT1-mCdHs-ABE#1-1) with the highest frequency of the desired corrected sequence (13.1%) (Figure 3B). To examine ABEmax-mediated genome-wide off-target effects in HT1-mCdHs-ABE#1-1, we performed restriction Endonuclease V (EndoV) enzyme coupled Digenome-seq (Kim et al., 2019a), a method for identifying *in vitro* off-target cleavage sites, which indicated that such cells have eleven *in vitro* cleavage sites, including the on-target site (Table S2). In addition, we determined ten potential off-target sites *in silico* using Cas-OFFinder software (Bae et al., 2014; Hwang et al., 2021) (Table S2). Then, we performed high-throughput sequencing for each site in HT1-mCdHs-ABE#1-1 and found no significant off-target editing compared with the control (HT1-mCdHs) (Figure S3).

Ex vivo therapeutic transplantation of cells from the corrected HT1-mCdHs-ABE#1-1 line into the livers of HT1 mice

We next tested whether the corrected mCdHs would exhibit a reliable repopulation capacity, and thus therapeutic potential, in HT1 mice. We performed intrasplenic transplantation of the partially corrected HT1-mCdHs-ABE#1-1 line, which was confirmed to lack significant off-target effects, into HT1 mice. Seven days before transplantation, NTBC was withdrawn from the drinking water of nine HT1 mice so that liver damage would be induced, thereby facilitating transplantation of the HT1-mCdHs-ABE#1-1 cells (Figure 3C). Phosphate-buffered saline (PBS) and HT1-mCdHs cells were used as negative controls, and PHs from wild-type mice (WT-mPHs) were used as a positive control. We emphasize that we did not use any chemical compounds such as retrorsine to enhance the cell transplantation efficiency. Furthermore, NTBC was completely withdrawn after 90 days. After transplantation, mice from the PBS injected (five mice) and HT1-mCdHs treated (five mice) groups rapidly died; all mice were dead by day 90 (Figure 3D). Furthermore, all animals (five mice) in the WT-mPHs treated group died at about 120 days. Under our experimental conditions (i.e., no retrorsine and complete withdrawal of NTBC), we found that the mice in

(C) Scheme of HT1-mCdHs-ABE transplantation into the HT1 mouse model.

(D) Kaplan-Meier survival curves of HT1 mice with or without cell transplantation. Shown are results for the negative control (PBS injected, five mice), HT1-mCdHs (five mice), HT1-mCdHs-ABE#1 (four mice), HT1-mCdHs-ABE#2 (seven mice), HT1-mCdHs-ABE#1-1 (nine mice), and WT-mPHs (five mice). NTBC was completely withdrawn at day 90.

(E) Serum levels of AST, ALT, total bilirubin, and ALB in the negative control and in the HT1-mCdHs, HT1-mCdHs-ABE#1, HT1-mCdHs-ABE#2, HT1-mCdHs-ABE#1-1, and WT-mPHs groups. The p value was calculated using the log-rank test. ***$p < 0.001$.

(F) Immunohistochemical staining of Fah in the liver at day 40, 130, and 180 after transplantation of HT1-mCdHs-ABE#1-1. Scale bars, 500 μm.

(G) Frequency of the converted nucleotide (G) in HT1-mCdHs-ABE#1-1 cells and liver tissue from HT1 mice at day 180 after transplantation with HT1-mCdHs-ABE#1-1. The position of the target site (A9) is counted from the 5′ end of the target sequence.

Please cite this article in press as: Kim et al., Adenine base editing and prime editing of chemically derived hepatic progenitors rescue genetic liver disease, Cell Stem Cell (2021), https://doi.org/10.1016/j.stem.2021.04.010

the WT-mPH-treated group often also failed to survive, similar to results from previous studies (Cheng et al., 2019; Huang et al., 2014; Karnezis et al., 2001; Michailidis et al., 2020). However, to our surprise, two mice from the HT1-mCdHs-ABE#1-1 treated group (nine mice in total) survived for more than 180 days, indicating a fundamental treatment-induced improvement of HT1 disease in the absence of NTBC. In the case of the mice that survived for more than 180 days, levels of serum biomarkers including aspartate transaminase (AST), alanine transaminase (ALT), total bilirubin (T.BIL), and ALB, showed that liver damage was significantly decreased after transplantation of HT1-mCdHs-ABE#1-1 cells (Figure 3E).

To confirm the repopulation capacity of HT1-mCdHs-ABE#1-1 cells, we examined Fah-positive cell populations in the mice from the HT1-mCdHs-ABE#1-1 transplanted group after 40 (n = 1), 130 (n = 3), and 180 (n = 3) days. Fah-positive cell populations were found around the portal triads at 40 days after transplantation (Figure 3F). After 130 days, the area occupied by Fah-positive cells had increased to about 15% of the liver slice, and further increased to almost 50% at 180 days, and these cells showed a morphology that differed from that of the original mPHs (Figure 3F). On the other hand, the Fah-positive cells were observed in about 5.1% area of the liver slice from the WT-mPHs transplanted group at 110 days, indicating the low therapeutic effect of WT-mPHs on HT1 mice (Figure S4A). To further determine *in vivo* hepatic differentiation capacity of HT1-mCdHs-ABE#1-1 cells, we measured mRNA expression levels of mature hepatocyte-specific markers from the re-isolated cells of a HT1-mCdHs-ABE#1-1 transplanted mouse liver at 180 days. Interestingly, the results showed that the gene expression levels in the re-isolated cells were much similar to those in HT1 mouse liver (Figure S4B), suggesting a relevant *in vivo* hepatocyte differentiation ability of mCdHs.

Furthermore, it is notable that the frequency of G at the target site (A9) had been largely maintained through day 180 in the livers of HT1-mCdHs-ABE#1-1 treated mice, whereas the frequency of G at a bystander site (A6) had decreased substantially (from 21.6% to 0.4%) (Figure 3G), indicating that cells containing the corrected alleles became dominant in the liver during cell duplication, similar to observations in previous studies (Song et al., 2020). Conversion of A6 to G will lead an amino acid mutation (serine to glycine, S235G) near the FAH enzyme active site (D233, K234), which would impede FAH enzyme function; thus, cells possessing an A6 substitution might be eliminated during NTBC withdrawal *in vivo*. In the transplantation experiments, we observed that two of the nine mice in the HT1-mCdHs-ABE#1-1 transplantation group and one of the five in the WT-mPHs transplantation group developed HCC. To investigate whether the hepatocarcinogenesis was mediated by the transplanted HT1-mCdHs-ABE#1-1 cells, we conducted sequencing analysis for cells in the HCC section. We did not observe the corrected sequences in these cells, suggesting that these HCCs were generated naturally (Figures S4C–S4E), similar to findings from a previous study that reported that HT1 model mice developed HCC when NTBC was absent or present at low concentration (Buitrago-Molina et al., 2013).

To investigate the reproducibility of our *ex vivo* gene editing strategy, we repeated the experiments with other corrected mCdHs lines, HT1-mCdHs-ABE#1, and HT1-mCdHs-ABE#2 (Figure 3B). We confirmed that the mice in the HT1-mCdHs-ABE#1 (four mice) and HT1-mCdHs-ABE#2 (seven mice) treated groups also survived for more than 130 days under NTBC withdrawal conditions (Figure 3D). In addition, levels of markers that indicate liver damage were decreased (Figure 3E). Likewise, Fah-positive cell populations in these two groups were observed to show similar patterns as those in the HT1-mCdHs-ABE#1-1 transplanted group (Figures S4F and S4G), although the frequency of sequences in which the mutation had been corrected was lower than in the HT1-mCdHs-ABE#1-1 group. These results indicate that our *ex vivo* gene editing strategy is a reliable and solid approach for HT1 disease treatment in mice.

Ex vivo therapeutic transplantation of a corrected HT1-mCdHs-PE3b cell population into the livers of HT1 mice

After the experiments with the HT1-mCdHs-ABE lines, we next sought to use HT1-mCdHs-PE3b cells, in which the disease mutation was corrected by PE3b, for *ex vivo* therapeutic transplantation. In this case, we decided to use a bulk cell population, instead of isolated clonal cell lines, because the bulk population of cells showed a sufficient editing efficiency (average 2.3%) and lacked bystander effects (Figures 2D and S2F). Similar to the above experiments, NTBC was withdrawn from the drinking water 7 days before transplantation to induce liver damage to facilitate cell transplantation (Figure 4A). Additionally, NTBC was completely withdrawn at day 60, and PBS-injected mice were used as negative controls. As expected, PBS-injected mice (9 mice) died rapidly, before 90 days. However, it is notable that 7 mice from the HT1-mCdHs-PE3b transplanted group (13 mice) survived for more than 160 days, indicating that HT1-mCdHs-PE3b cells also fundamentally treat HT1 disease in the absence of NTBC (Figure 4B). In the case of the mice that survived for more than 140 days, levels of the serum biomarkers AST, ALT, T.BIL, and ALB showed that liver damage was significantly decreased in the HT1-mCdHs-PE3b transplanted group compared with the control group, indicating recovery from liver injury (Figure 4C). Using the immunohistochemistry assay, we observed the Fah-positive cell population in HT1-mCdHs-PE3b transplanted liver after 140 days and confirmed the repopulation capacity of HT1-mCdHs-PE3b cells (Figure 4D), whereas Fah-positive cell populations were not observed in the PBS injected group. In addition, similar to the HT1-mCdHs-ABE#1-1 transplanted mice, the frequency of the edited nucleotide was increased in livers of HT1-mCdHs-PE3b transplanted mice (from 2.5% to 34.3%) (Figure 4E). Taken together, these results suggest that a PE-mediated *ex vivo* gene editing strategy is also feasible.

DISCUSSION

Human genetic disorders are often associated with severe pathological phenotypes, but few curative therapies are available. In this study, we successfully generated mCdHs from HT1 mice and corrected the pathogenic *Fah* gene mutation in these cells using both base editing and prime editing tools that were delivered via a non-viral, electroporation method. Furthermore, we demonstrated that the corrected mCdH population would expand in the liver after transplantation, allowing the mice to survive even under NTBC withdrawal conditions. Our *ex vivo* gene editing strategy, involving base correction in mCdHs, has several important advantages compared with previous strategies: (1) Exogenous genetic factors, which can cause unexpected genetic changes, are not required for the induction of hepatic progenitors from PHs. (2) We can assess the mutation correction rates and genome-wide off-target effects in the cells with a high degree of accuracy prior to transplantation, so we can select a cell line in which base correction is more efficient and that exhibits negligible off-target effects. (3) The gene editing efficiency is less critical than that in *in vivo* gene correction strategies because corrected cells can be enriched *in vitro*, and non-viral delivery of CRISPR tools is easily accomplished.

For our *ex vivo* gene editing strategy, we aimed to conduct the experiments through the safest method to ensure the possibility of further clinical applications. Therefore, we did not perform hepatectomy or inject retrorsine before the cell transplantation to improve liver regeneration, in contrast with other studies (Basma et al., 2009; Nagamoto et al., 2016; Sekiya and Suzuki, 2011; Unzu et al., 2019). Previous studies reported that the repopulation rate of transplanted cells such as PHs in mouse liver was significantly decreased in the absence of retrorsine treatment (Dahlke et al., 2003; Laconi et al., 1998; Michailidis et al., 2020). In addition, other studies have reported that in the absence of NTBC, HT1 mice transplanted with PHs showed a survival rate of less than 20%–30% within 60 days after transplantation (Huang et al., 2014; Karnezis et al., 2001; Zhang et al., 2018). Consistently, our results showed that the HT1-mPHs group did not completely recover, and none of these mice survived more than 120 days. Notably, however, the transplanted HT1-mCdHs, in which the disease-associated mutation was corrected via ABE or PE3b, stably repopulated the liver in HT1 mice without prior hepatectomy or retrorsine, and under the complete NTBC withdrawal condition. We interpret that it is mainly because of the high *in vivo* repopulation capacity of

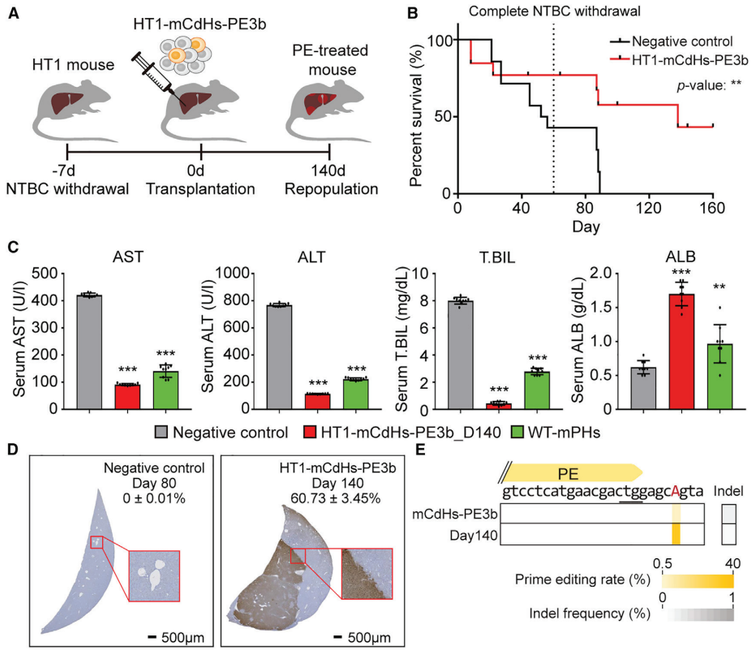

Figure 4. Therapeutic effects of a bulk population of HT1-mCdHs-PE3b cells in HT1 model mice

(A) Scheme of HT1-mCdHs-PE3b transplantation into the HT1 mouse model.

(B) Kaplan-Meier survival curves of HT1 mice with or without cell transplantation. Shown are results for the negative control (PBS injected, 9 mice) and HT1-mCdHs-PE3b (13 mice). NTBC was completely withdrawn at day 60. The p value was calculated using the log-rank test. **p = 0.008.

(C) Serum levels of AST, ALT, total bilirubin, and ALB in the negative control, HT1-mCdHs-PE3b, and WT-mPHs groups. Data were analyzed using the t test (*p < 0.05, **p < 0.01, and ***p < 0.001).

(D) Immunohistochemical staining of Fah in the liver at day 80 and 140 after transplantation of PBS and HT1-mCdHs-PE3b, respectively. Scale bars, 500 μm.

(E) Frequency of the edited nucleotide in HT1-mCdHs-PE3b cells and liver tissue from HT1 mice at day 140 after transplantation with HT1-mCdHs-PE3b.

Please cite this article in press as: Kim et al., Adenine base editing and prime editing of chemically derived hepatic progenitors rescue genetic liver disease, Cell Stem Cell (2021), https://doi.org/10.1016/j.stem.2021.04.010

mCdHs and conclude that CdHs can be a reliable alternative as a liver cell resource in regenerative medicine research, in terms of safety and effectiveness for clinical applications.

In this study, we established various gene correction strategies in mCdHs that involved several gene editing systems, including the canonical ABE that recognizes an NGG PAM (i.e., ABEmax), an ABE that recognizes an NG PAM (i.e., NG-ABE8e), and prime editing (i.e., PE3 or PE3b). We first demonstrated *ex vivo* therapeutic treatment with clonal cell lines derived from a population of ABEmax-treated mCdHs, showing that mice transplanted with such corrected cells survived under a condition of complete NTBC withdrawal. We next transplanted a bulk population of PE3b-treated mCdHs, which similarly improved HT1 symptoms. If gene-corrected cells by PE3b are further used instead of the bulk population, the therapeutic effect may be enhanced. To the best of our knowledge, our study is the first example of PE-mediated HT1 treatment. Our study highlights various pros and cons of ABEs and PEs. Although ABEs show high base conversion efficiency, they have a limited editing window and exhibit bystander base editing. When we used NG-ABEmax rather than ABEmax, the *Fah* mutation could be positioned within the editing activity window, but the efficiency decreased substantially. To overcome this limitation, we further tested NG-ABE8e and found that it showed higher editing frequencies than NG-ABEmax (9.2% versus 0.2%, respectively) (Figure 2D). Although NG-ABE8e also induced bystander mutations, they were located in *Fah* intron sites. On the other hand, although PEs did not induce detectable bystander mutations, these systems are associated with a relatively laborious optimization process. PE3 commonly generated undesired indel mutations (frequency 3%–7%), whereas PE3b caused a much lower frequency of indel mutations (<1%) (Figure S2F).

In summary, considering the high repopulation capacity of mCdHs and the precise editing activity of ABEs and PEs, our novel *ex vivo* therapeutic editing strategy opens a new avenue for treating not only HT1 disease but other genetic diseases that affect the liver. Small molecule-mediated cellular reprogramming and gene correction techniques provide the potential for new clinical applications in various cell types.

Limitations of study

In this study, we established chemically derived progenitor cells from HT1 mice and corrected the disease-causing mutation using both ABEs and PEs. ABEs enabled efficient base correction, but they also converted bystander bases. PEs could precisely correct the disease-causing mutation, but their editing efficiency was lower than that of ABEs. In addition, although ABE- and PE-corrected HT1-mCdHs showed therapeutic effects in HT1 model mice, we could not obtain a cell line in which all mutant alleles were corrected, because of the polyploid nature of HT1-mCdHs. We also found that under our experimental conditions (i.e., in the absence of retrorsine and NTBC), HT1 mice transplanted with WT-mPHs did not survive more than 120 days, whereas HT1-mCdHs-ABEs or HT1-mCdHs-PEs transplanted mice were frequently alive. This finding might be inconsistent with previous studies (Cheng et al., 2019; Huang et al., 2014; Karnezis et al., 2001) showing that WT-mPH-transplanted mice had survived until 100 days, although they all showed decreased tendencies of survival rates.

STAR★METHODS

Detailed methods are provided in the online version of this paper and include the following:

- KEY RESOURCE TABLE
- RESOURCE AVAILABILITY
  - Lead contact
  - Materials availability
  - Data and code availability
- EXPERIMENTAL MODEL AND SUBJECT DETAILS
  - Animals
  - Isolation of primary hepatocytes and cell culture
- METHOD DETAILS
  - Immunostaining
  - Isolation of mRNA and RT-PCR analysis
  - Library preparation and transcriptome sequencing
  - Bioinformatic analysis
  - Calculation of the doubling time
  - PAS staining and detection of ICG uptake
  - Construction of sgRNA- and pegRNA-expressing plasmids
  - Transfection of HT1-mCdHs
  - High-throughput sequencing
  - Endonuclease V-coupled Digenome-seq
  - *In vitro* transcription of sgRNAs
  - Transplantation
  - Analysis of ploidy
- QUANTIFICATION AND STATISTICAL ANALYSIS
  - Statistical analysis

SUPPLEMENTAL INFORMATION

Supplemental information can be found online at https://doi.org/10.1016/j.stem.2021.04.010.

ACKNOWLEDGMENTS

This research was supported by grants from the National Research Foundation of Korea (NRF; 2021M3A9H3015389 to S.B. and 2021M3A9H3015390 to D.C.) and grants from the Medical Research Center (2017R1A5A2015395) and Basic Science Research Program (2019R1F1A106114812) to D.C.

AUTHOR CONTRIBUTIONS

S.B. and D.C. conceived this project. Y.K., S.-A.H., and J.Y. performed and analyzed most of the experiments. J.E., K.J., S.Y., and D.H.H. assisted with *in vivo* experiments and histological analysis. D.S. assisted in the analysis of RNA-seq data. S.-N.L. and J.-S.W. performed protein-related experiments. Y.K., S.-A.H., and S.B. wrote the manuscript with the approval of all other authors. J.J., S.B., and D.C. supervised the research.

DECLARATION OF INTERESTS

Y.K., S.-A.H., J.J., S.B., and D.C. have filed a patent application on the basis of this work.

INCLUSION AND DIVERSITY

We worked to ensure sex balance in the selection of non-human subjects. We worked to ensure diversity in experimental samples through the selection of the genomic datasets.

Please cite this article in press as: Kim et al., Adenine base editing and prime editing of chemically derived hepatic progenitors rescue genetic liver disease, Cell Stem Cell (2021), https://doi.org/10.1016/j.stem.2021.04.010

CellPress

Cell Stem Cell
Short Article

Received: August 5, 2020
Revised: December 19, 2020
Accepted: April 12, 2021
Published: May 4, 2021

REFERENCES

Anzalone, A.V., Randolph, P.B., Davis, J.R., Sousa, A.A., Koblan, L.W., Levy, J.M., Chen, P.J., Wilson, C., Newby, G.A., Raguram, A., and Liu, D.R. (2019). Search-and-replace genome editing without double-strand breaks or donor DNA. Nature *576*, 149–157.

Bae, S., Park, J., and Kim, J.S. (2014). Cas-OFFinder: a fast and versatile algorithm that searches for potential off-target sites of Cas9 RNA-guided endonucleases. Bioinformatics *30*, 1473–1475.

Banas, A., Teratani, T., Yamamoto, Y., Tokuhara, M., Takeshita, F., Quinn, G., Okochi, H., and Ochiya, T. (2007). Adipose tissue-derived mesenchymal stem cells as a source of human hepatocytes. Hepatology *46*, 219–228.

Basma, H., Soto-Gutiérrez, A., Yannam, G.R., Liu, L., Ito, R., Yamamoto, T., Ellis, E., Carson, S.D., Sato, S., Chen, Y., et al. (2009). Differentiation and transplantation of human embryonic stem cell-derived hepatocytes. Gastroenterology *136*, 990–999.

Buitrago-Molina, L.E., Marhenke, S., Longerich, T., Sharma, A.D., Boukouris, A.E., Geffers, R., Guigas, B., Manns, M.P., and Vogel, A. (2013). The degree of liver injury determines the role of p21 in liver regeneration and hepatocarcinogenesis in mice. Hepatology *58*, 1143–1152.

Chen, Y.F., Tseng, C.Y., Wang, H.W., Kuo, H.C., Yang, V.W., and Lee, O.K. (2012). Rapid generation of mature hepatocyte-like cells from human induced pluripotent stem cells by an efficient three-step protocol. Hepatology *55*, 1193–1203.

Cheng, Z., He, Z., Cai, Y., Zhang, C., Fu, G., Li, H., Sun, W., Liu, C., Cui, X., Ning, B., et al. (2019). Conversion of hepatoma cells to hepatocyte-like cells by defined hepatocyte nuclear factors. Cell Res. *29*, 124–135.

Chinsky, J.M., Singh, R., Ficicioglu, C., van Karnebeek, C.D.M., Grompe, M., Mitchell, G., Waisbren, S.E., Gucsavas-Calikoglu, M., Wasserstein, M.P., Coakley, K., et al. (2017). Diagnosis and treatment of tyrosinemia type I: a US and Canadian consensus group review and recommendations. Genet. Med. *19* (12).

Crudele, J.M., and Chamberlain, J.S. (2018). Cas9 immunity creates challenges for CRISPR gene editing therapies. Nat. Commun. *9*, 3497.

Dahlke, M.H., Popp, F.C., Bahlmann, F.H., Aselmann, H., Jäger, M.D., Neipp, M., Piso, P., Klempnauer, J., and Schlitt, H.J. (2003). Liver regeneration in a retrorsine/CCl4-induced acute liver failure model: do bone marrow-derived cells contribute? J. Hepatol. *39*, 365–373.

Duncan, A.W., Taylor, M.H., Hickey, R.D., Hanlon Newell, A.E., Lenzi, M.L., Olson, S.B., Finegold, M.J., and Grompe, M. (2010). The ploidy conveyor of mature hepatocytes as a source of genetic variation. Nature *467*, 707–710.

Grompe, M., Overturf, K., al-Dhalimy, M., and Finegold, M. (1998). Therapeutic trials in the murine model of hereditary tyrosinaemia type I: a progress report. J. Inherit. Metab. Dis. *21*, 518–531.

Hickey, R.D., Mao, S.A., Glorioso, J., Elgilani, F., Amiot, B., Chen, H., Rinaldo, P., Marler, R., Jiang, H., DeGrado, T.R., et al. (2016). Curative ex vivo liver-directed gene therapy in a pig model of hereditary tyrosinemia type 1. Sci. Transl. Med. *8*, 349ra99.

Huang, P., Zhang, L., Gao, Y., He, Z., Yao, D., Wu, Z., Cen, J., Chen, X., Liu, C., Hu, Y., et al. (2014). Direct reprogramming of human fibroblasts to functional and expandable hepatocytes. Cell Stem Cell *14*, 370–384.

Hwang, G.H., Park, J., Lim, K., Kim, S., Yu, J., Yu, E., Kim, S.T., Eils, R., Kim, J.S., and Bae, S. (2018). Web-based design and analysis tools for CRISPR base editing. BMC Bioinformatics *19*, 542.

Hwang, G.H., Kim, J.S., and Bae, S. (2021). Web-based CRISPR toolkits: Cas-OFFinder, Cas-Designer, and Cas-Analyzer. Methods Mol. Biol. *2162*, 23–33.

Jeong, Y.K., Yu, J., and Bae, S. (2019). Construction of non-canonical PAM-targeting adenosine base editors by restriction enzyme-free DNA cloning using CRISPR-Cas9. Sci. Rep. *9*, 4939.

Karnezis, A.N., Dorokhov, M., Grompe, M., and Zhu, L. (2001). Loss of p27(Kip1) enhances the transplantation efficiency of hepatocytes transferred into diseased livers. J. Clin. Invest. *108*, 383–390.

Katsuda, T., Kawamata, M., Hagiwara, K., Takahashi, R.U., Yamamoto, Y., Camargo, F.D., and Ochiya, T. (2017). Conversion of terminally committed hepatocytes to culturable bipotent progenitor cells with regenerative capacity. Cell Stem Cell *20*, 41–55.

Kim, D., Kim, D.E., Lee, G., Cho, S.-I., and Kim, J.-S. (2019a). Genome-wide target specificity of CRISPR RNA-guided adenine base. Nat. Biotechnol. *37*, 430–435.

Kim, Y., Kang, K., Lee, S.B., Seo, D., Yoon, S., Kim, S.J., Jang, K., Jung, Y.K., Lee, K.G., Factor, V.M., et al. (2019b). Small molecule-mediated reprogramming of human hepatocytes into bipotent progenitor cells. J. Hepatol. *70*, 97–107.

Koblan, L.W., Doman, J.L., Wilson, C., Levy, J.M., Tay, T., Newby, G.A., Maianti, J.P., Raguram, A., and Liu, D.R. (2018). Improving cytidine and adenine base editors by expression optimization and ancestral reconstruction. Nat. Biotechnol. *36*, 843–846.

Laconi, E., Oren, R., Mukhopadhyay, D.K., Hurston, E., Laconi, S., Pani, P., Dabeva, M.D., and Shafritz, D.A. (1998). Long-term, near-total liver replacement by transplantation of isolated hepatocytes in rats treated with retrorsine. Am. J. Pathol. *153*, 319–329.

Lee, K.D., Kuo, T.K., Whang-Peng, J., Chung, Y.F., Lin, C.T., Chou, S.H., Chen, J.R., Chen, Y.P., and Lee, O.K. (2004). In vitro hepatic differentiation of human mesenchymal stem cells. Hepatology *40*, 1275–1284.

Lee, A.S., Tang, C., Rao, M.S., Weissman, I.L., and Wu, J.C. (2013). Tumorigenicity as a clinical hurdle for pluripotent stem cell therapies. Nat. Med. *19*, 998–1004.

Michailidis, E., Vercauteren, K., Mancio-Silva, L., Andrus, L., Jahan, C., Ricardo-Lax, I., Zou, C., Kabbani, M., Park, P., Quirk, C., et al. (2020). Expansion, in vivo-ex vivo cycling, and genetic manipulation of primary human hepatocytes. Proc. Natl. Acad. Sci. U S A *117*, 1678–1688.

Miura, K., Okada, Y., Aoi, T., Okada, A., Takahashi, K., Okita, K., Nakagawa, M., Koyanagi, M., Tanabe, K., Ohnuki, M., et al. (2009). Variation in the safety of induced pluripotent stem cell lines. Nat. Biotechnol. *27*, 743–745.

Nagamoto, Y., Takayama, K., Ohashi, K., Okamoto, R., Sakurai, F., Tachibana, M., Kawabata, K., and Mizuguchi, H. (2016). Transplantation of a human iPSC-derived hepatocyte sheet increases survival in mice with acute liver failure. J. Hepatol. *64*, 1068–1075.

Nishimasu, H., Shi, X., Ishiguro, S., Gao, L., Hirano, S., Okazaki, S., Noda, T., Abudayyeh, O.O., Gootenberg, J.S., Mori, H., et al. (2018). Engineered CRISPR-Cas9 nuclease with expanded targeting space. Science *361*, 1259–1262.

Nobili, V., Jenkner, A., Francalanci, P., Castellano, A., Holme, E., Callea, F., and Dionisi-Vici, C. (2010). Tyrosinemia type 1: metastatic hepatoblastoma with a favorable outcome. Pediatrics *126*, e235–e238.

Overturf, K., al-Dhalimy, M., Ou, C.N., Finegold, M., Tanguay, R., Lieber, A., Kay, M., and Grompe, M. (1997). Adenovirus-mediated gene therapy in a mouse model of hereditary tyrosinemia type I. Hum. Gene Ther. *8*, 513–521.

Pankowicz, F.P., Barzi, M., Legras, X., Hubert, L., Mi, T., Tomolonis, J.A., Ravishankar, M., Sun, Q., Yang, D., Borowiak, M., et al. (2016). Reprogramming metabolic pathways in vivo with CRISPR/Cas9 genome editing to treat hereditary tyrosinaemia. Nat. Commun. *7*, 12642.

Park, J., Lim, K., Kim, J.S., and Bae, S. (2017). Cas-analyzer: an online tool for assessing genome editing results using NGS data. Bioinformatics *33*, 286–288.

Rambhatla, L., Chiu, C.P., Kundu, P., Peng, Y., and Carpenter, M.K. (2003). Generation of hepatocyte-like cells from human embryonic stem cells. Cell Transplant. *12*, 1–11.

Richter, M.F., Zhao, K.T., Eton, E., Lapinaite, A., Newby, G.A., Thuronyi, B.W., Wilson, C., Koblan, L.W., Zeng, J., Bauer, D.E., et al. (2020). Phage-assisted evolution of an adenine base editor with improved Cas domain compatibility and activity. Nat. Biotechnol. *38*, 883–891.

Please cite this article in press as: Kim et al., Adenine base editing and prime editing of chemically derived hepatic progenitors rescue genetic liver disease, Cell Stem Cell (2021), https://doi.org/10.1016/j.stem.2021.04.010

Rong, Z., Wang, M., Hu, Z., Stradner, M., Zhu, S., Kong, H., Yi, H., Goldrath, A., Yang, Y.G., Xu, Y., and Fu, X. (2014). An effective approach to prevent immune rejection of human ESC-derived allografts. Cell Stem Cell *14*, 121–130.

Rossidis, A.C., Stratigis, J.D., Chadwick, A.C., Hartman, H.A., Ahn, N.J., Li, H., Singh, K., Coons, B.E., Li, L., Lv, W., et al. (2018). In utero CRISPR-mediated therapeutic editing of metabolic genes. Nat. Med. *24*, 1513–1518.

Sekiya, S., and Suzuki, A. (2011). Direct conversion of mouse fibroblasts to hepatocyte-like cells by defined factors. Nature *475*, 390–393.

Song, Z., Cai, J., Liu, Y., Zhao, D., Yong, J., Duo, S., Song, X., Guo, Y., Zhao, Y., Qin, H., et al. (2009). Efficient generation of hepatocyte-like cells from human induced pluripotent stem cells. Cell Res. *19*, 1233–1242.

Song, C.Q., Jiang, T., Richter, M., Rhym, L.H., Koblan, L.W., Zafra, M.P., Schatoff, E.M., Doman, J.L., Cao, Y., Dow, L.E., et al. (2020). Adenine base editing in an adult mouse model of tyrosinaemia. Nat. Biomed. Eng. *4*, 125–130.

Subramanian, Aravind, Mootha, Vamsi, Mukherjee, Sayan, Ebert, Benjamin, Gillette, Michael, Paulovich, Amanda, Pomeroy, Scott, Golub, Todd, Lander, Eric, and Mesirov, Jill (2005). Gene set enrichment analysis: a knowledge-based approach for interpreting genome-wide expression profiles. Proc Natl Acad Sci U S A *102* (43), 15545–15550, https://doi.org/10.1073/pnas.0506580102.

Sullivan, G.J., Hay, D.C., Park, I.H., Fletcher, J., Hannoun, Z., Payne, C.M., Dalgetty, D., Black, J.R., Ross, J.A., Samuel, K., et al. (2010). Generation of functional human hepatic endoderm from human induced pluripotent stem cells. Hepatology *51*, 329–335.

Unzu, C., Planet, E., Brandenberg, N., Fusil, F., Cassano, M., Perez-Vargas, J., Friedli, M., Cosset, F.L., Lutolf, M.P., Wildhaber, B.E., and Trono, D. (2019). Pharmacological induction of a progenitor state for the efficient expansion of primary human hepatocytes. Hepatology *69*, 2214–2231.

van Ginkel, W.G., Rodenburg, I.L., Harding, C.O., Hollak, C.E.M., Heiner-Fokkema, M.R., and van Spronsen, F.J. (2019). Long-term outcomes and practical considerations in the pharmacological management of tyrosinemia type 1. Paediatr. Drugs *21*, 413–426.

VanLith, C., Guthman, R., Nicolas, C.T., Allen, K., Du, Z., Joo, D.J., Nyberg, S.L., Lillegard, J.B., and Hickey, R.D. (2018). Curative ex vivo hepatocyte-directed gene editing in a mouse model of hereditary tyrosinemia type 1. Hum. Gene Ther. *29*, 1315–1326.

Wilkinson, P.D., Delgado, E.R., Alencastro, F., Leek, M.P., Roy, N., Weirich, M.P., Stahl, E.C., Otero, P.A., Chen, M.I., Brown, W.K., and Duncan, A.W. (2019). The polyploid state restricts hepatocyte proliferation and liver regeneration in mice. Hepatology *69*, 1242–1258.

Wu, X.B., and Tao, R. (2012). Hepatocyte differentiation of mesenchymal stem cells. Hepatobiliary Pancreat. Dis. Int. *11*, 360–371.

Yu, J., Vodyanik, M.A., Smuga-Otto, K., Antosiewicz-Bourget, J., Frane, J.L., Tian, S., Nie, J., Jonsdottir, G.A., Ruotti, V., Stewart, R., et al. (2007). Induced pluripotent stem cell lines derived from human somatic cells. Science *318*, 1917–1920.

Zacharias, D.G., Nelson, T.J., Mueller, P.S., and Hook, C.C. (2011). The science and ethics of induced pluripotency: what will become of embryonic stem cells? Mayo Clin. Proc. *86*, 634–640.

Zhang, K., Zhang, L., Liu, W., Ma, X., Cen, J., Sun, Z., Wang, C., Feng, S., Zhang, Z., Yue, L., et al. (2018). In vitro expansion of primary human hepatocytes with efficient liver repopulation capacity. Cell Stem Cell *23*, 806–819.e4.

Please cite this article in press as: Kim et al., Adenine base editing and prime editing of chemically derived hepatic progenitors rescue genetic liver disease, Cell Stem Cell (2021), https://doi.org/10.1016/j.stem.2021.04.010

CellPress

Cell Stem Cell
Short Article

STAR★METHODS

KEY RESOURCE TABLE

REAGENT or RESOURSE	SOURCE	IDENTIFIER
Antibodies		
Mouse anti-Cytokeratin 19	Santa Cruz Biotechnology	Cat# sc-376126; RRID:AB_10988034
Rabbit anti-SOX9	Abcam	Cat# ab185966; RRID:AB_2728660
Goat anti-Albumin	Abcam	Cat# ab19194; RRID:AB_777886
Mouse anti-E Cadherin	Abcam	Cat# ab76055; RRID:AB_1310159
Rabbit anti-EpCAM	Abcam	Cat# ab32392; RRID:AB_732181
Mouse anti-CD44	Cell Signaling Technology	Cat# 5640; RRID:AB_10547133
Rabbit anti-AFP	Invitrogen	Cat# PA5-21004; RRID:AB_11157055
Rabbit anti-HNF-4alpha	Santa Cruz Biotechnology	Cat# sc-8987; RRID:AB_2116913
Mouse anti-Cytokeratin 18	Abcam	Cat# ab668; RRID:AB_305647
Rabbit anti-ASGPR1	Invitrogen	Cat# PA5-32030; RRID:AB_2549503
Rabbit anti-FAH	Yecuris	Cat# 20-0034
Donkey anti-Goat, Alexa Fluor 488	Thermo Fisher Scientific	Cat# A-11055; RRID:AB_2534102
Goat anti-Mouse, Alexa Fluor 488	Thermo Fisher Scientific	Cat# A-11001; RRID:AB_2534069
Donkey anti-Rabbit, Alexa Fluor 594	Thermo Fisher Scientific	Cat# A-21207; RRID:AB_141637
Chemicals, peptides, and recombinant proteins		
Tris-EDTA	Sigma-Aldrich	Cat# T9285
Collagenase	Worthington Biochemical	Cat# LK002066
Percoll	Sigma-Aldrich	Cat# 17-5445-02
William's Medium E	GIBCO	Cat# A12176-01
DMEM/F-12	GIBCO	Cat# 10565-018
FBS	GIBCO	Cat# 16000-044
Insulin-Transferrin-selenium	GIBCO	Cat# 51500056
Dexamethasone	Sigma-Aldrich	Cat# D1756
Nicotinamide	Sigma-Aldrich	Cat# N3376
β-mercaptoethanol	Sigma-Aldrich	Cat# M3148
Penicillin/streptomycin	GIBCO	Cat# 15070-063
EGF	Peprotech	Cat# 315-09
HGF	Peprotech	Cat# 100-39H
A83-01	Sigma-Aldrich	Cat# SML0788
CHIR99021	Sigma-Aldrich	Cat# SML1046
TrypLE Express Enzyme	GIBCO	Cat# 12563029
Oncostatin M	Prospec	Cat# cyt-231
Matrigel	Corning	Cat# 356230
Collagen Type I	GIBCO	Cat# A10483-01
Indocyanine green	Sigma-Aldrich	Cat# 1340009
critical commercial assay		
Dako REAL EnVision Detection System	Dako	Cat# K500711
qPCR PreMix	Dyne Bio	Cat# DYRT1202
PAS stain kit	Abcam	Cat# ab150680
P3 Primary Cell 4D-Nucleofector X Kit	Lonza	Cat# V4XP-3032
Neon Transfection System 10 μL Kit	Invitrogen	Cat# MPK1096
SUN-PCR blend	Sun Genetics	SG-PT02
Expin PCR SV mini	GeneAll	Cat# 103-102
MiniSeq Mid Output Reagent Cartridge	Illumina	FC-420-1004
DNeasy Blood & Tissue Kit	QIAGEN	Cat# 69504

(*Continued on next page*)

Please cite this article in press as: Kim et al., Adenine base editing and prime editing of chemically derived hepatic progenitors rescue genetic liver disease, Cell Stem Cell (2021), https://doi.org/10.1016/j.stem.2021.04.010

Continued

REAGENT or RESOURSE	SOURCE	IDENTIFIER
Deposited data		
high-throughput sequencing data, identifier: PRJNA655370 and PRJNA717639	This study	https://www.ncbi.nlm.nih.gov/sra
Mendeley dataset 1	This study	https://doi.org/10.17632/rf6wscfvhw.1
Mendeley dataset 2	This study	https://doi.org/10.17632/zxxb72tkxk.1
Experimental models: Organisms/strains		
Mouse: *Fah*$^{-/-}$	From Hyoungbum (Henry) Kim	Gift
Mouse: C57BL/6N	Orient	N/A
Oligonucleotides		
Primers for qRT-PCR; see Table S3	This paper	N/A
Oligos for sgRNA, pegRNA, and ngRNA plasmid cloning; see Table S4	This paper	N/A
Oligos for sgRNA *in vitro* transcription; see Table S4	This paper	N/A
Primers for high-throughput sequencing; see Table S3	This paper	N/A
Recombinant DNA		
pRG2	Addgene	Addgene: 104174
pU6-pegRNA-GG-accepto	Addgene	Addgene: 132777
pCMV-ABEmax	Addgene	Addgene: 112095
pCMV-PE2	Addgene	Addgene: 132775
NG-ABE8e	Addgene	Addgene: 138491
Software and algorithms		
GraphPad Prism 7	GraphPad Software	Version 7.04
ZEN 2.3 (blue edition)	Zeiss	Version 2.3.64.0
Leica TCS SP5	Leica	https://www.leica-microsystems.com/products/confocal-microscopes/p/leica-tcs-sp5/
FUJI DRI-CHEM	Fuji film	NX700i
Cas-analyzer	Park et al., 2017	http://www.rgenome.net/cas-analyzer/
BE-analyzer	Hwang et al., 2018	http://www.rgenome.net/be-analyzer/
PE-analyzer		http://www.rgenome.net/pe-analyzer/
Cas-OFFinder	Bae et al., 2014	http://www.rgenome.net/cas-offinder/
Cluster3.0	Eisen lab	http://eisenlab.org/
GSEA	Subramanian et al., 2005	https://www.gsea-msigdb.org/gsea/index.jsp
Adobe illustrator	Adobe	https://www.adobe.com/products/illustrator.html

RESOURCE AVAILABILITY

Lead contact

Further information and requests for resources and reagents should be directed to and will be fulfilled by the Lead Contact, Sangsu Bae (sangsubae@hanyang.ac.kr).

Materials availability

All unique/stable reagents generated in this study are available from the Lead Contact with a completed Materials Transfer Agreement.

Please cite this article in press as: Kim et al., Adenine base editing and prime editing of chemically derived hepatic progenitors rescue genetic liver disease, Cell Stem Cell (2021), https://doi.org/10.1016/j.stem.2021.04.010

CellPress

Cell Stem Cell
Short Article

Data and code availability

High-throughput sequencing and RNA-seq data have been deposited in the NCBI Sequence Read Archive database (SRA; https://www.ncbi.nlm.nih.gov/sra) under accession numbers PRJNA655370 and PRJNA717639. Additional supplementary figures have been deposited to Mendeley Data as follows: https://doi.org/10.17632/rf6wscfvhw.1 (Dataset 1) and https://doi.org/10.17632/zxxb72tkxk.1 (Dataset 2)

EXPERIMENTAL MODEL AND SUBJECT DETAILS

Animals

HT1 mice were a gift from Hyoungbum (Henry) Kim. Experiments were performed on 6-8-week-old male and female mice. The mice were housed and cared for under specific pathogen-free conditions in accordance with the Principles of Laboratory Animal Care and the Guide for the Use of Laboratory Animals of HYU Industry-University Cooperation Foundation regulations (2018-0196A). Liver damage was induced in HT1 mice by withdrawal of NTBC for 1 week.

Isolation of primary hepatocytes and cell culture

To isolate *Fah*$^{-/-}$ mouse primary hepatocytes, livers in HT1 mice were perfused through the portal vein with solution A (0.19 g/L EDTA (Sigma-Aldrich), 8 g/L NaCl, 0.4 g/L KCl, 0.078 g/L $NaH_2PO4{\cdot}2H_2O$, 0.151 g/L $Na_2HPO4{\cdot}12H_2O$, and 0.19 g/L HEPES) for 5 min at 37°C, followed by solution B (0.3 g/L collagenase (Worthington Biochemical), 0.56 g/L $CaCl_2$, 8 g/L NaCl, 0.4 g/L KCl, 0.078 g/L $NaH_2PO4{\cdot}2H_2O$, 0.151 g/L $Na_2HPO4{\cdot}12H_2O$, and 0.19 g/L HEPES) for 8 min at 37°C. Viable primary hepatocytes were obtained by isodensity centrifugation in Percoll solution (GE Healthcare). Isolated *Fah*$^{-/-}$ mouse primary hepatocytes were seeded in a collagen-coated dish at 2,000 cells/cm^2. Cells were then cultured in William's E medium (GIBCO) in a humidified atmosphere containing 5% CO_2 at 37°C.

For generating chemically derived hepatic progenitors from the HT1 primary hepatocytes, 1 day after seeding the medium was changed to reprogramming medium [DMEM/F-12 medium containing 1% fetal bovine serum (FBS) (GIBCO), 1% insulin-transferrin-selenium (GIBCO), 0.1 μM dexamethasone (Sigma-Aldrich), 10 mM nicotinamide (Sigma-Aldrich), 50 μM β-mercaptoethanol (Sigma-Aldrich), 1% penicillin/streptomycin (GIBCO), 20 ng/mL epidermal growth factor (Peprotech), 20 ng/mL hepatocyte growth factor (Peprotech), 4 μM A83-01 (Sigma-Aldrich), and 3 μM CHIR99021 (Sigma-Aldrich)]. The reprogramming medium was changed every couple of days. Every 4 to 6 days, the cells were passaged by first dissociating them from the plates by treatment with 1X TrypLE Express Enzyme (GIBCO), diluting the released cells into fresh medium at a ratio of 1:4, and plating them in fresh collagen-coated dishes. After base editing, the bulk population of cells was diluted and seeded into 96-well plates so that single cell-derived clones could be picked.

For hepatic differentiation, HT1-mCdHs were seeded on collagen-coated dishes at 1,000 cells/cm^2. After a 1-day incubation, the medium was changed to differentiation medium consisted of the reprogramming medium supplemented with 20 ng/mL oncostatin M (Prospec) and 10 μM dexamethasone; the medium was changed every two days thereafter. After 6 days, the cells were covered with Matrigel (Corning) diluted with differentiation medium at a 1:7 ratio and cultured 2 more days.

For cholangiocytic differentiation, HT1-mCdHs were harvested by treatment with 1X TrypLE Express Enzyme and resuspended at a density of 1 × 10^5 cells/well in 6-well plates in DMEM/F-12 medium containing 10% FBS and 20 ng/mL hepatocyte growth factor [designated cholangiocyte differentiation medium (CDM)]. The CDM was mixed on ice with an equal volume of collagen type I (pH 7.0) and incubated for 30 min at 37°C for solidifying. Then, the cells were overlaid with mixtures consisted of CDM and collagen and cultured for 7 days. The medium was changed every two days.

To conduct comparison studies with CLiPs, mPHs were isolated by the methods described above and cultured with YAC-containing medium manufactured by Katsuda et al. (2017). CLiPs were cultured for 7 days and harvested for RT-qPCR analysis.

METHOD DETAILS

Immunostaining

For immunocytochemistry, the cells were fixed in 4% paraformaldehyde at 4°C overnight. The fixed cells were washed in PBS and then treated with PBS containing 0.2% Triton X-100 for 10 min at room temperature. Next, cells were treated with blocking solution consisting of 1% bovine serum albumin, 22.52 ng/mL glycine, and 0.1% Tween 20 in PBS for 1 hr at room temperature, after which the cells were incubated with primary antibodies diluted in blocking solution at 4°C overnight. After washing, the primary antibodies were detected using Alexa Fluor 488- or 594-conjugated secondary antibodies (Thermo Fisher Scientific). Nuclei were counterstained with Hoechst 33342 (1:10,000, Molecular Probes). Primary antibodies used in this study are listed in the Key Resources Table. Stained cells were visualized under a TCS SP5 confocal microscope (Leica).

For immunohistochemistry, liver tissue samples were fixed in 10% formalin and embedded in paraffin. Sections were subjected to immunohistochemical staining, which was performed using a Dako REAL EnVision Detection System (Dako). Anti-FAH antibody (Yecuris, 20-0034) was used as the primary antibody and nuclei were counterstained with hematoxylin. Stained tissues were viewed under a Virtual Microscope Axio Scan.Z1 (Zelss).

Please cite this article in press as: Kim et al., Adenine base editing and prime editing of chemically derived hepatic progenitors rescue genetic liver disease, Cell Stem Cell (2021), https://doi.org/10.1016/j.stem.2021.04.010

Isolation of mRNA and RT-PCR analysis

Total RNAs were isolated using Trizol Reagent (GIBCO) and RNeasy FFPE Kit (QIAGEN). Then, 1 μg RNA samples were reverse transcribed using a Transcriptor First Strand cDNA Synthesis Kit (Roche). RT-PCR was performed using a CFX Connect Real-Time PCR Detection system (Bio-Rad); each reaction contained 10 μL of qPCR PreMix (Dyne Bio), 1 μL of cDNA, and oligonucleotide primers. Reactions were analyzed in triplicate for each gene. The PCR cycles consisted of 40 cycles of 95°C for 20 s followed by 60°C for 40 s. Melting curves and melting peak data were obtained to characterize the PCR products. The primer sequences are listed in Table S3.

Library preparation and transcriptome sequencing

Total RNA concentrations were calculated using Quant-IT RiboGreen (Invitrogen, USA), and integrity values were accessed by the TapeStation RNA ScreenTape (Agilent Technologies, USA). Only high-quality RNA with an integrity number greater than 7.0 was used for library construction. A library was independently prepared with 1 μg of total RNA for each sample using an Illumina TruSeq Stranded mRNA Sample Prep Kit (Illumina, Inc., San Diego, CA, USA). The initial step of library preparation involved purifying poly-A containing mRNA molecules with poly-T-attached magnetic beads. After this step, the purified mRNA was fragmented into small pieces using divalent cations under elevated temperature. The cleaved mRNA fragments were copied into first strand cDNA using SuperScript II reverse transcriptase (Invitrogen) and random primers, and the reverse complement strand of the cDNA was synthesized using DNA polymerase I, RNase H, and dUTP. These cDNA fragments then underwent an end repair process, which included the addition of a single 'A' base and adaptor ligation. After these steps, the final cDNA libraries were created, purified, and enriched with PCR. The libraries were quantified using KAPA Library Quantification kits for the Illumina Sequencing platforms according to the qPCR Quantification Protocol Guide (Kapa Biosystems, USA) and qualified by the TapeStation D1000 ScreenTape (Agilent Technologies). Indexed libraries were then paired-end sequenced with Illumina HiSeq 2500 (Illumina, Inc.) at Macrogen, Inc. (Korea).

Bioinformatic analysis

The standard Illumina pipeline and real-time analysis tools were employed for the processing of raw images, base calling, and generation of FASTQ data from paired-end RNA-sequencing data. The 100 bp × 2 read sequences were preprocessed using Sickle (V1.33, https://github.com/najoshi/sickle) to trim poor quality sub sequences, and then aligned to the hg19 human reference genome (UCSC data from Illumina iGenomes, https://support.illumina.com/sequencing/sequencing_software/igenome.html) using RSEM (v1.2.31) with STAR (v2.5.2b) alignment software. The expression level of a transcript was measured as the score of transcripts per million kilobases for easier comparison of the proportion of reads that mapped to a gene in each sample. Clustering analysis was performed using Cluster3.0 (http://eisenlab.org/) and heatmap (v3.3.2, https://www.r-project.org).

Gene set enrichment analysis (GSEA) scores were generated for gene sets in the C5 and C8.bp datasets. Normalized enrichment scores and *p-value*s were calculated using GSEA software (https://www.gsea-msigdb.org/gsea/index.jsp).

Calculation of the doubling time

HT1-mCdHs were seeded at a density of 1×10^4 cells/well onto collagen-coated 6-well plates. Cell numbers were determined on day 3 and 7. The doubling time was calculated using the following formula:

$$\text{Doubling Time} = \text{duration} * \log(2)/[\log(\text{Final Concentration}) - \log(\text{Initial Concentration})]$$

as described at https://www.doubling-time.com/compute.php

PAS staining and detection of ICG uptake

To detect glycogen, cells were stained with PAS reagent using a PAS staining kit (Abcam) in the presence or absence of diastase (Sigma) as recommended by the supplier. To detect ICG (Dongindang Pharmaceutical) uptake, cells were incubated in medium containing 1 mg/mL of ICG for 30 min at 37°C and examined under a phase-contrast microscope.

Construction of sgRNA- and pegRNA-expressing plasmids

To construct sgRNA-expressing plasmids, complementary oligos representing the target sequences were annealed and cloned into pRG2 (Addgene #104174). To construct pegRNA-expressing plasmids, complementary oligos representing the target sequences, sgRNA scaffold, and 3′ extensions were annealed and cloned into pU6-pegRNA-GG-acceptor (Addgene #132777). The oligos are listed in Table S4.

Transfection of HT1-mCdHs

Electroporation was performed using an Amaxa 4-D device (Lonza) or a Neon Transfection System (Thermo Fisher). For the Amaxa 4-D device, a P3 Primary Cell 4D-Nucleofector X Kit (program EX-147) was used. 200,000 HT1-mCdHs were electroporated with 750 ng of ABEmax-encoding plasmid (Addgene, #112095) and 250 ng of sgRNA-encoding plasmid. Using the Neon Transfection System, 100,000 HT1-mCdHs were transfected with 900 ng of PE2-encoding plasmid (Addgene #132775), 300 ng of pegRNA-encoding plasmid, and 83 ng of nicking sgRNA- encoding plasmid or 900 ng of NG-ABE-encoding plasmid (NG-ABE8e, Addgene #138491) and 250 ng of sgRNA-encoding plasmid with the following parameters: voltage, 1,200; width, 50 ms; number, 1. The NG-ABEmax-encoding plasmid was constructed in our lab based on the appropriate backbone plasmids (Addgene # 112095).

Please cite this article in press as: Kim et al., Adenine base editing and prime editing of chemically derived hepatic progenitors rescue genetic liver disease, Cell Stem Cell (2021), https://doi.org/10.1016/j.stem.2021.04.010

CellPress
Cell Stem Cell
Short Article

The transfected cells were cultured in reprogramming medium for 3 days. Three days after transfection, the cells were harvested using TrypLE Express Enzyme followed by centrifugation in preparation for freezing and high-throughput sequencing. For freezing, the cells were resuspended in reprogramming medium containing 10% DMSO and stored at −80°C. For high-throughput sequencing, the cell pellet was resuspended in 100 μl of Proteinase K extraction buffer [40 mM Tris-HCl (pH 8.0) (Sigma), 1% Tween-20 (Sigma), 0.2 mM EDTA (Sigma), 10 mg of proteinase K, 0.2% nonidet P-40 (VWR Life Science)], incubated at 60°C for 15 min, and heated to 98°C for 5 min.

High-throughput sequencing

ABE and PE target sites were amplified from extracted genomic DNA using SUN-PCR blend (Sun Genetics). The PCR products were purified using Expin PCR SV mini (GeneAll) and sequenced using a MiniSeq Sequencing System (Illumina). The results were analyzed using Cas-Analyzer (http://www.rgenome.net/cas-analyzer/) (Park et al., 2017), BE-Analyzer (http://www.rgenome.net/be-analyzer/) (Hwang et al., 2018), and PE-analyzer (http://www.rgenome.net/pe-analyzer/). The primers are listed in Table S3.

Endonuclease V-coupled Digenome-seq

Genomic DNA was extracted from HT1-mCdHs using a DNeasy Blood & Tissue Kit (QIAGEN). 8 μg of the genomic DNA was incubated with 32 μg of ABE pre-incubated with 24 μg of *in vitro* transcribed sgRNA at room temperature for 5 min, after which 300 μL of 2X BF buffer (Biosesang) was added and the reaction volume brought to 600 μL. That mixture was incubated at 37°C for 16 h. After RNase A (50 μg/mL, Thermo Scientific) treatment at 37°C for 15 min, the ABE-treated genomic DNA was purified using a DNeasy Blood & Tissue Kit (QIAGEN). 3 μg of the purified DNA was digested with 8 units of Endo V (New England Biolabs) in a 200 μL reaction at 37°C for 2 h. EndoV recognizes inosine and cleaves the second phosphodiester bond 3′ to inosine, resulting in double strand breaks *in vitro*. The genomic DNA was then purified using a DNeasy Blood & Tissue Kit (QIAGEN). Whole genome sequencing was performed with 1 μg of the digested DNA and intact genomic DNA as a negative control using a HiSeq X Ten Sequencer (Illumina) at Macrogen (South Korea).

In vitro transcription of sgRNAs

To generate a template for *in vitro* transcription, a forward oligo containing a T7 RNA polymerase promoter and the target sequence and a reverse oligo containing a guide RNA scaffold were purchased from Macrogen (South Korea) and extended using Phusion DNA polymerase (Thermo Scientific). The extended DNA products were purified using Expin PCR SV mini (GeneAll) and transcribed by T7 RNA polymerase (New England Biolabs). After incubation at 37 °C for 16 h, DNA templates were degraded with DNase I (New England Biolabs), and the RNA products were purified with Expin PCR SV mini (GeneAll). The oligos are listed in Table S4.

Transplantation

Seven days before cell transplantation into mice, NTBC was withdrawn from the drinking water. 1×10^6 cells in 100 μL PBS were transplanted into the inferior pole of the spleen. NTBC was transiently given every 3 days when mice reached 80% of their original weight. NTBC was completely withdrawn from the drinking water at days 90 and 60 for HT1-mCdHs-ABE and -PE3b transplanted mice, respectively. After transplantation, serum was collected for biomarker analysis. Serum was diluted at a ratio of 1:4 to obtain means.

Analysis of ploidy

HT1 mPHs, mCdHs, and mCdHs-ABE cells were dissociated from plates by trypsinization and then incubated with 15 μg/mL of Hoechst 33342 and 5 μM of reserpine for 30 min at 37°C. Cell ploidy was analyzed with a FACS Aria II (Beckman coulter) as described by Duncan et al. (2010).

QUANTIFICATION AND STATISTICAL ANALYSIS

Statistical analysis

Doubling time experiments and qRT-PCR were performed in triple biological replicates. Quantitative data are presented as means ± standard deviations (SDs) with inferential statistics (p values). Survival was analyzed as a Kaplan-Meier curve using GraphPad Prism 7 (GraphPad). Statistical significance was evaluated by two-tailed t tests with significances set at * $p < 0.05$, ** $p < 0.01$, and *** $p < 0.001$.

역대 수상자

제1회

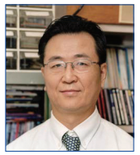

본상
고재영 울산대학교 의과대학 신경과학 교실

Non-proteolytic Neuroprotection by Human Recombinant Tissue Plasminogen Activator. Science, 1999;284:647-50.

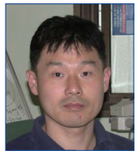

젊은 의학자상
이석형 가톨릭대학교 의과대학 병리학 교실

Alterations of Fas(APO-1/CD95) Gene in Transitional Cell Carcinomas of Urinary Bladder. Cancer Research, 1999;59:5683-6.

제2회

본상
이현철 연세대학교 의과대학 내분비내과

Remission in Models of Type 1 Diabetes by Gene Therapy Using A Single-chain Insulin Analogue. Nature, 2000;408:483-8.

젊은 의학자상
이철환 울산대학교 의과대학 심장내과

Pressure-derived Fractional Collateral Blood Flow: A Primary Determinant of Left Ventricular Recovery after Reperfused Acute Myocardial Infarction. Journal of the American College of Cardiology, 2000;35:949-55.

제3회

본상
고규영 포항공과대학교 생명과학부

Angiopoietin-1 Reduces VEGF-stimulated Leukocyte Adhesion to Endothelial Cells by Reducing ICAM-1, VCAM-1, and E-Selectin Expression. Circulation Research, 2001;89:477-9.

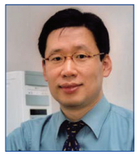

젊은 의학자상
강덕현 울산대학교 의과대학 심장내과

Long-term Clinical and Echocardiographic Outcome of Percutaneous Mitral Valvuloplasty. Journal of the American College of Cardiology, 2000;35:169-75.

제4회

본상 (공동수상)
이동수 서울대학교 의과대학 핵의학과

Cross-modal Plasticity and Cochlear Implants.
Nature, 2001;409:149-50.

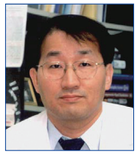

본상 (공동수상)
박국인 연세대학교 의과대학 소아과

The Injured Brain Interacts Reciprocally with Scaffolds Seeded with Neural Stem Cells to Reconstitute Lost Tissue. Nature Biotechnology, 2002;20:1111-7.

젊은 의학자상
박용범 연세대학교 의과대학 류마티스내과

Atherosclerosis in Rheumatoid Arthritis: Morphologic Evidence Obtained by Carotid Ultrasound. Arthritis & Rheumatism, 2002;46:1714-9.

제5회

기초의학연구 부문
한기훈 울산대학교 의과대학 심장내과

Monocyte Chemoattractant Protein-1-induced Angiogenesis is Mediated by Vascular Endothelial Growth Factor-A. Blood, 2005;105:1405-7.

임상의학연구 부문
임재준 서울대학교 의과대학 호흡기내과

Discrepancy Between the Tuberculin Skin Test and the Whole-Blood Interferon-gamma Assay for the Diagnosis of Latent Tuberculosis Infection in an Intermediate Tuberculosis-Burden Country. Journal of the American Medical Association, 2005;293:2756-61.

제6회

기초의학연구 부문
정두현 서울대학교 의과대학 병리학 교실

FcgammaRIII engagement Provides Activating Signals to NKT Cells That Promote Antibody-induced Joint inflammation.
Journal of Clinical Investigation, 2006;116(9):2484-92.

임상의학연구 부문
이석구 성균관대학교 의과대학 소아외과

Hepatocyte Transplantation for Glycogen Storage Disease Type Ib.
Cell Transplantation, 2007;16(6):629-37.

제7회

기초의학 부문
신재국 인제대학교 의과대학 약리학 교실

Genetic Polymorphism of Hepatocyte Nuclear Factor-4α Influences Human Cytochrome P450 2D6 Activity. Hepatology, 2008;48:635-45.

임상의학 부문
이용철 전북대학교 의학전문대학원 호흡기·알레르기 내과

Mast Cells Can Mediate Vascular Permeability through Regulation of the PI3K-HIF-1α-VEGF Axis.
American Journal of Respiratory and Critical Care Medicine, 2008;178:787-97.

제8회

기초의학 부문
박종완 서울대학교 의과대학 약리학 교실

Sirtuin 1 Modulates Cellular Responses to Hypoxia by Deacetylating Hypoxia-Inducible Factor 1α. Molecular Cell, 2010;38(6):864-78.

임상의학 부문
박재용 경북대학교 의학전문대학원 내과

Polymorphisms in the CASPASE Genes and Survival in Patients With Early-Stage Non-Small-Cell Lung Cancer. Journal of Clinical Oncology, 2009;27(34):5823-9.

제9회

기초의학 부문
김우현 전북대학교 의학전문대학원 생화학 교실

Ca^{2+} Signaling Tools Acquired from Prostasomes are Required for Progesterone-induced Sperm Motility. Science Signaling, 2011;4:ra31.

임상의학 부문
김흥동 연세대학교 의과대학 소아과학 교실

Resective Pediatric Epilepsy Surgery in Lennox-Gastaut Syndrome.
Pediatrics, 2010;125(1)e58-e66.

제10회

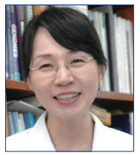

기초의학 부문
조은경 충남대학교 의학전문대학원 미생물학 교실

Host Cell Autophagy Activated by Antibiotics is Required for their Effective Antimycobacterial Drug Action. Cell Host & Microbe, 2012;11(5):457-68.

임상의학 부문
김완욱 가톨릭대학교 의과대학 내과학 교실

A Novel Pathogenic Role of the ER Chape-rone GRP78/BiP in Rheumatoid Arthritis.
The Journal of Experimental Medicine, 2012;209(4):871-86.

제11회

기초의학 부문
김인겸 경북대학교 의학전문대학원 약리학 교실

Histone Deacetylase Inhibition Attenuates Transcriptional Activity of Mineralocorticoid Receptor through its Acetylation and Prevents Development of Hypertension.
Circulation Research, 2013;112(7):1004-12.

임상의학 부문
윤영호 서울대학교 의과대학 의과학과

Web-Based Tailored Education Program for Disease-Free Cancer Survivors With Cancer-Related Fatigue: A Randomized Controlled Trial.
Journal of Clinical Oncology, 2012;30(12):1296-303.

제12회

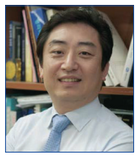

기초의학 부문
남석우 가톨릭대학교 의과대학 병리학 교실

Histone Deacetylase Inhibition Attenuates Transcriptional Activity of Mineralocorticoid Receptor through its Acetylation and Prevents Development of Hypertension.
Circulation Research, 2013;112(7):1004-12.

임상의학 부문
고원중 성균관대학교 의과대학 내과학 교실

Macrolide Treatment for Mycobacterium abscessus and Mycobacterium massiliense Infection and Inducible Resistance.
American Journal of Respiratory and Critical Care Medicine, 2012;186:917-925.

제13회

기초의학 부문
김철훈 연세대학교 의과대학 약리학 교실

mGluR5 in the Nucleus Accumbens is Critical for Promoting Resilience to Chronic Stress.
Nature Neuroscience, 2015;18(7):1017-24.

임상의학 부문
이은봉 서울대학교 의과대학 내과학 교실

Tofacitinib versus Methotrexate in Rheumatoid Arthritis.
The New England Journal of Medicine, 2014;370(25):2377-86.

제14회

기초의학 부문
국 현 전남대학교 의과대학 약리학 교실

Cross-modal Plasticity and Cochlear Implants.
Nature, 2001;409:149-50.

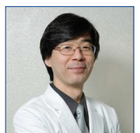

임상의학 부문
홍명기 연세대학교 의과대학 내과학 교실

Effect of intravascular ultrasound-guided vs. angiography-guided everolimus-eluting stent implantation: the IVUS-XPL randomized clinical trial. JAMA, 2015;314(20):2155-63.

중개의학 부문
남도현 성균관대학교 의과대학 신경외과학 교실

Clonal evolution of glioblastoma under therapy. Nature Genetics,2016;48(7):768-76.

제15회

기초의학 부문
김형범 연세대학교 의과대학 약리학 교실

In vivo high-throughput profiling of crisPr-cpf1 activity.
Nature Methods,2017;14[2]:153-159.

임상의학 부문
홍수종 울산대학교 의과대학 소아청소년과학 교실

Prenatal maternal distress affects atopic dermatitis in offspring mediated by oxidative stress. Journal of Allergy and Clinical Immunology,2016;138[2]:468-475.

중개의학 부문
이필휴 연세대학교 의과대학 신경과학 교실

Mesenchymal stem cells enhance α-synuclein clearance via M2 microglia polarization in experimental and human parkinsonian disorder. Acta Neuropathologi ca,2016;132[5]:685-701.

제16회

기초의학 부문

김응국 충북대학교 의과대학 생화학 교실

Nigral dopaminergic PAK4 prevents neurodegeneration in rat models of Parkinson's disease. Science Translational Medicine, 2016; 8.367ra170.

임상의학 부문

김재민 전남대학교 의과대학 정신건강의학 교실

Effect of Escitalopram vs Placebo Treatment for Depression on Long-term Cardiac Outcomes in Patients With Acute Coronary Syndrome A Randomized Clinical Trial. Journal of the American Medical Association, 2018;320(4):350-357

중개의학 부문

송재관 울산대학교 의과대학 내과학 교실

Dipeptidyl Peptidase-4 Induces Aortic Valve Calcification by Inhibiting Insulin-Like Growth Factor-1 Signaling in Valvular Interstitial Cells. Circulation, 2017;135:1935-1950

제17회

기초의학 부문

이상훈 한양대학교 의과대학 생화학 . 분자생물학교실

Cografting astrocytes improves cell therapeutic outcomes in a Parkinson's disease model (Journal of Clinical Investigation, 2018;128(1):463-482)

임상의학 부문

박상민 서울대학교 의과대학 가정의학교실

Association of Blood Pressure Classification in Korean Young Adults According to the 2017 American College of Cardiology/American Heart Association Guidelines With Subsequent Cardiovascular Disease Events (JAMA, 2018;320(17):1783-1792)

중개의학 부문

손명현 연세대학교 의과대학 소아과학교실

Activated Leukocyte Cell Adhesion Molecule Stimulates the T-Cell Response in Allergic Asthma (Am J Respir Crit Care Med, 2018;197(8):994-1008)

제18회

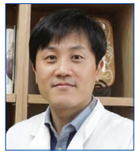

기초의학 부문

선 웅 고려대학교 의과대학 해부학교실

Drp1-Zip1 Interaction Regulates Mitochondrial Quality Surveillance System (Molecular cell, 73. 2. 364-376, 2019)

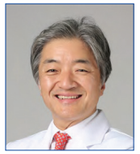

임상의학 부문

김병극 연세대학교 의과대학 내과학교실

Effect of Ticagrelor Monotherapy vs Ticagrelor With Aspirin on Major Bleeding and Cardiovascular Events in Patients With Acute Coronary Syndrome: The TICO Randomized Clinical Trial (JAMA, 323(23), 2407-2416, 2020)

중개의학 부문

강훈철 연세대학교 의과대학 소아과학교실

Precise Detection of Low-Level Somatic Mutation in Resected Epilepsy Brain Tissue (Acta Neuropathol, 2019 Dec;138(6):901-912)

중개의학 부문

이승표 서울대학교 의과대학 내과학교실

Assessment of Inflammation in Pulmonary Artery Hypertension by 68 Ga-Mannosylated Human Serum Albumin (Am J Respir Crit Care Med, 201, 1, 95-106, 2020)